Dr. med. Hsiang-Hao Hsu

Mechanisms of angiotensin II signaling on cytoskeleton of podocytes

2007

Biologie

Mechanisms of angiotensin II signaling on cytoskeleton of podocytes

Inaugural-Dissertation
zur Erlangung des Doktorgrades
der Naturwissenschaften im Fachbereich Biologie
der Mathematisch-Naturrwissenschaftlichen Fakultät
der Westfälische Wilhelms-Universität Münster

vorgelegt von
Dr. med. Hsiang-Hao Hsu
aus Taipei
-2007-

Dekan:	Prof. Dr. Norbert Sachser
Erste Gutachter:	Prof. Dr. Andreas Püschel
Zweiter Gutachter:	Prof. Dr. Hermann Pavenstädt
Tage der mündlichen Prüfung:	04. 03. 2008
Tage der Promotion:	11. 04. 2008

Abstract

Podocytes are critical for establishing the selective permeability of the glomerular filtration barrier. Sustained rennin-angiotensin system activation is crucial in the pathogenesis of podocyte injury and proteinuria. Mechanisms of angiotensin II (Ang II) modulating actin cytoskeletal dynamics of podocytes in physiological or injurious stimuli remain unclear. This work demonstrated increased expression of Rac-1 and phosphorylated ezrin/radixin/moesin (ERM) proteins in cultured mouse podocytes stably expressing Ang II type 1 receptor (AT1R) and in glomeruli of AT1R transgenic rats (Neph-hAT1 TGRs). In mouse podocytes, Ang II caused a reactive oxygen species (ROS)–dependent rearrangement of cortical F-actin, stress fiber attenuation and a migratory phenotype switch. Ang II–induced actin cytoskeletal remodeling was provoked by activated Rac-1 and phosphorylated ERM proteins. Phosphorylation of ERM proteins may indicate a high actin cytoskeletal turnover state. Heparin, a potent G-coupled protein kinase 2 inhibitor, abolished ERM protein phosphorylation in Ang II-treated podocytes. However, inhibition of Rho kinase, p38 MAPK or protein kinase C had no effect on phosphorylation. The free radical scavenger DMTU abolished Ang II–induced cell migration, ERM protein phosphorylation and cortical F-actin ring formation, suggesting that ROS mediates the effect of Rac-1 in podocyte AT1R signaling. Proteomic analysis of AT1R podocytes revealed Ang II suppressed expression of peroxiredoxin 2 (Prx2), an anti-oxidative protein. SiRNA experiments targeting Prx2 in cultured podocytes demonstrated that Prx2 is a cellular redox reaction modulator. Decreased Prx2 expression in podocytes favors an oxidative cellular environment. Moreover, Ang II signaling triggered a down-regulation of α actinin-4 and decreased focal adhesion expression in podocytes. The Ang II–induced phenotype shift from dynamically stable to adaptively migratory may eventually exhaust podocytes with a high actin cytoskeletal turnover, leading to podocyte depletion and focal segmental glomerulosclerosis.

Table of Contents

1. Introduction

1.1. The kidney, Nephron and Glomerular Filtration

The kidneys perform their most important function by "clearing" unwanted substances from blood and excreting these substances in the urine while returning needed substances back to the blood. The ability of the kidney to perform many of its functions depends on the three fundamental functions—*filtration*, *reabsorption*, and *secretion*. Each human kidney is made up of approximately 1 million nephrons, each capable of generating urine. Figure 1.1.1 displays the embryonic development and functional parts of a nephron. Each nephron is composed of a tuft of glomerular capillaries called the glomerulus, through which substantial amounts of fluid are filtered from the blood (filtration), a capsule around the glomerulus called Bowman's capsule, and a long tubule in which filtered fluid is converted into urine on its way to the renal pelvis (reabsorption and secretion), which receives urine from all nephrons.

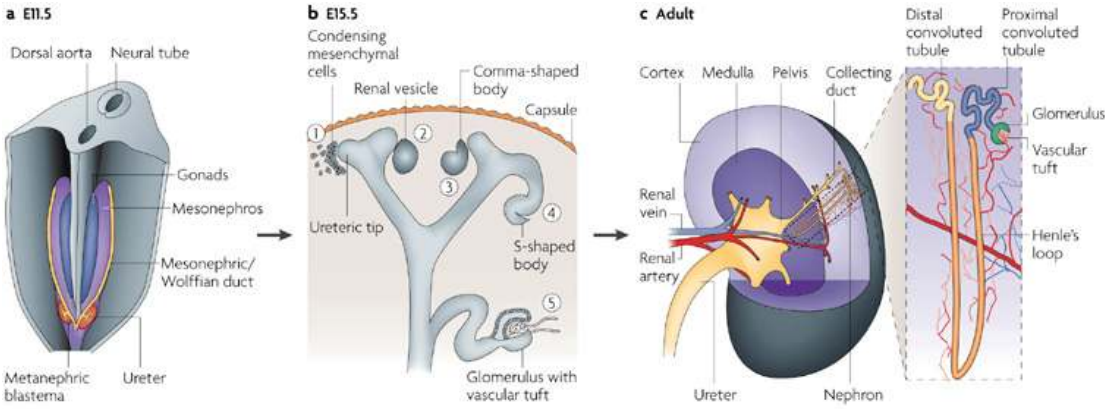

Fig. 1.1.1 Embryonic development and anatomy of kidney (a) The metanephros develops from reciprocal interactions between the mesonephric duct (giving rise to the ureter) and metanephric mesenchyme at the caudal end of the nephrogenic cord. At embryonic stage E11.5, the ureter has invaded and branched once in the mesenchyme. **(b)** Nephrons are continuously induced at the ureter tips and undergo a well-defined series of morphological transformations: first, condensation of mesenchymal cells; second, mesenchymal-to-epithelial transition with formation of the renal vesicle; third, the comma-shaped body transformation; fourth, the S-shaped body transformation with invasion of endothelial cells; and, fifth, formation of the glomerulus and patterning of the nephron into its segments. **(c)** Anatomy of an adult kidney and nephron position and arrangement. Schedl A. Nature Reviews Genetics, 2007

The glomerulus is a ball of capillaries surrounded by the Bowman's capsule, a hollow capsule of the tubular epithelium through which urine is filtered. The glomerulus also contains mesangial cells, which comprise a scaffold supporting capillary loops and have contractile and phagocytic characteristics. Blood enters the glomerular capillaries through an afferent arteriole and exits via an efferent arteriole rather than venule. Vasoconstriction of this efferent arteriole generates high hydrostatic pressure in the glomerular capillary, forcing water, iron, and small molecules through the filtration barrier into Bowman's capsule. Whether a substance is filtered depends on both its molecular size and charge (Fig. 1.1.2).

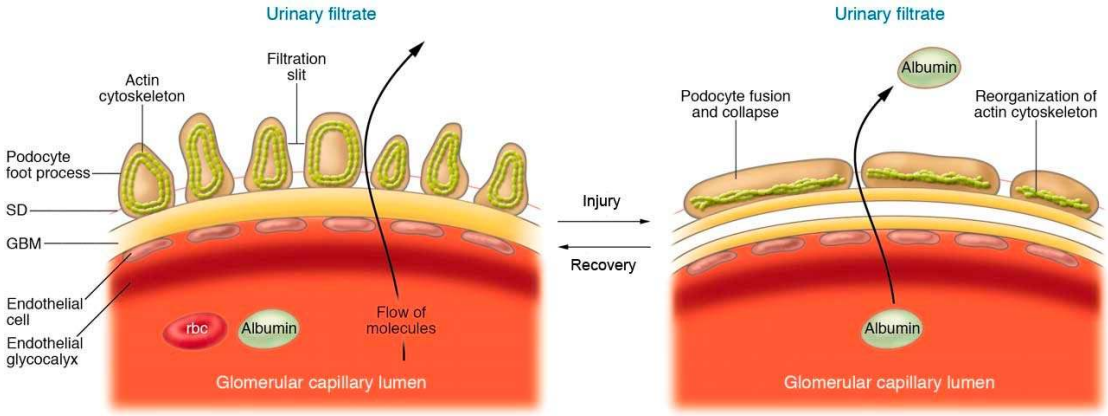

Fig. 1.1.2 The glomerular filtration barrier Blood enters glomerular capillaries and is filtered across the endothelium and glomerular basement membrane, and through the filtration slits between podocyte foot processes to generate the urine filtrate. In healthy glomeruli, this barrier restricts the passage of macromolecules (e.g. albumin). Ronco P J. Clin. Invest. 2007

The filtration barrier has three layers: *Endothelial cells.* The endothelial cells of the glomerular capillary wall are thin, with many 70 nm pores filled with negatively charged glycoproteins—mostly podocalyxin. *Glomerular basement membrane.* This membrane is a specialized capillary basement membrane that also contains negatively charged glycoproteins. This basement membrane has two layers, comprised of type IV collagen, heparin sulfate proteoglycans, laminin, podocalyxin and low levels of type III and V collagen, fibronectin, and entactin. The type IV collagen forms helical strands arranged into a three-dimensional framework on to which other components

are attached. *Epithelial cells*. The epithelial cells or so-called podocytes have long projections from which foot processes arise and attach to the urinary side of the glomerular basement membrane. Foot processes from differentiated podocytes interdigitate, leaving filtration slits 25–65 nm in diameter between foot processes from adjacent podocytes. Across these slits, a highly organized network of several glycoproteins forms 'slit pores' through which filtration occurs and which prevent the passage of large molecules such as albumin.

1.2. Podocyte and Slit Diaphragm

Podocytes have a significant role in generating selective permeability of the glomerular filtration barrier. Podocyte injury can cause proteinuria, a sign of glomerular diseases.[1] Differentiated podocytes are mesenchymal-like cells that arise from epithelial precursors during renal development. These differentiated podocytes consist of three morphologically and functionally different segments: a cell body (CB); major processes (MPs); and, foot processes (FPs). Major processes arise from the CB and split into FPs. Podocyte FPs comprise a highly branched interdigitating network with FPs of neighboring podocytes connected by the slit diaphragm (SD), which is a multiprotein complex similar to adheren junctions and covers filtration slits (regions between opposing podocyte FPs), thereby establishing the final barrier to urinary protein loss (Fig. 1.2).

Slit diaphragm-interconnected FPs cover the exterior basement membrane surface of the glomerular capillary, stabilize glomerular architecture by counteracting distensions of the glomerular basement membrane,[2] and maintain a large filtration surface through the SDs.[3] Thus, SD-interconnected FPs are responsible for approximately 40% of filtration barrier hydraulic resistance. The contractile structures of podocyte foot processes typically respond to vasoactive hormones and thereby modulate the ultrafiltration coefficient K_f.[2;4] Podocytes contribute to specific size and charge characteristics of the glomerular filtration barrier, and podocyte damage results in retraction of their FPs and proteinuria.[5;6] Podocytes are the injury target of many

glomerular diseases. Podocyte cell shape changes, such as retraction of FPs and even podocyte loss, occur in minimal-change nephropathy, membranous nephropathy, focal segmental glomerulosclerosis, chronic glomerulonephritis, and diabetic nephropathy.[7-11] Despite decades of research, the physiological and molecular mechanisms of glomerular filtration and its disturbances remain unclear.

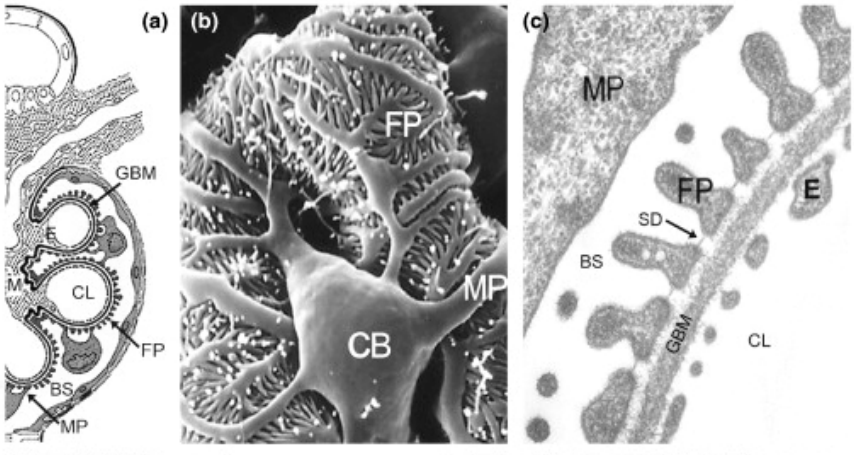

Fig. 1.2 Podocyte and slit diaphragm (a) Glomerular endothelial cells (E) embracing the capillary lumen (CL) and mesangial cells (M) are located on the blood side of the glomerular basement membrane (GBM), whereas podocytes cover the outer aspect of the GBM facing Bowman's space (BS). **(b)** Scanning electron microscopy illustrates the complexity of podocyte morphology. Podocytes consist of a cell body (CB), major processes (MPs) and foot processes (FPs). Only FPs directly contact the GBM. They also interdigitate with FPs of neighboring cells and form filtration slits (shown in **(c)**, interposed slit diaphragms (SDs) cover the filtration slits). Faul *et al*. Trends Cell Biol. 2007

1.3. Actin Cytoskeleton of Podocyte

Podocytes function is largely based on their complex cell architecture, and, in particular, on the maintenance of the normal FP structure. FPs contain an actin-based cytoskeleton linked to the GBM in focal contacts (the basal membrane domain (BMD), also known as sole plate). These FPs are further characterized by a cortical network of short branched actin filaments (the apical membrane domain (AMD)), and the presence of highly ordered, parallel, contractile actin filament bundles,[4] which are believed to modulate filtration barrier SD permeability through changes in FP morphology. All three domains—AMD, BMD and SD—are physically and

functionally linked to the actin cytoskeleton (Fig. 1.3); thus, actin is the common denominator in podocyte function and dysfunction.[12] Interference with any of these three FP domains transforms the actin cytoskeletons arising from parallel contractile bundles into a dense network with FP effacement (reflected by the simplification of the FP structure and loss of normal interdigitating pattern) and proteinuria. Foot process effacement requires active reorganization of actin filaments.[13-15] Therefore, proteins regulating the plasticity of the podocyte actin cytoskeleton are extremely important for maintenance of glomerular filter function.

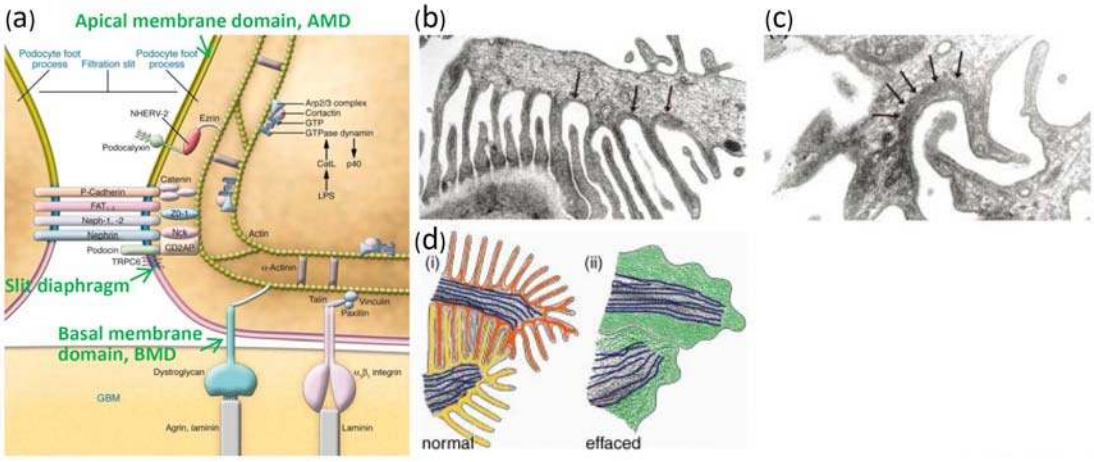

Fig. 1.3 All three foot process domains are physically and functionally linked to the actin cytoskeleton of podocytes (a) This schematic displays the connections between the cortical actin cytoskeleton, slit diaphragm, and components of the podocyte basolateral portion. The membrane domains are marked: apical cell membrane domain (green); SD domain (blue); and, "sole" of the FP (pink). **(b)** The origin of several FPs from a MP. The cytoskeleton of MPs predominantly consists of microtubules and intermediate filaments. The FPs contain bundles of parallel actin filaments (arrows) that connect neighboring FPs. **(c)** At high magnification (×65000), the well-organized parallel actin bundles (arrows) are clearly visible. **(d)** Top view of normal and effaced podocyte FPs. (i) In healthy podocytes, FPs regularly interdigitate. The highly organized actin bundles of interdigitating FPs from two adjacent podocytes are in red and yellow, respectively. Microtubules of MPs are blue. (ii) In effaced podocytes, a meandering cell border exists between effaced FPs. A continuous sheet of cytoplasm develops that is filled with reorganized, short, branched actin filaments (green). Modified from Ronco P J. Clin. Invest. 2007 and Faul *et al*. Trends Cell Biol. 2007

1.4. Focal Segmental Glomerulosclerosis (FSGS)

Focal and segmental glomerulosclerosis (FSGS) is a very common primary glomerular disease that terminates as end-stage renal disease (ESRD).[16;17] In most series, the ten-year survival rate is 40–60%.[18-21]

1.4.1. Pathological Features

Focal and segmental glomerulosclerosis is a pattern of injury defined by a segmental scar, which involves only some glomeruli. The classic scar is defined by a segmental scar located either at the capillary hilum or in the glomerular periphery (Fig. 1.4.1 a). The scar comprises either obliteration of glomerular architecture and replacement by collagen or segmental glomerular collapse (Fig. 1.4.1 b). The overlying parietal and visceral epithelium may be prominent, especially when associated with an adhesion. This lesion is frequently associated with hyalinosis and adhesions. Detailed morphological analysis in rodents largely corresponds to that for human pathology, and demonstrates that this disease entity is a result of a primary dysfunction of the podocyte (‘podocytopathy’) (Fig. 1.4.1 c).

1.4.2. Pathophysiological Mechanisms

Severe damage to podocytes by numerous damaging mechanisms results in a local loss of the separation between the tuft and Bowman’s capsule.[10] This happens affixation of either parietal epithelial cells (PECs) to the glomerular basement membrane (characteristic of degenerative mechanisms such as hypertension or direct toxic effects to podocytes) or affixation of podocytes to the parietal basement membrane (characteristic of inflammatory diseases such as anti-GBM nephritis). This adhesion develops either into a proteinaceous crescent based on misdirected filtration common in degenerative diseases,[22-24] or into a cellular or mixed crescent, which are generally associated with inflammatory diseases.[25-27] The progression of both crescents may stop by evolving into an adherent segmental scar (synechia)—the

hallmark of segmental glomerulosclerosis. Conversely, a crescent may progress to global sclerosis and finally cause nephron degeneration and fibrosis.[26]

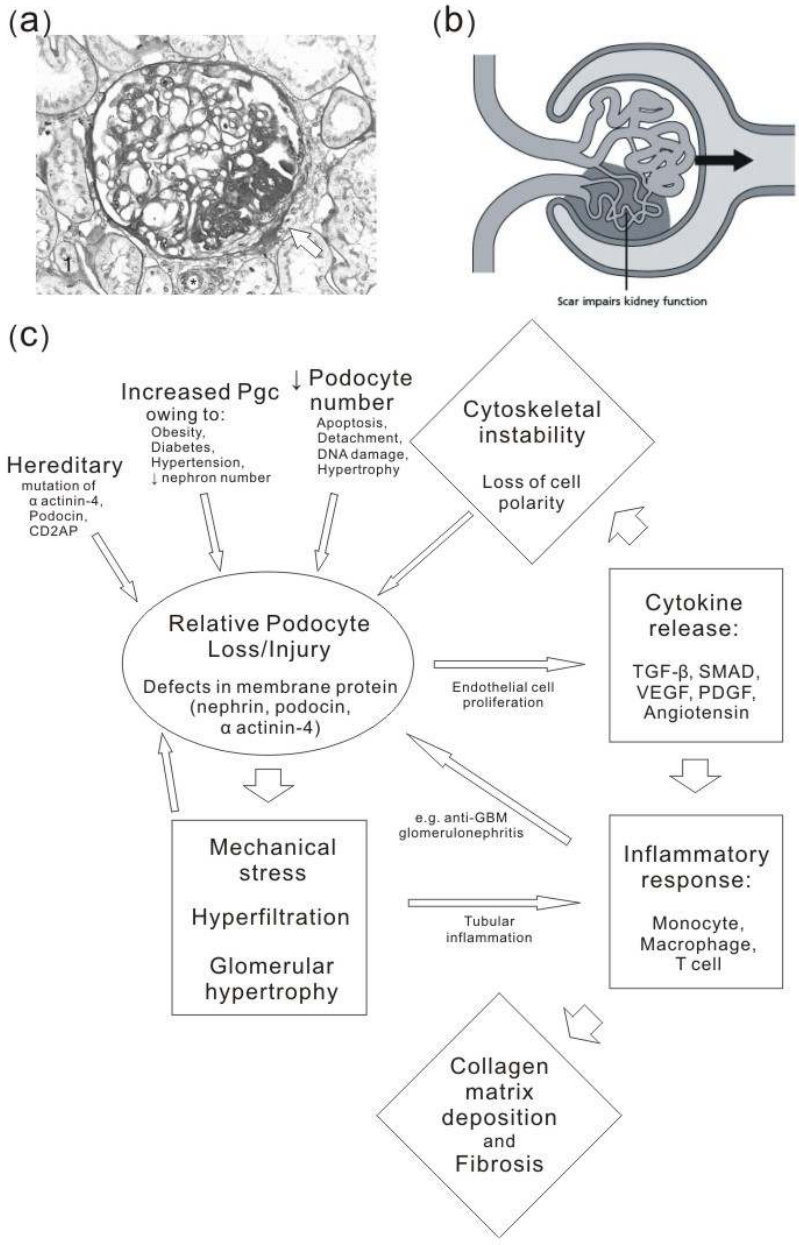

Fig. 1.4.1 Pathology, pathophysiology and factors involved in the progression of FSGS to ESRD **(a)** Typical features of classic form FSGS (periodic acid-Schiff stain): A segmental scar with an adhesion to Bowman's capsule (white arrow) and hyalinosis is present in the perihilar region of the glomerulus. Hilar arteriole (∗). **(b)** The sclerotic lesion (scar) is characterized by focally increased matrix within the glomerular tuft with obliteration of the glomerular capillary lumen. Intraglomerular scar impairs normal filtration function resulting in renal insufficiency. **(c)** Initial loss or injuries to podocytes (related to hereditary factors, increased glomerular pressure (Pgc), reduced podocyte numbers, defects in membrane proteins or cytoskeletal instability) leads to cytokine release, mechanical stress, hyperfiltration, and glomerular hypertrophy. These factors result in up-regulation of an inflammatory response. The end result is collagen matrix deposition, fibrosis and progression to ESRD. Modified from Shankland SJ Kidney Int. 2006; Reidy K and Kaskel FJ Pediatr Nephrol. 2007 and Chun *et al*. J Am Soc Nephrol. 2004.

1.4.3. Recent Findings for FSGS Pathogenesis

Strong mechanistic evidence indicating that podocyte depletion is the central mechanism in FSGS development has been established by targeting damage directly and specifically to podocytes; no study of FSGS-induced by damage targeted to parietal epithelial, endothelial or mesangial cells has been presented. The notion that the inability of podocytes to replicate cells is the initial cause of glomerular diseases dates to the early 1990s.[28;29] Detailed descriptive and correlative evidence has since been provided in numerous studies demonstrating that severe damage to podocytes follows a loss of podocytes, which underlies the development of classic FSGS.[26] Recently, two studies—a study of rats by Wiggins,[30] and a study of mice by Ichikawa[31-33]—clearly demonstrated that the degree of podocyte depletion predicts sclerosis severity. Both studies utilized transgenic rodents, and specifically addressed damage to podocytes. Notably, glomerulosclerosis in these rodent models did not start before the number of podocytes declined, and, thus, started after the onset of podocyte lesions and proteinuria.

1.4.4. Podocyte Cytoskeleton and FSGS

Gene mutations associated with podocyte development and function have taken center stage in hereditary glomerular diseases. Two basic groups of diseases can be identified: those with early onset, indicating that lesions have already occurred in fetal or neonatal life; and, those with late onset. Late onset diseases typically emerge predominantly due to impaired function of the podocyte cytoskeleton, whereas early onset diseases are rooted in severe structural deficiencies of various components (GBM and slit membrane) or defects in major signaling networks for development and maintenance.[34] Notably, α actinin-4 and synaptopodin are actin–associated proteins with specific relevance for actin bundling in podocytes. Mutations in the α actinin-4 gene in humans lead to an autosomal dominant form of familial late onset FSGS (see Introduction, Section 1.8 Alpha actinin-4).[35;36]

1.5. Renin-Angiotensin System

The renin-angiotensin system (RAS) has a significant homeostatic role in blood pressure regulation, water and salt balance, and tissue growth control under physiological conditions. Conversely, the involvement of the RAS in the pathophysiology of cardiovascular and renal diseases is supported by basic and clinical data. In particular, angiotensin II (Ang II), the biological effector of the RAS, can induce a number of relevant structural and functional abnormalities via activation of numerous cellular effects primarily mediated via Ang II binding with type 1 angiotensin (AT1) subtype receptors. Through the binding of Ang II with specific G protein–coupled receptors present on the cellular membranes of numerous tissues, Ang II is the terminal biological effector of the RAS and is responsible for important and diverse functions that have fundamental relevance in human physiology and pathology.[37;38]

1.5.1. Enzymatic Cascade of the RAS and Angiotensin II

The RAS is typically viewed as an enzymatic proteic cascade, which, through the generation of intermediate peptidic products, finally leads to production of Ang II, a small octapeptide. Ang II has a central role in regulation of cardiovascular homeostasis (Fig. 1.5.1). Acting on both the "content" and "container," Ang II regulates blood volume and vascular resistance. The wide spectrum of Ang II target tissues encompasses the adrenals, kidney, brain, pituitary gland, vascular smooth muscle, and sympathetic nervous system. Angiotensin is a blood-borne hormone that is produced by enzymatic cleavage of angiotensinogen and acts in circulation, and is formed in many tissues such as the brain, kidney, heart, and blood vessels. Thus, researchers have suggested that Ang II may also function as a paracrine and autocrine hormone that induces cell growth and proliferation and controls extracellular matrix formation.[39-41] Other angiotensin-derived metabolites, such as angiotensin 2–8 (Ang III), angiotensin 1–7, or angiotensin 3–8 (Ang IV), have biological activities (Fig. 1.5.1 b).[42-46]

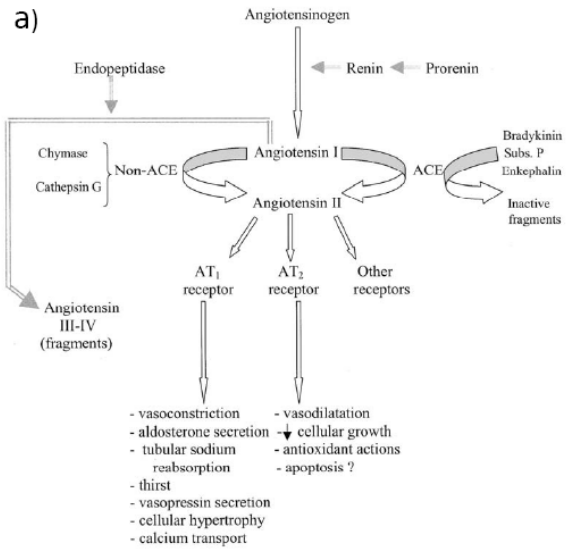

b)

Precursors and metabolites	1 2 3 4 5 6 7 8 9 10 11 12 13 14
Angiotensinogen	Asp-Arg-Val-Tyr-Ile-His-Pro-Phe-His-Leu-Leu-Val-Tyr-Ser
Ang I	Asp-Arg-Val-Tyr-Ile-His-Pro-Phe-His-Leu
Ang II	Asp-Arg-Val-Tyr-Ile-His-Pro-Phe
Ang III	Arg-Val-Tyr-Ile-His-Pro-Phe
Ang IV	Val-Tyr-Ile-His-Pro-Phe
Angiotensin 1-7	Asp-Arg-Val-Tyr-Ile-His-Pro

Fig. 1.5.1 Renin-angiotensin system (a) Diagram of the conventional renin-Ang II pathway with its receptors and general biological effects **(b)** Amino acid sequences of Ang II precursors and metabolites.

1.5.2. The Type 1 Angiotensin (AT1) Receptor

The human type 1 angiotensin (AT1) receptor contains 359 amino acids;[38] its sequence is reported in the SwissProt file under No. 30556 (P30556); the gene coding for the receptor (abbreviated as AGTR1) is located on chromosome 3q. Similarly, the structural coding for rat and mouse AT1 receptors is (rat) 359 amino acids, P29089, P25095 and (mouse) 359 amino acids, P29754, P29755 as two subtypes A and B exist in rats and mice located on chromosomes 17 and 2, and 13 and 3, respectively.

Figure 1.5.2 presents the secondary structure and consensus sequence of the mammalian angiotensin AT1 receptor. The amino acid sequence shown is based on derived sequences for five individual cloned mammalian AT1 receptors. The amino acid residues that are highly conserved among G protein-coupled receptors are indicated by bold letters. The positions of the three extracellular carbohydrate chains and two extracellular disulfide bonds are also indicated.

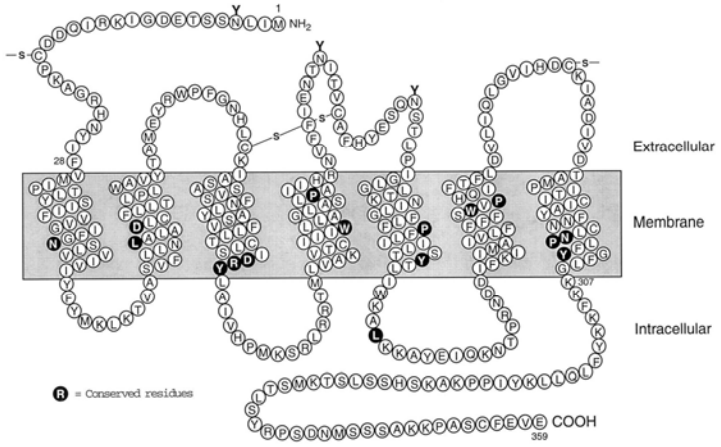

Fig. 1.5.2 Secondary structure and consensus sequence of the mammalian angiotensin AT1 receptor The amino acid sequence shown is based on derived sequences for five individual cloned mammalian AT1 receptors. The amino acid residues that are highly conserved among G protein-coupled receptors are indicated by bolded letters. The positions of the three extracellular carbohydrate chains, and two extracellular disulfide bonds are also indicated. de Gasparo *et al*. Pharmacol Rev. 2000

The AT1 receptor mediates all known physiological actions of Ang II in cardiovascular, renal, neuronal, endocrine, hepatic, and other target cells. These actions comprise regulation of arterial blood pressure, electrolyte and water balance, thirst, hormone secretion, and renal function. The AT1 receptor belongs to the G protein-coupled receptor (GPCR) superfamily and is predominantly coupled via pertussis toxin-insensitive G proteins to activate phospholipase C and calcium signaling. The AT1 receptors of several mammalian species have been cloned and their amino acid sequences identified from their respective cDNAs. Ang II binding to the AT1 receptor causes conformational change in the receptor molecule, thereby promoting the receptor's interaction with the G protein(s), which in turn mediates signal transduction via several plasma membrane effector systems. These systems include enzymes, such as phospholipase C, phospholipase D, phospholipase A2, and adenylyl cyclase, and ion channels such as L-type and T-type voltage-sensitive calcium channels. In addition to activating several intracellular signaling pathways that mediate agonist-induced phenotypic responses in various Ang II target cells, the agonist-occupied AT1 receptor undergoes desensitization and internalization in the same manner as many other GPCRs.

1.5.3. Renal Protective Effects of RAS Blockage

The RAS blockage with angiotensin-converting enzyme inhibitors (ACEIs) or AT1R antagonists (AT1RBs) were primarily conceived for treating hypertension. Reduction of Ang II levels by ACEIs or AT1RBs is renoprotective in human glomerular diseases, especially in diabetic nephropathy.[47-49] The RAS blockage decreases proteinuria and moderates reduction in glomerular filtration rate in human diseases and experimental animal models.[50-54] The beneficial anti-proteinuric effects of ACEIs and AT1RBs have been partially explained by their hemodynamic effects on the glomerulus. Nevertheless, increasing clinical and experimental data demonstrate that Ang II targets influence and damage podocytes directly and specifically.

1.5.4. The AT1 Receptors in Podocytes

Within the glomerulus, Ang II was thought to influence preferentially mesangial cell function. However, experimental and clinical data has indicated that AT1RBs ameliorate glomerular function, and, in contrast to other antihypertensive agents, decrease podocyte hypertrophy in rat kidneys following subtotal nephrectomy,[55] implying that podocyte morphology can be directly impacted by Ang II. In literatures, convincing evidence indicates that Ang II directly regulates podocyte function.[49;56;57] It has been demonstrated that Ang II depolarized podocytes *ex vivo* with a patch clamp technique of isolate intact rat glomerulus.[58] Fluorescence measurements with a laser scanning microscope indicated that podocytes in glomerulus responded to Ang II with a reversible increase of intracellular calcium.[59] Moreover, podocyte-specific overexpression of AT1R is suggestive of considerable involvement when the RAS in FSGS development is due to hypertension.[60] Rats (Neph-hAT1 transgenic rats (TGRs)) with podocyte-specific enhanced AT1–mediated signaling developed proteinuria and glomerular damage that progressed to FSGS mimicking the structural details identified in hypertensive models of FSGS development.[61] These studies support a conclusion that beneficial effects of ACEIs or AT1RBs slow progression of chronic disease—in addition to their beneficial effects in lowering blood pressure—stem from

prevention of increased AT1R signaling in podocytes.

1.6. Rac-1

The mammalian Rho guanosine-5'-triphosphate hydrolase (GTPase) family currently consists of seven distinct proteins: Rho (A, B, and C isoforms), Rac (1 and 2 isoforms), Cdc42 (Cdc42Hs and G25K isoforms), RhoD, RhoG, RhoE, and TC10. Like other members of the Ras superfamily, Rho proteins act as molecular switches that control cellular processes by cycling between active GTP-bound and inactive GDP-bound states.

During cell migration, Rho family GTPases organize the actin cytoskeleton in all eukaryotic cells.[62] Activation of Rho in fibroblasts causes bundling of actin filaments into stress fibers, and clustering of integrins and associated proteins into focal adhesion complexes; activation of Rac promotes *de novo* actin polymerization at the cell periphery to form lamellipodia extensions and membrane ruffles; activation of Cdc42 triggers actin polymerization to form filopodia or microspikes (Fig. 1.6). Considerable crosstalk exists within and between Ras and Rho GTPase families. Activation of Cdc42 results in localized activation of Rac, and, hence, filopodia are closely associated with lamellipodia; in fact, in these cells, identifying filopodia unless Rac activity is first inhibited is difficult. Quiescent Swiss cells have no detectable stress fiber, and activation of Rac under these conditions results in a weak and delayed activation of Rho, thereby producing only a few weak stress fibers. However, activation of Rac in cells growing in serum, which already have very pronounced and abundant stress fibers, results in a loss of stress fibers.

Notably, Rac-1 exhibits a ubiquitous expression pattern and is a crucial component of Nicotinamide adenine dinucleotide phosphate (NADPH) oxidase, which mediates Ang II–induced ROS production.[63-65] Furthermore, very recent experimental data demonstrate that Rho GTPases (RhoA and Rac) have different involvements in cytoskeletal effects of Ang II in rat adrenal glomerulosa cells.[66] This work investigates

the effects of Rac-1 on podocyte cytoskeletons in AT1R signaling.

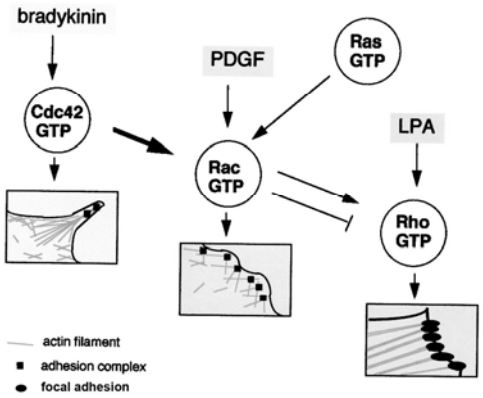

Fig. 1.6 The activation of Rho, Rac, and Cdc42 by extracellular agonists induces changes to actin cytoskeletons and cell-matrix interaction In these cells, lysophosphatidic acid (LPA, a major constituent of tissue culture serum) activates Rho, leading to assembly of actin-myosin stress fibers and associated integrin adhesion complexes (focal adhesions). Notably, Rac can be activated by Platelet-derived growth factor (PDGF) or by insulin, thus leading to actin polymerization at the cell periphery, causing lamellipodia extensions and membrane ruffling activity. Lamellipodia, also associated with integrin adhesion complexes, contain many of the same constituents as classical focal adhesions, but are markedly smaller. Lamellipodia are not required for actin polymerization, but may be required for cell movement. Bradykinin induces Cdc42 in these cells to generate filopodia or microspikes and associated integrin complexes. Mackey *et al*. J Biol Chem. 1998

1.7. Ezrin/radixin/moesin ERM proteins

Ezrin, discovered 20 years ago, is a major component of the microvillus cytoskeleton and the chicken intestinal cell brush border.[67] Recent studies determined that ezrin together with radixin and moesin[68;69] define a family of closely related proteins (ezrin, radixin and moesin (ERM) proteins) that can potentially link actin microfilaments to the plasma membrane. Since this pioneering work, ERM proteins have been implicated in myriad cellular functions, ranging from regulation of cell extension to polarity, migration and growth.[70]

Understanding the functions of ERM proteins has become important to human health as ezrin is now recognized as a primary regulator of tumor metastasis.[71;72] Initial attempts to inactivate ERM proteins in cultured cells utilized antisense nucleotides or

laser-assisted inactivation methods, and demonstrated that ERM proteins are involved in control of cell shape and adhesive characteristics.[73;74]

The ERM proteins have three structural domains: the N-terminal domain (major functional domains, N-ERMAD); a coiled midregion; and, the C-terminal domain (C-ERMAD). The N-ERMAD domain of ERM protein interacts with an increasing number of integral membrane proteins, such as I-Cam, CD44, CD43 and Nhe3.[70] Additionally, the N-ERMAD domain interacts with adaptor proteins (EBP50 or NHE-RF,[75] and NHE type 3 kinase A regulatory protein (E3KARP)[70]) and is involved in signal transduction. The C-ERMAD domain of the ERM protein binds to actin filaments.

Furthermore, the N- and C-ERMAD domains, which are connected by a flexible α-helical region, are also capable of intramolecular interaction.[76] As this N-ERMAD–C-ERMAD interaction masks the two regions involved in binding to membrane proteins and F-actin,[77;78] this hairpin-like intramolecular interaction results in a closed or dormant configuration of ERM proteins. The ERM proteins therefore must be activated to generate an open conformation,[79] enabling these proteins to interact with their heterotypic partners (Fig. 1.7). Although the mechanism is not fully understood, activation of ERM proteins involves both binding of phosphatidylinositol (4,5)-bisphosphate [PtdIns(4,5)P2] to N-ERMAD domain,[80;81] and phosphorylation of a threonine residue of the F-actin-binding domain, which is located at the C terminus.[82]

Ezrin has recently been identified as a part of podocyte actin cytoskeleton, and little is known about its functional characteristics.[83-85] As mentioned, small GTP-binding proteins of the Rho family integrate extracellular signals from diverse receptor types and initiate rearrangements of F-actin. Activation of Rho GTPases induces actin polymerization by increasing the availability of actin filament barbed ends. However, the induced spatial pattern of F-actin depends on associated actin-binding proteins or cross-linking proteins such as ezrin and α actinin-4 (see Introduction, Section 1.8

Alpha actinin-4). This study investigates the factors that regulate these processes, and how these factors may in turn respond to messages from the Rho family GTPases.

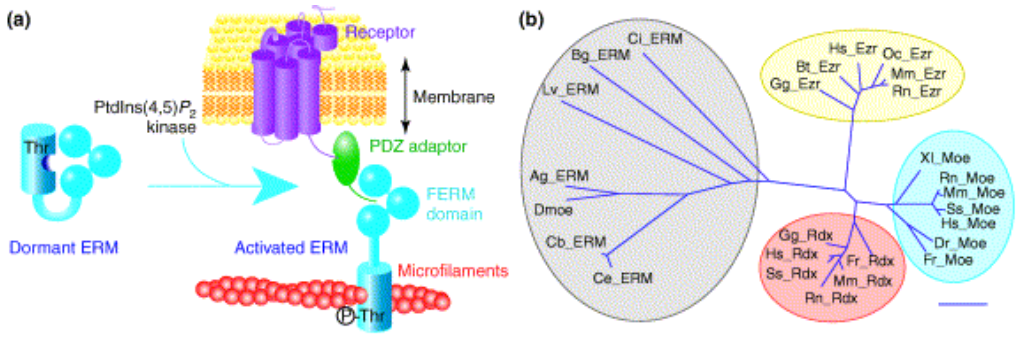

Fig. 1.7 Schematic representation of ERM protein structures and activation The intramolecular interaction between N-ERMAD (FERM) and C-ERMAD (cylinder) keeps ERM proteins in a dormant configuration in cytoplasm. Upon activation via binding of phosphatidylinositol (4,5)-bisphosphate [PtdIns(4,5)P_2] and phosphorylation of a conserved threonine residue of C-ERMAD, ERM proteins switch to an open configuration unmasking protein-binding regions. The FERM domain binds directly, or through a PDZ adaptor, to membrane proteins, whereas the C-terminal region of ERM proteins binds to actin filaments. Polesello *et al.* Trends Cell Biol. 2004

1.8. Alpha actinin-4

Alpha actinin is a ubiquitously expressed protein that is regarded as the ancestral molecule within a family of actin-binding proteins that includes spectrin, dystrophin, and utrophin, each of which regulates the organization of the actin cytoskeleton in a cell-type-specific manner.[86] The α actinin is a rod-shaped antiparallel dimer of two 100-kDa monomers; this configuration positions its actin-binding calponin homology (CH) motifs at either end of the rigid rod, an arrangement that allows α actinin to efficiently cross-link actin filaments into tight bundles.[87;88]

In skeletal and cardiac muscle, α actinin is found in the Z disk, where it cross-links antiparallel actin filaments from adjacent sarcomeres (Fig. 1.8a). Interactions between α actinin and titin likely play a role in controlling Z disk assembly.[89;90] In nonmuscle cells, α actinin is a ubiquitously expressed cytoskeletal protein and cross-links actin

filaments at sites of cell-cell (adhesion junctions) and cell-matrix (focal adhesion) junctions (Fig. 1.8 b), and at the leading edges (focal complex) of cell membranes of migrating cells.

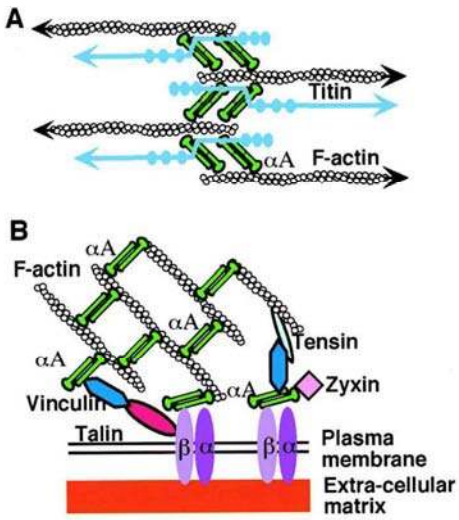

Fig. 1.8 Function of α actinin in the sarcomeric Z disk and in focal contacts (a) In the muscle Z disk, α actinin cross-links antiparallel actin filaments from adjacent sarcomeres. Titin acts as a molecular ruler for sarcomere and interacts with two different parts of α actinin, at the center of the α actinin rod and with the calmodulin-like domain. **(b)** A simplified representation of a focal contact displaying α actinin linking the actin cytoskeleton to membrane-associated structures. Focal contacts are points where cultured cells are attached tightly to the extracellular matrix via transmembrane receptors such as integrins (α and β). α actinin has been shown to interact with β integrins and with focal contact components vinculin and zyxin. Thus, α actinin may connect integrins to actin filaments either directly or indirectly. Djinović-Carugo *et al.* Cell 1999 (αA: α actinin)

In podocytes, α actinin-4 is encoded by the FSGS gene ACTN4,[35] which serves as an actin-binding and cross-linking protein localized to podocytes in the renal glomerulus, predominantly in FPs. *In vitro*, FSGS-associated mutations increase the strength of α actinin-4 binding to actin filaments.[91] The same effect can be expected *in vivo*, and results in alteration of glomerular podocyte mechanical characteristics. Recently, a experimental study showed that α actinin-4 null mice have severe glomerular disease,[91] and α actinin-4 is required for normal podocyte adhesion.[92]

Little is known about the effects of α actinin-4 on Ang II–related actin cytoskeletal change in podocytes. This work examined the function of α actinin-4 in AT1R signaling and the associated mechanisms leading to FSGS in Neph-hAT1 TGRs.

1.9. Nephrin

Nephrin, the product of the gene NPHS1 mutated in congenital nephrotic syndrome (NS) of the Finnish type (CNF), was the first podocyte protein identified by research into hereditary NS. Notably, CNF is common in Finnish people and has also been identified in various ethnic groups wourldwide.[93] CNF develops *in utero* causing premature infants with low birth weights for their age. Severe NS is frequently present at birth and resistant to steroids and immunosuppressive drugs.[93;94] Before the development of adequate treatments, patients typically died of various complications within the first 6 months of life.[94]

Using the positional cloning, Kestilä *et al*. identified a new gene on chromosome 19 called NPHS1 that is mutated in CNF.[95] Nephrin, the gene product, is a transmembrane protein of the Ig family of cell adhesion molecules that is located at the podocyte SD.[96] Inactivation of Nphs1 in mice results in massive proteinuria, effacement of podocyte FPs, absence of SDs, and neonatal death.[97] These effects suggest that nephrin is a primary component of the glomerular filter. Protein tomography data from the Tryggvason group suggest that nephrin molecules from adjacent podocytes connect via their Ig-like extracellular domains and form zipper-like structures, according to the SD model developed by Rodewald and Karnovsky (Fig. 1.9).[98]

Unlike α actinin-4, which links actin filaments to the GBM in focal contacts (the basal membrane domain) and cross-links the parallel actin bundles in the apical membrane domain of the podocyte FPs, nephrin connects the SD to the actin cytoskeleton in FPs.[99;100] The SD is formed by extracellular domains of specific transmembrane proteins, such as nephrin, Neph proteins, and two large cadherins, FAT1 and FAT2. Intracellularly, proteins important to podocyte structure—ZO-1, podocin, and CD2AP—are located in the SD region and are believed to play a role in connection of the SD to actin microfilaments.[101]

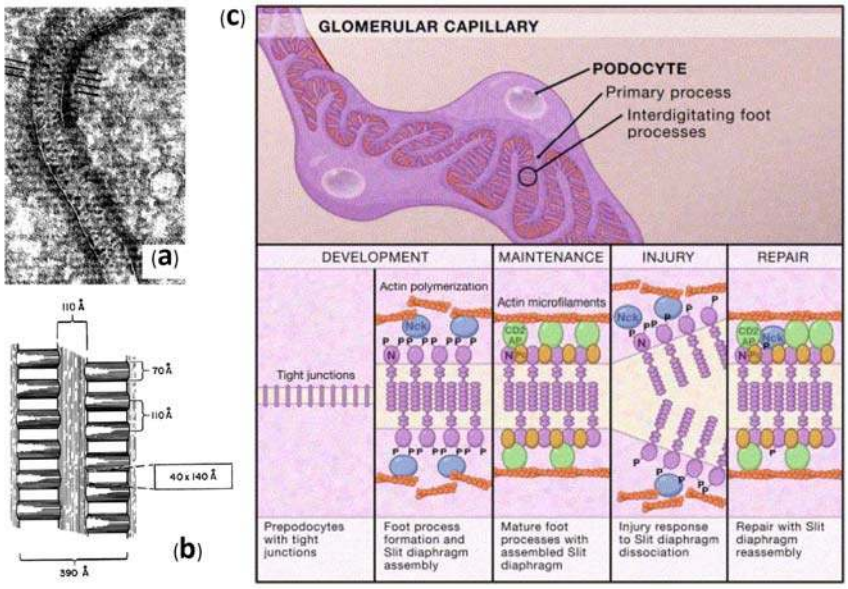

Fig. 1.9 Nephrin and slit diaphragm (a) and **(b)** The slit diaphragm (SD) structure proposed by Rodewald and Karnovsky in 1974. A central filament is connected to the podocyte membranes by alternating bridge fibers. This view is in the direction of filtrate flow. **(c)** (Top panel) Podocytes cover the outside wall of glomerular capillaries and extend primary processes attached to the surface of the glomerular basement membrane. Secondary FPs extend from the primary processes to interdigitate with FPs of a neighboring podocyte. The slit between the FPs contains a thin porous filter called the SD. (Bottom panel) Prior to formation of FPs and the SD, prepodocytes covering glomerular capillaries are connected via tight junctions. During formation of FPs, nephrin (N) becomes phosphorylated (P), likely upon contact with its extracellular ligand, resulting in recruitment of Nck adaptor proteins and induction of actin polymerization. Once the SD is assembled, the nephrin molecules are dephosphorylated and nephrin is connected to actin through CD2AP, podocin (Pc), and possibly other proteins. Following injury to the SD, which leads to FP effacement and proteinuria, nephrin molecules become clustered, thereby inducing their phosphorylation, Nck association, and actin polymerization. Finally, upon injury repair, nephrin molecules are dephosphorylated and the SD-actin filament complex is restored as in normal mature FPs. Modified from Rodewald R and Karnovsky MJ J. Cell Biol. 1974 and Tryggvason *et al*. Cell 2006

One important question is whether cytoskeletal dysregulation of podocytes has pathological consequences for the structure/function of the SD and filtration barrier? This study therefore analyzes the impact of AT1R signaling on nephrin.

1.10. Peroxiredoxin 2

Organisms living under aerobic conditions develop various anti-oxidative mechanisms for protection from damage by reactive oxygen species (ROS) such as hydrogen peroxide and superoxide.[102] A novel family of antioxidative proteins, peroxiredoxin (Prx), was identified 20 years ago and currently comprises six members in

mammals.[103-105] Prxs share a common reactive cystine residue in the N-terminal region, and serve as a peroxidase and involve thioredoxin and/or glutathione as the electron donor. Prxs protect against oxidative damage in cells via their peroxidase activity ($ROOH + 2e^- \rightarrow ROH + H_2O$), whereby hydrogen peroxide, peroxynitrite and numerous organic hydroperoxides (ROOH) are reduced and detoxified. (Fig. 1.10)

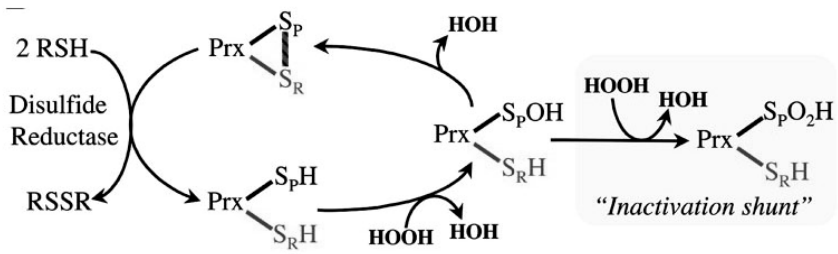

Fig. 1.10 The catalytic cycle of 2-Cys peroxiredoxin (Prx) Peroxidatic cysteine is depicted as a thiol (S_PH), sulfenic acid (S_POH), sulfinic acid (S_PO_2H), or in a disulfide with resolving cysteine (S_RH). Colors differentiate the cysteines from different dimer subunits, and the striped bar is the intersubunit disulfide bond. The disulfide reductase varies with organisms, typically a thioredoxin or flavoenzyme containing a thioredoxin-like domain. Wood *et al*. Science 2003.

Among the six isoforms (Table 1.10), Prx1 to Prx4 have an additional cystine residue in the conserved C-terminal region, and are cross members as determined by amino acid sequence similarity. Notably, Prx5 also contains an additional cystine in its C-terminal region, which is less conserved than that of Prx1–4. Conversely, Prx6 has only 1 unique cystine. These Prx family members are distributed in cytosol, mitochondria, peroxisome and plasma, all of which are potential sites of ROS production. In addition to their roles as a peroxidase, however, a growing body of evidence suggests that individual family members also have different functions associated with various biological processes such as detoxification of oxidants, cell proliferation, differentiation and gene expression.

Prx subtype	PrxI (2-Cys)	PrxII (2-Cys)	PrxIII (2-Cys)	PrxIV (2-Cys)	PrxV (atypical 2-Cys)	PrxVI (1-Cys)
Previous nomenclature	TPx-A NKEF A MSP23 OSF-3 HBP23 PAG	TPx-B NKEF B PRP Calpromotin Torin Band-8 TSA	AOP-1 SP22 MER5	AOE372 TRANK	AOEB166 PMP20 AOPP	ORF06 LTW4 AOP2
Polypeptide length	199 aa	198 aa	256 aa (cleaved at 63–64)[a]	271 aa (cleaved at 36–37)[a]	214 aa (cleaved at 52–53)[a]	224 aa
Human chromosomal location	1q34.1	13q12	10q25–q26	10p22.13	11q13	1q23.3
Cellular location	Cytosol, nucleus	Cytosol, membrane	Mitochondria	Cytosol, Golgi, secreted	Mitochondria, peroxisome, cytosol	Cytosol
Genbank	AAA50464	AAA50465	BAA08389	AAB95175	AAF03750	BAA03496
SwissProt	tdx2_human P35703	tdx1_human P32119	tdxm_human P30048	tdxn_human Q13162	aopp_human P30044	aop2_human P30041
Interactions with proteins and other ligands	c-Abl Presenilin-1 Heme Macrophage migration inhibitory factor Cyclophilin	Protein 7.2b (stomatin) Presenilin-1 Erythrocyte membrane Cyclophilin	Cyclophilin Abrin A-chain	Heparin Cyclophilin	DNA Cyclophilin	Cyclophilin

Abbreviation: aa, amino acids.
[a]These proteins are post-translationally processed.

Table 1.10 Six isoforms of the peroxiredoxin family Peroxiredoxins (Prxs) are divided into three classes: typical 2-Cys Prxs; atypical 2-Cys Prxs; and 1-Cys Prxs. Although varying in cellular location and interacting protein partners, all Prxs share the same basic catalytic mechanism. Wood et al. Trends Biochem Sci. 2003

Recent experimental data suggest that Prxs regulate peroxide-mediated signaling cascades. *In vivo*, Prxs are required for Myc-mediated transformation and apoptosis,[106] can regulate NF-κB activation,[107;108] and their overexpression can decrease intracellular hydrogen peroxide generated in response to tumor necrosis factor-α, p53, epidermal growth factor, and thyrotropin.[109;110] Additionally, overexpression of Prxs is common in several cancers and is correlated with resistance to apoptosis induced by radiation therapy or the anticancer drug cisplatin.[111;112] However, the function of Prx2 in podocytes has never been investigated.

1.11. Principal Objectives of this Work

Little is known about the signaling mechanisms of AT1R in podocytes, particularly because no reliable cultured podocyte model functionally expressing AT1R exists. Furthermore, the mechanisms resulting in dynamic change of the actin cytoskeleton in podocytes are poorly understood. This study therefore investigates the mechanisms of Ang II–mediated regulation of actin cytoskeletal organization in podocytes and has the following aims.

- Establishing a stable Ang II-responsive podocyte cell line
- Identify effectors and effects of AT1R signaling in cultured podocytes
- Functional characterization of AT1R signaling in podocytes
- Confirm signal mechanisms *in vivo* — in Neph-hAT1 TGRs
- Proteomic analysis of AT1R-activated cultured podocytes
- Lose of function studies—SiRNA technique in cultured podocytes

2. Materials

2.1. Equipment

Equipment Name	Type and Number	Supplier
Autoclave	Varioklav	H+P Labortechnik GmbH
Bioluminescence detecting system	Lumat LB9501	Berthold
Bacterial culture incubator	B5050	Heraeus
Bacterial incubator shaker	Certomat® IS	B.Braun Biotech International
Chemiluminescent signal analyzer	Lumi-Imager F1	Roche
Centrifuges	Mikro 200 R Allegra ™ X-22R Multifuge 3S-R	Hettich Beckman Heraeus
Cell culture incubator	Heracell 240	Heraeus
Digital electronic balance	Scout™Pro Explorer®Pro	OHAUS
DIGE fluorescent gel image system	Typhoon 9200	GE Healthcare
Electroporesis apparatus (vertical)	Criterion® 3 Cell	Bio-Rad
Electroporesis apparatus (PAA gel)	Novex Mini-Cell	Invitrogen
Electroporesis apparatus (agarose gel)	Model B1	Peqlab Biotechnologie GmbH
Film developer	Optimax X-Ray Film Processor	PROTEC Medizintechnik

Equipment Name	Type and Number	Supplier
Isoelectric Focusing Cell	PROTEAN IEF cell	Bio-Rad
Lamina flow hood for cell culture	HERAsafe	Heraeus
Luminance detector	Lumat LB9501	Berthold GmbH
Microscope for immunoflurescence	AXIOVERT 100	Zeiss
Microscope for life cell imaging	AXIOVERT 25	Zeiss
Microscope for intracellular calcium measurement	AXIOVERT 125	Zeiss
PCR thermal cyclers	GeneAmp® PCR-System 2700	Applied Biosystems
pH-meter	RS-232-C	Schott
Photometer	Smart Spec ™	Bio-Rad
Power supply for blotting and electrophoresis	Power Pac HC™	Bio-Rad
Thermomixer	Comfort	Eppendorf
Ultra pure water system	Ultra Clear	SG Wasseraufbereitung und Regenerierstation GmbH
UV transilluminator	IL-200-M	H. Saur Laborbedarf D-Reutlingen
Video camera	XC-ST70C	Hamatsu/Sony
Vortexer	VortexGenie2	Scientific Industries, Inc. N.Y. USA
Western-Blot apparatus	Semidry Transfercell	Bio-Rad

2.2. Chemicals and Laboratory Requirements

Material Name	Brand/Supplier
1 kb DNA ladder	Promega
100 bp DNA ladder	Promega
2-Propanol	Roth
6 x Loading Dye Solution	MBI Fermentas
β-Mercaptoethanol (β-ME)	Sigma-Aldrich
Acetic acid	Roth
Agarose	Roth
Ammonium Chloride	Roth
Ammonium Persulfate (APS)	Sigma-Aldrich
Bio-Lyte 3/10 Ampholyte, 100x	Bio-Rad
Bromphenolblue	Bio-Rad
Calcium Chloride	Sigma-Aldrich
Calcium gluconate	Sigma-Aldrich
Calphostin C (Pan PKC inhibitor)	Calbiochem
Coomassie brilliant blue R-250	Sigma-Aldrich
CHAPS	Sigma-Aldrich
Crystal Clear Mounting Medium	Sigma-Aldrich
D-glucose monohydrate	AppliChem
Dimethyl sulfoxide (DMSO)	Sigma-Aldrich
Dithio-1,4-threitol (DTT)	Sigma-Aldrich
Dimethylthiourea (DMTU)	Sigma-Aldrich
Ethanol	Roth

Material Name	Brand/Supplier
Ethidium bromide	AppliChem
Ethylenediamine tetraacetic acid (EDTA)	Omnilab
Ethylene glycol tetraacetic acid (EGTA)	Sigma-Aldrich
Fura-2-acetomethyl ester	Molecular Probe
Geniticin (G418)	PAA
Glycerin (Glycerol)	Roth
Glycin	Roth
HCl (37 %)	Roth
Hydrogen Peroxide (H_2O_2) 30 %	Sigma-Aldrich
Iodoacetamide	Sigma-Aldrich
KH_2PO_4, potassium dihydrogen phosphate	Sigma-Aldrich
K_2HPO_4, dipotassium phosphate	Sigma-Aldrich
LB-Broth Powder	Sigma-Aldrich
Lucigenin	Sigma-Aldrich
Losartan (AT1R specific antagonist)	Merck & Co.
Magnesium Chloride	Sigma-Aldrich
Methanol	Roth
N, N, N´, N´-Tetramethylendiamin (TEMED)	Fluka
NaCl, sodium chloride	Fluka
NaH_2PO_4, sodium dihydrogen phosphate	Fluka
NaDS, sodium dodecyl sulfate (SDS)	AppliChem
NaF, sodium fluoride	Sigma-Aldrich
Na_3VO_4, sodium orthovanadate	Sigma-Aldrich
Paraformaldehyde (PFA)	Fluka

Material Name	Brand/Supplier
PD123319 (AT2R specific antagonist)	Sigma-Aldrich
PEG 4000	Roth
PMSF	AppliChem
Ponceau S solution	Sigma-Aldrich
Polybrene	Sigma-Aldrich
Polyester seiving net, Ø100 µm und Ø51 µm	Reichelt Chemietechnik, Heidelberg
Precision Plus Protein Dual Colour Standard	BioRad
SB203580 (p38 MAPK inhibitor)	Calbiochem
SCH51344 (Rac specific inhibitor)	Calbiochem
Tris(hydroxymethyl)aminomethan (Tris, Trizma® Base)	Sigma-Aldrich
Triton® X-100	Sigma-Aldrich
Thiourea	Sigma-Aldrich
Trypsin	GE Healthcare
Urea	Sigma-Aldrich
Xanthine and xanthine oxidase	Sigma-Aldrich
Y27632 (Rho kinase specific inhibitor)	Calbiochem

2.3. Buffers and Solutions

Solution Name	Contents and Supplier
1 x PBS	*Dulbecco´s Phosphate buffered Saline* with or without Ca^{2+} & Mg^{2+}, PAA

Solution Name	Contents and Supplier
2 x HEBS	HEPES acid 10 g, NaCl 16 g, KCl 0.74 g, Na_2HPO_4 x H_2O 0.25 g, glucose 2 g, 10 ml 10x PBS, add H_2O to 1 litre, adjust pH to 7.05, sterile by filtering and stored in -20°C
2DE lysis buffer	7 M Urea, 2 M Thiourea, 4% CHAPS, and 30 mM Tris)
2DE 2X sample buffer	7 M urea, 2 M Thiourea, 4% CHAPS, 100 mM dithiothreitol (DTT) and 8% IPG buffer (Bio-Lyte 3-10)
2DE equilibrating buffer I	37.5 mM Tris-HCl (pH 8.8), 6 M urea, 20% glycerol, 2% SDS, and 1% DTT
2DE equilibrating buffer II	37.5 mM Tris-HCl (pH 8.8), 6 M urea, 20% glycerol, 2% SDS, 0.002% bromophenol blue, and 2.5% iodoacetamide
Acrylamide solution	40 % acrylamide/bis-acrylamide Solution, Bio-Rad, 4°C
Calcium Chloride solution	0.25 M
Column buffer	200 mM NaCl, 20 mM Tris/HCl [pH 7.4], 1 mM EDTA, 4°C
Collagen A	1 mg/ml Biochrom, 4°C
Coomassie ready-use solution	Coomassie stock solution with H_2O 1:10 dilution
Coomassie stock solution	0.6 % (w/v) Coomassie *brilliant blue*, 10 % acetic acid in H_2O
Coomassie gel destaining solution (*Destaining Solution*)	5-20 % methanol, 7 % acetic acid in H_2O
KREBS solution	99 mM NaCl, 4.7 mM KCl, 1.8 mM $CaCl_2$, 1.2 mM $MgCl_2$, 25 mM $NaHCO_3$, 1.03 mM K_2HPO_4, 20 mM Na-HEPES, and 11.1 mM glucose (pH 7.35]

Solution Name	Contents and Supplier
Fixing Solution for Coomassie	25 % isopropanol, 10 % acetic acid in H_2O
Fixing Solution for SyproRuby	10 % methanol, 7 % acetic acid in H_2O
Hepes 1M	PAA, 4°C (long-term storage -20°C)
Interferon γ	Roche, -20°C
IP-buffer ready-use solution	IP-buffer stock solution + 0.25 mM PMSF (in EtOH) + 5 mM Na_3VO_4, fresh make before use
IP-buffer stock solution	1 % Triton X-100, 20 mM Tris/HCl [pH 7.5], 25 mM NaCl, 50 mM NaF, 15 mM EDTA, 4°C
KERBS solution	99 mM NaCl, 4.7 mM KCl, 1.8 mM $CaCl_2$, 1.2 mM $MgCl_2$, 25 mM $NaHCO_3$, 1.03 mM K_2HPO_4, 20 mM Na-HEPES, and 11.1 mM glucose [pH 7.35]
Laemmli-sample buffer 2 x	20 % (v/v) glycerol, 125 mM Tris/HCl [pH 6.8], 10 % (w/v) SDS, 0.2 % (w/v) Bromphenolblue, 5 % (v/v) β-ME in H_2O, -20°C
Na_3VO_4 (Tyrosine-Phosphatase-Inhibitor)	100 mM stock solution, Sigma , -20°C
Paraformaldehyde,(PFA	2 % (w/v) Paraformaldehyde, 4% (w/v) Saccharose in 1x PBS, -20°C
Phenylmethanesulphonylfluoride, PMSF	10mg/ml PMSF in EtOH stock solution, AppliChem, -20°C
Protein-electrophoresis (PAGE) buffer 10x, (10x *Running buffer*)	2 M glycine, 0.5% (w/v) SDS, 250 mM Tris-Base
Ringer solution	145 mM NaCl, 1.6 mM K_2HPO_4; 0.4 mM KH_2PO_4; 5 mM D-glucose; 1 mM $MgCl_2$; 1.3 mM Ca^{2+}-gluconate (pH 7.4)
STET-buffer	8 % (w/v) Saccharose, 50mM EDTA, 5 % (v/v) TritonX-100, 50 mM Tris/HCl [pH 8]

Solution Name	Contents and Supplier
TAE-buffer	AppliChem
TBS-T (Tris-buffered Saline + Tween)	10 mM Tris [pH 7.4], 0.05 % Tween-20, 150 mM NaCl
TE Buffer	10 mM Tris [pH 8.0], 1 mM EDTA
Transfer-buffer 10x	144 g glycine, 30 g Tris-base, add H_2O to1 liter
Transfer-buffer 1x	1/10 10x Transfer-buffer, 10-20% methanol, add H_2O to 1 liter
Trypsin-EDTA	PAA, ready to use solution stored in 4°C, long-term storage in -20°C

2.4. Medium

Unless otherwise stated, sterile medium are stored at 4°C.

2.4.1. Medium for Bacterial Culture

2.4.2. LB Medium (Luria-Bertani Medium)

Per liter:

To 950 ml of deionized water, add

trypton	10g
yeast extract	5g
NaCl	10g

The solutes were shaken until they dissolved. The pH was adjusted to 7.0 with 5 N NaOH. Solution volume was adjusted to 1 liter with deionized water. Solution was sterilized by autoclaving for 20 min at 15 psi (1.05 Kg/cm^2) on the liquid cycle.

For antibiotic resistant selection, 100 µg/ml Ampicillin or 35 µg/ml Kanamycin were added. Agar plates with LB medium were made by adding an additional 20 g/l agarose.

2.4.2.1. SOB Medium

Per liter:

To 950 ml of deionized water, add

trypton	10g
yeast extract	5g
NaCl	10g

Solutes were shaken until dissolved; 10 ml 250 nM solution of KCl was then added. Medium pH was adjusted to 7.0 with 5 N NaOH, and solution volume was adjusted to 1 liter with deionized water. Solution was sterilized by autoclaving for 20 min at 15 psi (1.05 Kg/cm^2) on the liquid cycle. Just prior to use, 5 ml 2 M $MgCl_2$ was added to solution.

2.4.2.2. SOC Medium

After the SOB medium was autoclaved, it was allowed to cool to 60°C or less, and 20 ml sterile 1 M solution of glucose was added.

2.4.3. Medium for Eukaryotic Cell Culture

Cell Type	Content and Supplier
Mouse podocyte (PCLs)	RPMI 1640 (PAA) + 5 % FCS (+ 75-300 mg/L Geniticin 418 for transducted cells selection) Cultivated in 33°C: + 10 U/ml γ-Interferon
Human podocytes (AB8)	RPMI 1640 (PAA) + 5 % FCS + 0.8 % *Supplements*
Supplements	0.1 % non-essential aminoacids(Bio Whittaker) 100 µM Sodium pyruvate 10 µg/ml Insulin-Transferrin-Natrium-Selenit (Roche) 5 mM HEPES
FCS	BioChrom AG

Cell Type	Content and Supplier
HEK 293T cells	DMEM (+L-Glutamin+high Glucose 4.5 g/l) PAA + 10 % FCS (or CS/Fe)
Type I collagen	#C3867, Sigma-Aldrich, 4°C

2.5. Consumptive Materials and Commercial Kits

Material Name	Supplier
Advanced Protein Assay™ agents	Cytoskeleton
Alexa Fluor® 594 Phalloidin	Molecular Probes
Alexa Fluor® 488/594 conjugated secondary antibodies	Molecular Probes
Bacterial culture dish / sterile inoculation loop	Sarstedt
BigDye Terminator v1.1 / 3.1 Sequencing Buffer(5x)	Applied Biosystems
Blotting paper	Schleicher & Schüll
Complete protease inhibitor	Roche
Cell / tissue culture dish / flask	Greiner
Cy2,Cy3,Cy5-CyDye DIGE Fluor minimal dyes	GE Healthcare
Coverslides / slide for microscope	VWR
DAPI (4'-6-Diamidino-2-phenylindole)	Molecular Probes
ECL-Film	FUJIFILM Super RX
Flexi-Strip Schaber	BiWeX, Tilburg Holland
LumiLight (chemoluminescencent substrate)	Roche Diagnostics
M2 (anti-Flag antibody-conjugated) beads	Sigma-Aldrich
oligo(dT) primer	Promega
Pipettenspitzen	Sarstedt

Material Name	Supplier
Plasmid Miniprepkit, Wizard® Plus SV Minipreps	Promega
Protein G–sepharose beads	Amersham Biosciences
PureLinkHiPure Plasmid Filter Maxiprep Kit	Invitrogen
PVDF-Immobilon Membrane (0.45µm)	Millipore
QIAquick Gel Extraction Kit QIAquick PCR Purification Kit	Qiagen
ReadyStrip™ IPG Strip	Bio-Rad
RNeasy Minikit	Qiagen
Safe-Lock Tubes (“Epp1s”)	Eppendorf, Roth
Sterile filter	Millipore
SyproRuby gel staining solution	Bio-Rad
Vectashield Hard Set™	Axxora
Centrifuge test tube 15ml / 50ml	BD Falcon

2.6. Enzymes

Enzyme Name	Supplier
Calf Intestine Alkaline Phosphatase, 1.000 U	Promega
Pfu Turbo DNA Polymerase	Stratagene
Go Taq DNA Polymerase	Promega
Lysozyme	Roth
M-MLV Reverse Transcriptase	Promega
Phusion High Fidelity DNA-Polymerase	Finnzymes
Proteinase K (PNK)	Promega

Enzyme Name	Supplier
RNase A	AppliChem
RNase-Free DNase	Promega
Restriction enzyme (restriction endonuclease)	NEB, Promega
T4 DNA Ligase	MBI Fermentas
T4 Polynucleotide Kinase	Promega

2.7. Antibodies

Specificity	IF	WB	Supplier
α actinin-4 (#210-356)	1:200	1:2000	Alexis
β-tubulin (sc-9104)	-	1:1000	Santa Cruz
β-tubulin (TUB 2.1)	1:200	1:2000	AbCam
AT1R (sc-1173)	-	1:1000	Santa Cruz
AT2R (sc-9040)	-	1:500	Santa Cruz
Actin (sc-1616)	-	1:500	Santa Cruz
Catalase (LF-PA0060)	-	1:1000	Ab-Frontier
ezrin/radixin/moesin (#3142)	1:200	1:2000	Cell signaling
FLAG (M2)	-	1:10000	Sigma-Aldrich
Focal Adhesion Kinase	1:100	-	Cell signaling
phospho-ezrin(Thr567)/radixin(Thr564) /moesin(Thr558) (#3141)	1:50	1:1000	Cell signaling
Peroxiredoxin 1 (rabbit, LF-PA0007)	-	1:3000	Ab-Frontier
Peroxiredoxin 2-cys (6E5, LF-MA0073)	-	1:1000	Ab-Frontier
Peroxiredoxin 2 (rabbit, LF-PA0007)	-	1:3000	Ab-Frontier

Specificity	IF	WB	Supplier
Peroxiredoxin 2 (mouse, LF-MA0071)	-	1:1000	Ab-Frontier
Nephrin (rabbit polyclonal)	-	1:1000	Larry Hotzmann
Nephrin (GP-N1, guinea pig polyclonal)	1:50	1:500	Progen
Nephrin (GP-N2, guinea pig polyclonal)	-	1:500	Progen
Rac-1 (#610650)	1:100	1:2000	BD Biosciences
Wilm's tumor 1 (WT1, 6F-H2)	1:200	-	Dako
Horseradish peroxidase conjugates goat anti-rabbit IgG (H+L)	-	1:500 ~1:2000	Jackson ImmunoResearch
Horseradish peroxidase conjugates goat anti-mouse IgG (H+L)	-	1:500 ~1:3000	Jackson ImmunoResearch
Horseradish peroxidase conjugates donkey anti-goat IgG (H+L)	-	1:500 ~1:2000	Jackson ImmunoResearch
Horseradish peroxidase conjugates goat anti-guinea pig IgG	-	1:1000	Jackson ImmunoResearch

2.8. Bacteria

Species	Genotype	Supplier
BL21	F^- *ompT gal dcm lon hsd*S_B(r_B^- m_B^-)	Invitrogen
DH5α	F^-Φ80 *lac*ZΔM15 Δ(*lac*ZYA-*arg*F)U169 *deo*R *rec*A1 *end*A1 *hsd*R17(r_k^-, m_k^+) *pho*A *sup*E44 *thi*-1 *gyr*A96 *rel*A1 λ^-	Invitrogen
TOP10	F^-*mcr* AΔ (*mrr-hsd*RMS-*mcr*BC) Φ80 *lac*ZΔM15 Δ *lac*X74 *rec*A1 *ara*D139 *gal*U *gal*K Δ(*ara-leu*)7697 *rps*L (Str^R)*end*A1 *nu*G	Invitrogen

2.9. Eukaryotic cells

Cell Name	Description	Reference
HEK 293T	Human embryonic kidney cells generated by transformation of cultures of normal human embryonic kidney cells with sheared adenovirus 5 DNA. Cultured in 37°C, 5% CO_2	ATCC-Nr.CRL-1573
AB8 cells	Immortalized cultured human podocytes Proliferation culture: 33°C, 5% CO_2 Differentiation culture: 37°C, 5% CO_2	Saleem *et al*. 2002
PCLs	Immortalized cultured mouse podocytes Proliferation culture: 33°C, 5% CO_2 Differentiation culture: 38°C, 5% CO_2	Schiwek *et al*. 2004

2.10. Oligonucleotides

Name	Sequenz (5´→ 3´)
hAT1R-EcoR-Kozar for	cgc ggg gaa ttc gcc acc atg att ctc aac tct tct act gaa gat gg
hAT1R-Not-Stop-Flag rev	cc cgc ggg gcg gcc gc tta tta ttt gtc gtc atc gtc ttt gta gtc cat tca ctc aac ctc aaa aca tgg tgc agg c
hAT1R-sequence for	gtt tgc cag cta taa tcc atc g
hAT1R-sequence rev	cca gca gcc aaa tga tga tgc
hAT1R+Flag for	cca tgt ttt gag gtt gag gca atg gac tac aaa gac g
hAT1R+Flag rev	cgt ctt tgt agt cca ttg cct ca acct caa aac atg g

Name	Sequenz (5´→ 3´)
hAT1R-RTPCR for	caa tga agt ccc gcc ttc gac gc
hAT1R-RTPCR rev	ctt tgt agt cca ttg cct caa cc
mAT1Ra-RTPCR for	cgt cat cta ctt tta cat gaa g
mAT1Ra-RTPCR rev	gcc cag gat gtt ctt ggt tag g
mAT1Rb-RTPCR for	gaa tct cag aac tca aca ctc c
mAT1Rb-RTPCR rev	gtt gat aac cct gca tgc gac c
mAT2R-RTPCR for	gtg caa agt gtt tgg ttc ttt tc
mAT2R-RTPCR rev	cat agt ctc tct ctt gcc ttg ga
mGAPDH-RTPCR for	aac ttt ggc att gtg gaa gg
mGAPDH-RTPCR rev	aca cat tgg ggg tag gaa ca
ShRNA sequence, sh1 (sense strend)	gaa gta cgt ggt cct ctt t (target human Prx2 a.a position: 105-124)
ShRNA sequence, sh2 (sense strend)	gaa gta cgt gga cct ctt t (target mouse Prx2 a.a position: 105-124)
ShRNA sequence, sh3 (sense strend)	gtg gat gac agc aag gaa t (target human and mouse Prx2 a.a position: 559-577)

2.11. Software and Internet Program

Software/Program	Supplier
AMIRA	TGS Inc., San Diego, CA, USA
Axiovision 4.2	Zeiss
HiPic32, Hamatsu Photonics Deutschland GmbH	Hersching
BioEdit sequence alignment editor	Ibis Biosciences

Software/Program	Supplier
DeCyder™ v6.5 Differential Analysis Software	GE Health Life Science
Blockit RNAi	Invitrogen
GPS Explorer software	Applied Biosystems
ImageQuant™ TL analysis software	GE Health Life Science
http://jura.wi.mit.edu/bioc/siRNAext/reference.php	Whitehead Institut
http://rsb.info.nih.gov/ij/	Image J
http://www.expasy.org/	*Expert Protein Analysis System,* Swiss Institute of Bioinformatics
http://www.matrixscience.com/search_intro.html	MASCOT

2.12. Plasmid Construct Maps

Plasmid:	**pCXhAT1S**	**Original vector:**	**pCXGFP**
Insert:	**hAT1-SV40 polyA**	**Restriction:**	**Eco RI / Bam HI**
Bacterial strain:	**D5Hα**	**Antibiotic resistance:**	**Ampicillin**

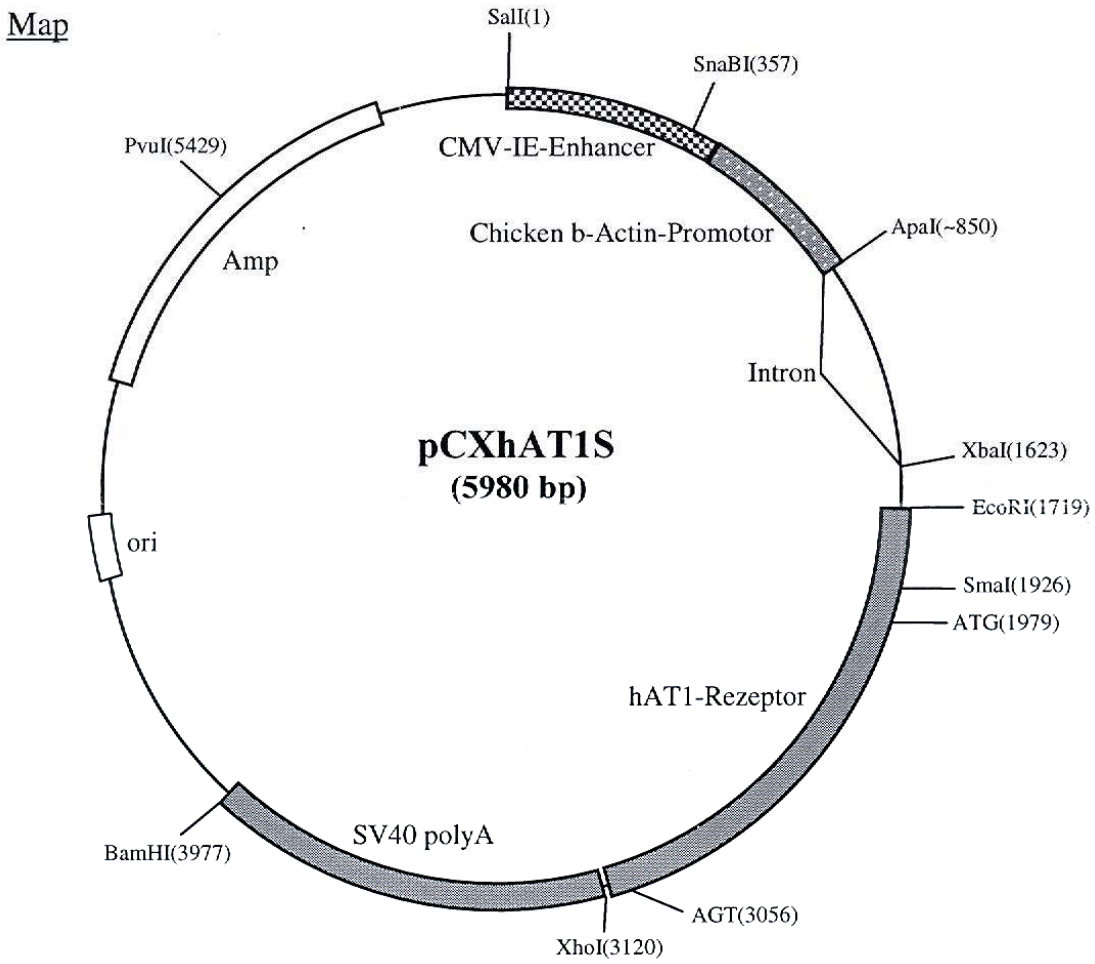

Discription:

A 1.1-kb fragment of the human angiotensin II type 1 receptor (hAT1R) cDNA containing the entire coding region (a gift from T. Inagami, Vanderbilt University School of Medicine, Nashville, Tennessee) was subcloned to PCR2.1 vector containing a 1.25-kb fragment of the human nephrin promoter (NPHS1). A novel transgenic rat (TGR) model with overexpression of the human AT1R in podocytes was developed by this 3.5-kb transgene excised with BstXI and BamHI out of the cloning vector to study the consequences of an increased AT1 signaling on the structure and function of the glomerular filter.

Plasmid: **pLXSN.hAT1R.FL.Flag** **Original vector:** **pLXSN**

Insert: **hAT1R.Flag** **Restriction:** **Eco RI / Not I**

Bacterial strain: **D5Hα** **Antibiotic resistance:** **Ampicillin**

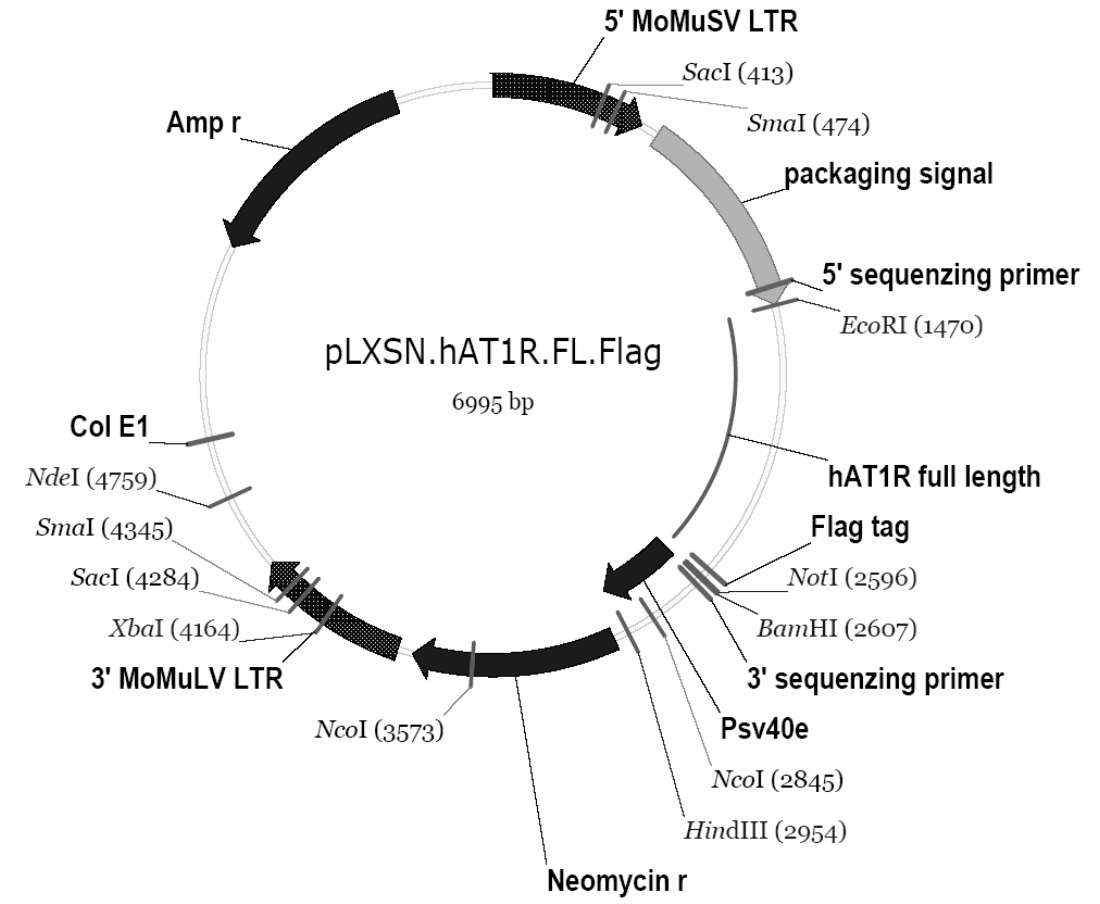

Reference:

Mann, R., Mulligan, R. C. & Baltimore, D. (1983) Construction of a retrovirus packaging mutant and its use to produce helper-free defective retrovirus. Cell 33:153–159.

Discription:

pLXSN can be used to transfect a packaging cell line and produce retrovirus, which is then collected from the supernatant and used to efficiently transduce cells. The target gene is expressed from the 5' LTR promoter; neomycin (G418) can be used for antibiotic selection.

Promoter: 5' LTR
Selection: prokaryotic—ampicillin
eukaryotic—neomycin
Replication: prokaryotic—Col E1
GenBank Accession No. M28248

Plasmid:	**pMD.G**	**Original vector:**	**pXF3**
Insert:	**VSV-G**	**Restriction:**	**EcoR I / EcoR I**
Bacterial strain:	**D5Hα**	**Antibiotic resistance:**	**Ampicillin**

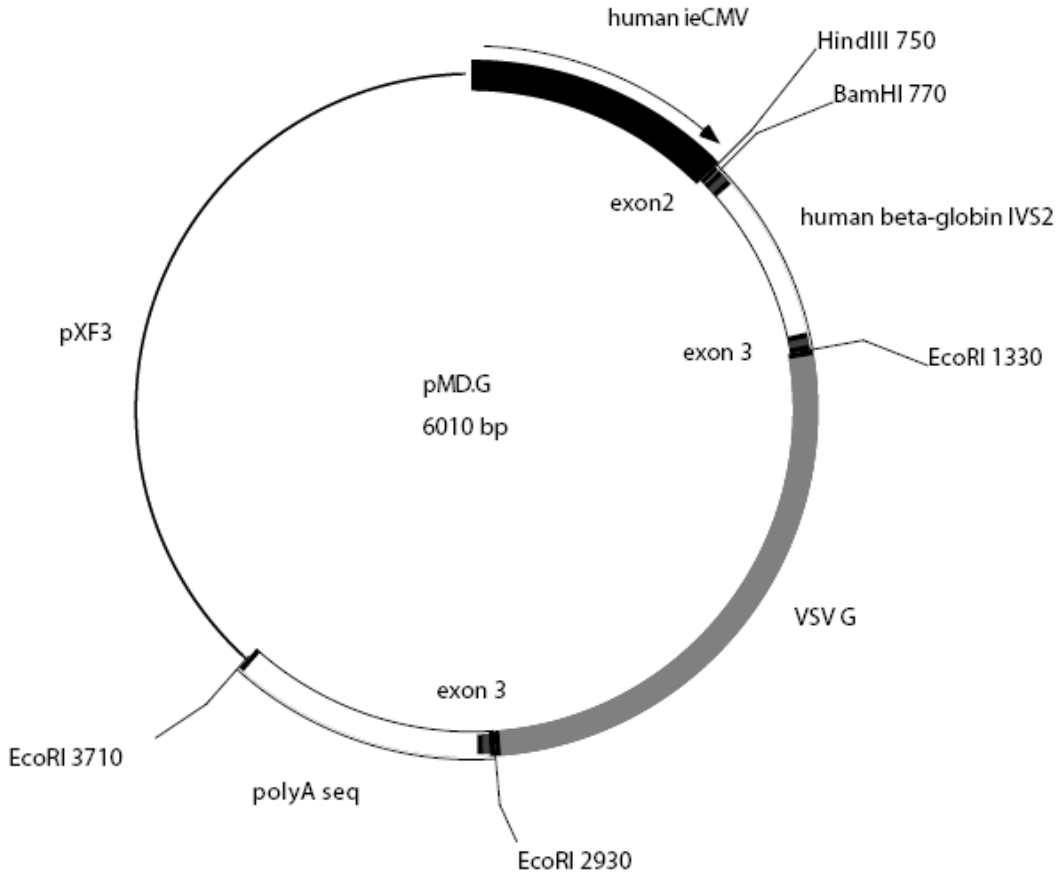

Reference:

Miyake K, Suzuki N, Matsuoka H, Tohyama T, Shimada T. (1998) Stable integration of human immunodeficiency virus-based retroviral vectors into the chromosomes of nondividing cells. Hum Gene Ther 9:467-475.

Discription:

This vector helps to produce a VSV-G pseudotyped retrovirus with higher transduction efficiency to target cells of gene delivery.

Constructed by: Daniel Ory
Construction date: August 25, 1994
Comments/References: human CMV promoter is from pBC12/CMV/IL2 (B. Cullen, Cell 46, 1986), human beta globin sequence (exons 2 and 3, IVS2, polyA) is from pucMdBs(R)S (gift M. Sadelain).
VSV G from pSVGL.

Plasmid: **pMD.gag/pol** **Original vector:** **pMD2**

Insert: **gag and pol genes** **Restriction:** **Eco RI / Eco R**

IBacterial strain: **D5Hα** **Antibiotic resistance:** **Ampicillin**

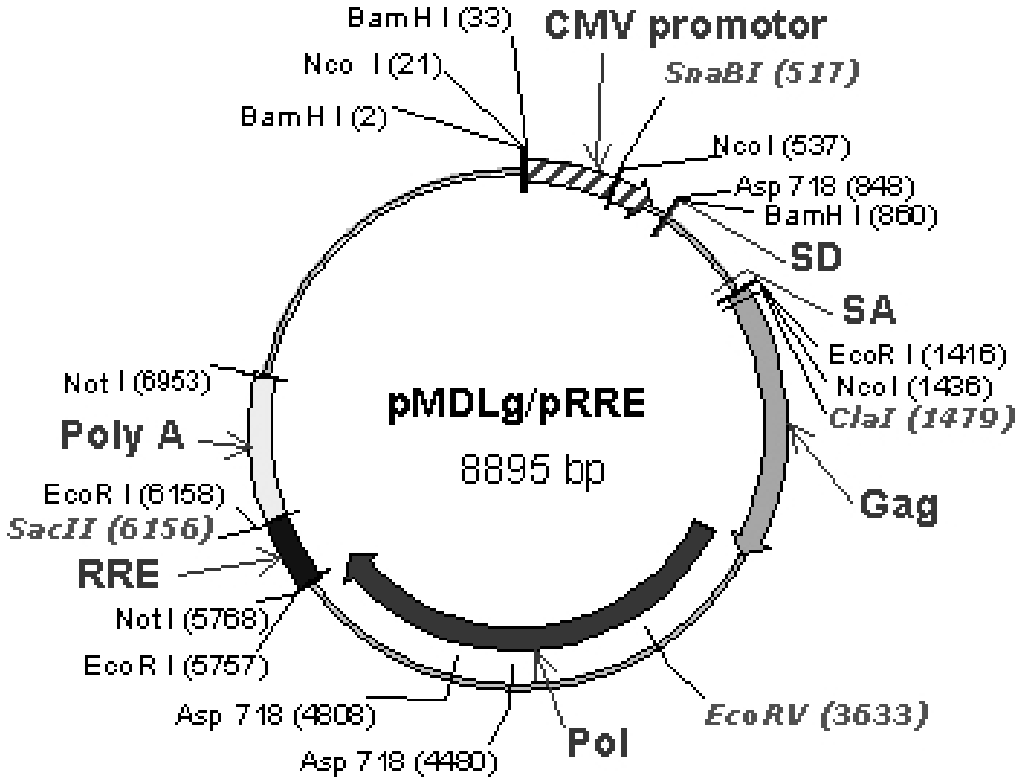

Reference:

Dull T, Zufferey R, Kelly M, Mandel RJ, Nguyen M, Trono D, Naldini L. (1998) A Third-Generation Lentivirus Vector with a Conditional Packaging System. J Virol. 72: 8463–8471

Discription:

pMD.g/p (pMD.gag/pol) is a packaging construct that contains gag and pol gene. During retrovirus assembly, the polyprotein Gag directs protein multimerization, membrane binding, and RNA packaging. The pol gene h encodes the reverse transcriptase which is involved in virus integration.

pMDLg/p is a CMV-driven expression plasmid that contains only the gag and pol coding sequences from HIV-1. pMDLg/pRRE differs from pMDLg/p by the addition of a 374-bp RRE-containing sequence from HIV-1 (HXB2) immediately downstream of the pol coding sequences.

Plasmid: pRNA-TH1.4/Retro-mPrdx2/SH1

Original vector: pRNA-TH1.4/Retro **Restriction: Mlu I / Xho I**

Insert: short hairpin sequence (for mouse peroxiredoxin 2)

Bacterial strain: D5Hα **Antibiotic resistance: Ampicillin**

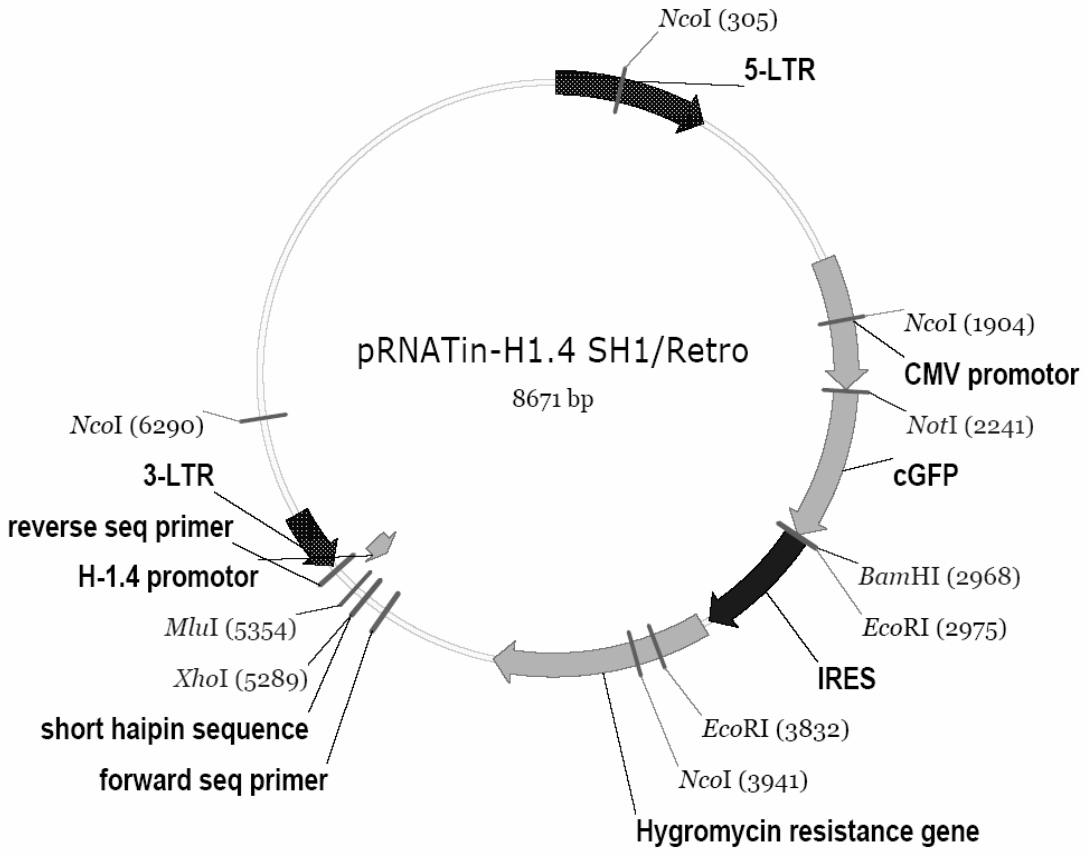

Reference:

Yu JY, DeRuiter SL, Turner DL. (2002) RNA interference by expression of short-interfering RNAs and hairpin RNAs in mammalian cells. Proc Natl Acad Sci U S A. 99(9):6047-6052.

Discription:

pRNA-H1.1/Retro siRNA expression vector is compatible with Clontech Retro-X Expression System. An H1 promoter drives the siRNA expression with the siRNA insert cloned between Mlu I and Xho Isites. The vector contains a hygromycin resistance gene under the control of cytomegalovirus (CMV) promoter for establishing stable cell line. The vector uses CMV enhancer/promoter joined MSV 5'LTR (CMV/MSV 5'LTR) and MSV 3'LTR for viral transcription and packaging.

Packaging signal: 757-1566
ColE1 ori: 6456-7342
SV40 ori & promoter: 6012-6356
Ampicillin: 7402-8262

3. Methods

3.1. Molecular Cloning Methods

Techniques for DNA manipulations for various purposes are modifications of those in "*Molecular Cloning: A Laboratory Manual (Third Edition)*" by Joseph Sambrook and David Russell (Cold Spring Harbor Laboratory Press, 2001).

3.1.1. Amplification of Double–Strand DNA by PCR

The following procedure was applied to subclone a 1.1-kb fragment of the human Ang II type 1 receptor (hAT1R) cDNA containing the entire coding region (a gift from T. Inagami, Vanderbilt University School of Medicine, Nashville, TN, USA) was subcloned into the retroviral gene delivery vector (pLXSN-hAT1R-Flag).

Oligonucleotide primers complementary to two different regions of the DNA fragment of interest were designed. For instance, two oligonucleotide primers were designed for hAT1R.

Primer 1: 5` atg att ctc aac tct tct act gaa gat gg 3`

Primer 2: 5` tca ctc aac ctc aaa aca tgg tgc agg c 3`

In a 0.2 m1 thin-walled PCR tube on ice, set up a standard reaction by adding the following in the order listed:

5X Amplification buffer (10 µl)

ddH_2O (10 µl)

Mixture of four dNTPs (1.25 mM each) (8.5 µl)

Primer 1 (50 to 100 ng) in ddH_2O (5 µl)

Primer 2 (50 to 100 ng) in ddH_2O (5 µl)

dsDNA in TE buffer (100 to 250 ng) (2 µl)

Phusion High Fidelity DNA-Polymerase (5 units/µ1) (0.5 µl)

Add H_2O to a final volume of 50 µl.

Carry out 25–35 cycles of PCR amplification in a PCR machine. The conditions of PCR, including primer annealing temperatures, extension times, and number of cycles, were optimized. An example of retroviral gene delivery vector (pLXSN-hAT1R-Flag) is as follows.

Cycle	Denaturation	Annealing	Polymerization
First cycle	30 sec at 98°C	-	-
Subsequent cycles (2–34)	10 sec at 98°C	30 sec at 60°C	45 sec at 72°C
Last cycles	10 sec at 98°C	30 sec at 60°C	45 sec at 72°C

Finally, hold at 4°C until the sample is removed.

The purity of the amplified cDNA on an agarose gel was assessed and the fragment of interest was eluted by the standard procedures in a QIAquick Gel Extraction Kit. The fragment was ligated to an appropriate cloning vector, and an appropriate E. coli host was transformed in preparation for minipreps. The ligation reaction was as follows:

Ligase 10X buffer (2 μl)

Vector (0.1 pg)

cDNA inserts (0.5 μg)

T4 DNA ligase (10 Weiss units)

Add ddH2O to a final volume of 20 μl.

The ligation reactions were incubated at 16°C for 12 h before proceeding to subcloning.

To identify the correct clones and verify the sequence, mimprep DNA of at least 20 colonies after E. coli transformation was prepared. These preps were cut with flanking restriction enzymes and fragments were run on a 1% agarose gel to identify clones with the correct size fragment. The DNA molecules were then directly sequenced by combining PCR technology and the dideoxynucleotide chain termination method—*Cycle Sequencing and Automated Sequencing*. The ligation reaction setup was as follows.

DNA template (40-800 fmol, 5μl)

BigDye 3.1 buffer (2 μl)

BigDye 3.1 mix (2 μl)

Primer (5 μM, 1 μl)

Start with the following cycling program:

Cycle	Denaturation	Annealing	Polymerization
Total 25 cycles	10 sec at 96°C	5 sec at 50°C	4 min at 60°C

The samples were purified for injection and sequence chromatograms were analyzed using the BioEdit sequence alignment editor.

3.1.2. Reverse transcription PCR

Reverse transcription PCR (RT-PCR) is a powerful approach for cDNA cloning and gene expression analysis when specific primers are available. Total RNA or mRNA is TRY first reverse transcribed into cDNA, which is then amplified by PCR. Briefly, specific primers are designed according to conserved nucleic acid motifs in two different regions of known genes or their protein products. The primers are annealed to the first strand of cDNA synthesized from an mRNA template. Double-stranded cDNAs can be generated and amplified using Taq DNA polymerase.

Isolation of total RNA and purification of poly(A)$^+$ RNA from cultured cells were performed using standard protocols in the RNeasy Minikit provided by Qiagen. The first strand of cDNAs was synthesized from the isolated total RNAs or mRNAs using reverse transcriptase and oligo(dT) as a primer. Total RNA (1 pg) or 50 ng mRNA template was annealed with 2 μg oligo(dT) primer in a sterile RNasefree microcentrifuge tube. Nuclease-free dd H_2O was added to a total volume of 15 μl. The tube was heated to 70°C for 5 min and allowed to slowly cool to room temperature to complete annealing. Briefly, the mixture was spun down to the bottom. First strand synthesis was as follows.

5X M-MLV reverse transcriptase buffer (5 μl)

M-MLV reverse transcriptase (1 µl)

1µg isolated RNA

dNTPs (10M, 1.25 µl)

Add H_2O to a final volume of 20 µl, incubate at 40°C for 1 h.

The oligonucleic primers were designed based on conserved amino acid sequences in two different regions of the specific gene product (protein) of interest. Amplification of the specific cDNA of interest was performed by PCR using specific primers.

3.2. Cellular Biologic Methods

Molecular and cellular methods for various purposes are modified versions of those in the "*Handbook of Molecular and Cellular Methods in Biology and Medicine (Second Edition)*" by Leland J. Cseke *et al.*, CRC Press, 2003.

3.2.1. Cell Culture

A recently generated conditionally immortalized mouse podocyte cell line was cultivated as reported elsewhere.[113] Briefly, podocytes were maintained in Roswell Park Memorial Institute (RPMI) 1640 medium (PAA, Cölbe, Germany) supplemented with 10% fetal bovine serum (FBS) (Biochrom, Berlin, Germany) in a humidified atmosphere of 5% CO_2. To stimulate podocyte proliferation, cells were cultivated at 33°C (permissive conditions). The culture medium was supplemented with 10 U/ml mouse recombinant γ-interferon (Roche, Mannheim, Germany) to induce expression of the temperature-sensitive large T antigen. To induce differentiation, podocytes were maintained at 38°C without γ-interferon (nonpermissive conditions) for at least 2 weeks.

The HEK293 cells were cultured in Dulbecco/Vogt modified Eagle's minimal essential medium (DMEM) (PAA, Cölbe, Germany) supplemented with 10% FBS. For immunofluorescence studies and intracellular Ca^{2+} measurements, podocytes were seeded on glass coverslips pre-coated with 0.1 mg/ml mouse collagen (Biochrom,

Berlin, Germany) for 30 min at room temperature.

All cells were FBS-deprived for 24 h prior to each experiment. To analyze living cells, podocytes were cultivated in a 25-cm² culture flask with plug seal cap (BD Falcon, Germany).

3.2.2. Calcium Phosphate Transfection

The principle of calcium phosphate–mediated transfect ion is that the DNA to be transferred is mixed with $CaCl_2$ and phosphate buffer to form a fine calcium phosphate precipitation containing the DNA. The precipitate is then placed on a cell monolayer. Calcium phosphate precipitate binds/attaches to the plasma membrane and enters the cell via endocytosis. This method, which is most widely used for transient and stable transfection, was carried out as follows.

Cell monolayers were prepared the day before the transfection experiment. The cell monolayers should have 50–70% confluence. The old culture medium was removed and cells were fed with 5–10 ml fresh culture medium.

A transfection mixture for each 100 mm dish was prepared as follows:

2.5 M $CaCl_2$ solution (50 µl)

Recombinant reporter DNA construct (10 to 30 µg)

Add ddH_2O to a volume of 0.5 ml.

The transfection mixture solution was vortexed well, and then the DNA mixture was slowly added dropwise to 0.5 ml of well-suspended 2X Hepes-Buffered Saline (HEBS) buffer by continuous mixing by vortexing. The mixture was incubated at room temperature for 30–40 min to allow for coprecipitation.

The precipitated mixture was slowly added dropwise to the dish containing the cells while the plate was continuously swirled to achieve a good mix. For each 100 mm dish containing the cells, 1 ml of the DNA mixture was added. For each 60 mm dish, 0.5 ml

of the DNA mixture was added. The plate containing the cells was incubated overnight in a 37°C CO_2/air (2–5% CO_2) incubator.

The medium was removed and the monolayer washed once with 10 ml serum-free DMEM medium and once with 10 ml PBS. Fresh culture medium was added and the Petri dishes were returned to the incubator. Typically, cells can be harvested 48–72 h after transfection for transient transfer analysis.

3.2.3. Retroviral Gene Delivery

The apical membrane of podocytes is negatively charged due to the presence of surface anionic proteins podocalyxin. Subsequently cultured podocytes are resistant to conventional methods of transient gene delivery.

Retroviruses can be utilized as effective vectors for gene transfer in mammalian systems. Retroviral gene delivery has the following advantages over SV40-based plasmid vectors: (1) the retroviral genome can stably integrate into the host chromosomes of infected cells and be passed from generation to generation, thereby providing an excellent vector for stable transformation; (2) retroviruses have a broad infectivity and expression host range for any animal cells via viral particles; (3) integration is site specific with respect to the viral genome at long terminal repeats (LTRs), which can easily preserve gene structure that remains intact after integration; and, (4) viral genomes are very plastic and allow for a high degree of delivered gene size manipulation.

Retroviruses, such as Rous sarcoma virus (RSV) and Moloney murine leukemia virus (MoMLV), are ribonucleic acid (RNA) viruses that cause a variety of diseases, including tumors in humans. These viruses contain two transfer RNA (tRNA) primer molecules, two copies of genomic RNA (38S), reverse transcriptase, RNase H, and integrase, which are packaged within an envelope. The viral envelope contains glycoproteins that determine degree of host infection. When a virus or virion attaches itself to a host cell, the viral glycoproteins in the envelope bind to specific receptors in

the host cell plasma membrane. The bound complex then facilitates internalization of the virus, which loses its coat as it passes through host cell cytoplasm. In the cytoplasm, the reverse transcriptase contained in the viral genome catalyzes the formation of a double-stranded DNA molecule from the single-stranded viral RNA. The DNA molecule circularizes, enters the nucleus, and integrates into host cell chromosomes, thereby forming a provirus. Subsequently, the integrated provirus functions as a transcriptional template for both messenger RNAs (mRNA) and viral genomic RNAs. Such transcription is catalyzed by host RNA polymerase II. The mRNAs undergo translation to generate viral proteins and enzymes using host machinery. All of these components are packaged in viral core particles. The particles move through the cytoplasm, attach to the plasma membrane inner side and bud off. This cycle of infection, reverse transcription, transcription, translation, virion assembly, and budding is repeated endlessly, thus infecting new host cells.

Retroviruses are single-stranded RNA viruses that can infect a number of organisms, including humans and many other mammals. Following infection, the virus genome is reversely transcribed into double-stranded DNA, which is integrated into the host chromosome via integration mechanisms. The ability to infect target cells, their stable replication and high-level gene expression make retroviruses very attractive as gene transfer vectors. The retroviral vectors developed in this stuffy proved highly efficient for gene delivery and achieved stable long-term expression of transgenes.

Retroviral gene delivery was performed using methods described elsewhere.[114] The plasmid pLXSN was provided by D. Miller (Fred Hutchinson Cancer Research Center, Seattle, WA, USA). The pMD.G and pMD.gag/pol plasmids were gifted by R. Mulligan (Harvard Medical School, Boston, MA, USA). A 1.1-kb fragment of human Ang II type 1 receptor (hAT1R) cDNA containing the entire coding region (from T. Inagami, Vanderbilt University School of Medicine, Nashville, TN, USA) was subcloned into the retroviral gene delivery vector using standard cloning techniques (pLXSN.hAT1R.FL.Flag). The hAT1R gene-containing virus was produced by co-transfecting HEK293 cells with three plasmids (2.5 μg pMD.G, 7.5 μg

pMD.gag/pol and 10 μg pLXSN.hAT1R.FL.Flag) using the calcium phosphate method. The supernatant was harvested, centrifuged to remove cellular debris and filtered. Podocytes cultivated in permissive conditions were infected by virus soup with 8 μg/ml polybrene and then selected 4 days following viral transduction in geniticin (250 μg/ml) to achieve 100% positive cells.

3.2.4. Intracellular Calcium Measurement

Measurement of cytosolic Ca^{2+} using Ca^{2+}-sensitive dye and Fura-2-acetomethyl ester (Molecular Probes) was performed using an inverted fluorescence microscope.[115] Podocytes were cultivated in collagen-coated coverslips and loaded with Fura-2-acetomethyl ester dye (5 μM, 45 min at room temperature). Coverslips were then placed into the microscopic chamber with continuous fluid flow. The initial superfusing solution was standard Ringer solution (145 mM NaCl, 1.6 mM K_2HPO_4; 0.4 mM KH_2PO_4; 5 mM D-glucose; 1 mM $MgCl_2$; 1.3 mM Ca^{2+}-gluconate [pH 7.4]) followed by superfusing with varying Ang II concentrations.

The $[Ca^{2+}]_i$ was measured by alternately exciting the dye with a beam at 340 and 380 nm while monitoring the emission at 530 nm with a single-photon counting tube (H3460–04; Hamamatsu, Herrsching, Germany). The Fura-2-acetomethyl ester fluorescence signal was calibrated after each experiment using Ca^{2+} ionophore ionomycin (1 μM) and Ringer solutions with the standard Ca^{2+} concentration or without Ca^{2+}. The $[Ca^{2+}]_i$ concentration was calculated using the fluorescence ratio of 340:380 nm and the equation developed by Grynkiewicz *et al*.[116]

3.2.5. Measuring NADPH Oxidase Activity and Superoxide Generation

Podocytes were rinsed twice with ice-cold PBS, scraped with KREBS solution (99 mM NaCl, 4.7 mM KCl, 1.8 mM $CaCl_2$, 1.2 mM $MgCl_2$, 25 mM $NaHCO_3$, 1.03 mM K_2HPO_4, 20 mM Na-HEPES, and 11.1 mM glucose [pH 7.35]) and centrifuged (200 × *g*, 4°C, 5 min). The supernatant was discarded and the pellet was resuspended in fresh KREBS buffer. The cell suspension was added to the KREBS solution containing 5 μM lucigenin and stimulated with 100 μM NADPH. Bioluminescence was measured

using a Lumat LB9501 (Berthold GmbH, Wildbad, Germany).

Cells were subsequently lysed, and protein concentrations were determined using Advanced Protein Assay™ agents (Cat.#ADV01, Cytoskeleton, USA). To calculate superoxide production, total counts were determined by integrating the area under the signal curve by luminescent signal intensity multiplying with time. These values were compared with a standard curve generated by xanthine/xanthine oxidase reaction as described elsewhere.[117] Superoxide generation was expressed as nanomole $O_2^{\cdot-}$ generated per mg cellular protein per min (nmol $O_2^{\cdot-}$/mg protein/min). Superoxide for podocyte stimulation was also generated by the xanthine/xanthine oxidase reaction.

3.2.6. In Vitro Wound Healing ('scratch') Assay

Twelve-well plates were pre-coated with type 1 collagen (#C3867, Sigma-Aldrich), and a sufficient number of AT1R podocytes were plated such that they were confluent in the wells immediately after differentiation (~14 days). Before creating a scratch wound, cells were FBS-starved for 24 h and then treated with Ang II (100 nM) and/or other inhibitors (losartan, PD123319, SCH51344, DMTU) for another 24 h. The same areas of each well were then displaced by scratching a cross through the layer using a pipette tip. Floating cells were removed by washing with PBS. Medium containing 2.5% FBS was added to the wells and incubated for an additional 48 h.

Images of the scratched areas in each cross wound were photographed at 24 and 48 h using an inverted phase-contrast microscope (Axiovert 100, Zeiss, Germany). Three independent experiments were performed, and 12 cross wounds were created for each group (n = 12). To estimate relative cell migration, the number of cells moving across a 1 mm wound border was calculated at 24 and 48 h.

3.2.7. Life Cell Imaging

Lamellipodium activities and membrane ruffles of individual podocytes were observed by time lapse video microscopy, as described elsewhere.[118] Twelve hours before experiments, the culture medium for differentiated sparsely cultivated podocytes was

changed to a vehicle medium (FBS-free and bicarbonate-free RPMI medium at pH 7.40), and the culture flask caps were sealed. After adding Ang II (final concentration of 100 nM) to the vehicle medium, the culture flasks with cells were resealed and placed in an electronically controlled heating chamber at 37°C on the stage of an inverted phase-contrast microscope (Axiovert 25, Zeiss, Germany). Images were taken using time-lapse video recordings at 10-min intervals for 24 h and stored as stacks of tiff files.

3.2.8. Cellular ROS Determination

Intracellular oxidative stress was monitored by measuring changes in fluorescence resulting from intracellular probe oxidation. Dihydroethidine (DHE, Molecular Probes, USA) enters the cell and is oxidized by ROSs, particularly superoxide, to yield fluorescent ethidium. Ethidium binds to DNA (Eth-DNA), further amplifying its fluorescence.[119] Thus, nuclei are the primary fluorescent structures labeled and increases in DHE oxidation to Eth-DNA (i.e., increases in Eth-DNA fluorescence) are indicative of superoxide generation.

By simply incubating experimental samples (cryosection of tissues or living cells) in the presence of DHE (5 μmol/l, 30–40 min at room temperature) followed by analysis of fluorescence allows for rapid and specific detection of intracellular oxidative stress due to superoxide anion generation. Dihydroethidium stains the cytoplasm of living cells blue (excitation at 370 nm and emission at 420 nm) and chromatin of living cells red (excitation at 535 nm and emission at 610 nm).

3.3. Protein Biochemistry Methods

3.3.1. Immunoprecipitation and Western Blotting

Using monoclonal antibodies that specifically recognize Flag-tag (M2 antibody) (Sigma-Aldrich), Flag-tagged hAT1R protein expression in cultured podocytes was evaluated with immunoprecipitation methods.

For immunoprecipitation, cells were washed with ice-cold PBS and homogenized in ice-cold lysis buffer (12 mM Tris base, 8 mM HEPES, 50 mM NaCl, 15 mM KCl, 1.5 mM $MgCl_2$, 1 mM EGTA, 10 mM $Na_2H_2P_2O_7$, 1 mM ATP, 20 mM NaF, 1 mM Na_3VO_4, 1% Triton X-100 and complete protease inhibitor [Roche]) on ice. Lysates rested on ice for 30 min and then centrifuged for 1 h at 16000g. Supernatants were pre-cleared by incubation with protein G-sepharose beads (Amersham Biosciences) coupled with actin antibody (sc-1616, Santa Cruz) for 6 h at 4°C on a rotary wheel. The pre-cleared protein extracts were then incubated with anti-Flag antibody-conjugated beads (M2 beads) (Sigma-Aldrich) overnight at 4°C on a rotary wheel. The M2 beads were then washed twice with lysis buffer without NaF, Na_3VO_4, ATP and Triton X-100. Precipitates were resolved by sodium dodecyl sulfate-polyacrylamide gel electrophoresis and analyzed by immunoblotting the AT1 receptor antibody (sc-1173, Santa Cruz). Pre-cleaned protein extracts with equal volumes were also resolved by SDS-PAGE and subsequent β-tubulin antibody (sc-9104, Santa Cruz) immunoblotting for total protein input control.

For conventional Western blotting, cells or rat kidney tissues were washed with ice-cold PBS and homogenized in ice-cold lysis buffer on ice. Lysates were left to rest on ice for 30 min and then centrifuged for 1 h at 16000g. Protein concentrations of supernatants were measured using Advanced Protein Assay™ agents (Cat.#ADV01, Cytoskeleton, USA), and each sample was measured three times to acquire average results. Equal amounts of protein extract were resolved by SDS-PAGE and analyzed by immunoblotting specific antibodies, followed by subsequent peroxidase-labeled secondary antibodies. Chemiluminescent signals (LumiLight, Roche Diagnostics, Germany) were detected with a Lumi-Imager and quantified using the LumiAnalyst program (Roche Diagnostics, Mannheim, Germany). The entire sodium dodecyl sulfate-polyacrylamide gel was subsequently stained with SyproRuby (Bio-Rad, USA) for total protein, and quantified and visualized by a Lumi-Imager (300 nm UV illumination) to ensure that amounts of protein loaded were approximately equal. Chemiluminescent signal intensity detected in each experiment was further standardized with total protein staining of a quantity of the representative lane in the

quantitative SYPRO Ruby gel-staining method. For each experiment, the matching results of SYPRO Ruby gel staining are included in figures containing Western blot results (labeled as “loading control”).

3.3.2. Two-dimensional electrophoresis followed by immunoblotting

Two-dimensional electrophoresis (2DE) was utilized to quantify the expression level of the AT1R protein in cultured podocytes with increased sensitivity and specificity. Total proteins can be separated by isoelectric point during the first dimension electrophoresis, and then separated again by molecular weight in the second dimension electrophoresis. Details of 2DE are described in Methods, Section 3.5—2-D DIGE System and Proteomics.

Cells were homogenized in 2DE lysis buffer (7 M Urea, 2 M Thiourea, 4% CHAPS, and 30 mM Tris) with a micro tissue grinder (model 440630; Radnoti, USA) followed by three rounds of sonication (1 min) in an ice bath sonicator at 4°C. Lysates rested on ice for 30 min and were then centrifuged for 1 h at 16000g. Supernatant protein concentrations were determined as described previously.

For 2DE, 215 μl buffer containing 7 M urea, 2 M Thiourea, 4% CHAPS, 100 mM dithiothreitol (DTT) and 8% IPG buffer (Bio-Lyte 3-10, Cat.#163-2094, Bio-Rad, USA) were added to each channel in the rehydration tray for overnight rehydration of the 11cm IPG Strips, pH 3–10 nonlinear (Cat.#163-2016, Bio-Rad, USA) in accordance with the ReadyStrip™ IPG Strip instruction manual (Bio-Rad) for cup loading. The first dimension separations were performed by the PROTEAN ® IEF cell (Cat. #165-4000, Bio-Rad, USA) by the cup loading method. Equal amounts of each sample (400–600 μg) were loaded into the sample cups in the focus tray, and focusing was performed at 1000 V for 90 min (slow ramp), 3500 V for 90 min (slow ramp) and 7000 V for 120 min (rapid ramp).

For the second dimension-electrophoresis TRY 2DE, the focused IPG strips were equilibrated in a reduction buffer (37.5 mM Tris-HCl, pH 8.8, 6 M urea, 20% glycerol,

2% SDS, and 1% DTT) at 25°C for 15 min. The strip was then equilibrated in an alkylation buffer (37.5 mM Tris-HCl, pH 8.8, 6 M urea, 20% glycerol, 2% SDS, 0.002% bromophenol blue, and 2.5% iodoacetamide) at 25°C for 15 min. The SDS-PAGE was performed in a 12% polyacrylamide gel cast in the Criterion® 3 Cell (Bio-Rad, USA) at 120 volt (V) during the first 15 min and at 200 V until the tracking dye reached the lower edge of the gel. Separated proteins were then electro-transblotted onto a nitrocellulose membrane for 2DE-immunoblotting. Chemiluminescent signals of AT1 receptors and actin were quantitatively detected using a Lumi-Imager.

3.3.3. Animal Tissue Preparations

All animal experiments were performed using Neph-hAT1R TGRs and age-matched wild-type (WT) littermates. The rats were maintained on a 12-h light-dark cycle with 55% humidity at an ambient temperature of 23 ± 2°C and given free access to a standard pellet diet (Sniff, Soest, Germany) and tap water. Glomeruli and tubuli were isolated from rat kidneys by sequential sieving as described elsewhere.[60] All studies were approved by the institutional animal care review committee and conducted according to the guiding principles of governmental authorities.

3.4. Immunofluorecent Stainings

The fluorescent antibody method, which is also known as the fluorescence-labeled antibody method and immunofluorescence staining, is an immunohistochemical staining technique that detects antigenic substances as markers of fluorescent anti-Ig antibodies based on the principle that clear fluorescence is observed against a dark background even when a fluorescent body is extremely small. This scheme can detect very small and distinct amounts of antigenic substances in renal tissue.

When a substance is detected using the fluorescent antibody approach, the following two conditions must be met: the substance must be antigenic and specific antibodies must be produced in reaction to it; and, the antigenic substance must be insoluble in

tissue and present in a certain minimum amount (sensitivity) under stable conditions.

3.4.1. Cultured Cells and Cortical F-actin Score Index

Cells on coverslips were fixed in ice-cold trichloroacetic acid for 15 min (specifically for pERM and ERM protein staining) or 4% paraformaldehyde and 4% sucrose in PBS for 10 min at room temperature. Cells were permeabilized in 0.1% Triton X-100 for 10 min at room temperature, blocked in 10% BSA in PBS for 1h and incubated with the phospho-ezrin(Thr567)/radixin(Thr564)/moesin(Thr558) antibody or ezrin/radixin/moesin antibody or α actinin-4 antibody followed by subsequent fluorophore-conjugated secondary antibodies and/or phalloidin (Alexa Fluor® 488/594; Molecular Probes, USA) detection. Some cells were incubated briefly in 4'-6-Diamidino-2-phenylindole (DAPI) (Molecular Probes) for nuclei visualization. Images were acquired using an inverted fluorescent microscope (Axiovert 100; Zeiss, Germany).

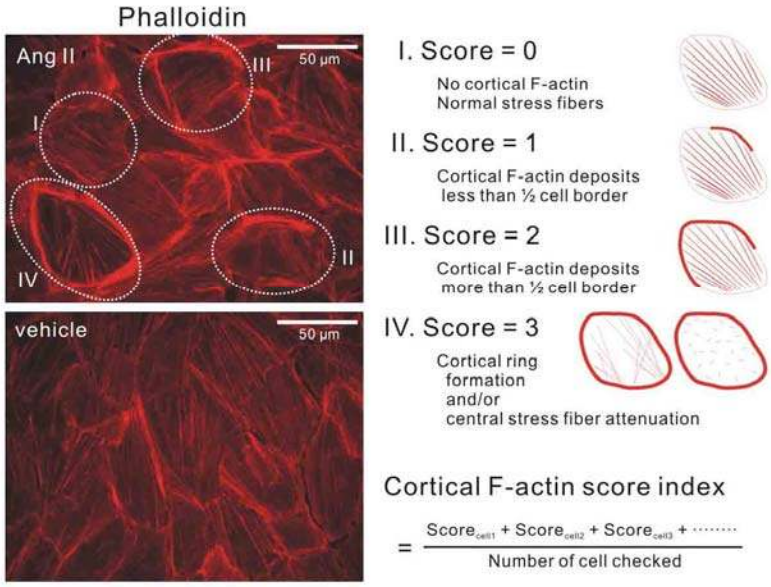

Fig. 3.4.1 The design of CFS index The extent of F-actin cytoskeletal reorganization for each individual cell was assessed and scored on a scale from 0 to 3 based on the degree of cortical F-actin formation. At minimum three independent experiments were performed, and over 600 cells were scored in each group. The CFS index for Ang II or vehicle-treated podocytes is the average score of cells counted ± SEM.

Three independent experiments were performed for cortical F-actin score (CFS) index determinations. Cells were fixed, permeablized and then stained with fluorophore-conjugated phalloidin and DAPI as described. Twelve low-magnification images (400×) were taken randomly from each group. All cells in these images were counted (by DAPI-stained nuclei) and individually scored according to the criteria defined in Fig. 3.4.1 (by phalloidin F-actin staining). At minimum 600 cells were examined in the 12 images from each group, and the CFS index was generated by averaging counted cells.

3.4.2. Cryosectioned Human Kidney Tissues

3.4.2.1. Tissue Preparation and Storage

Immediately after removing the renal tissue, it was wrapped in saline gauze and then specimens were prepared using a scalpel. Immediately freezing the tissue for the fluorescence antibody method is essential; that is, freezing and embedding must be performed immediately after removing the tissue. First, optimum cutting temperature (OCT) compound was added to a level of roughly 1–2 mm in the aluminum container and the tissue was floated on top. Then additional OCT compound was added to a level of 5–6 mm. If necessary, the tissue specimen was moved to the center using a scalpel. The upper part of the aluminum foil container was held using Nan forceps and the lower one-third to one-fourth of the container was immersed in the acetone–dry ice solution for freezing and embedding. Freezing was complete just before the top surface of the OCT compound became completely opaque. The frozen tissue was maintained at −80°C; this tissue can be used for several years if placed in thick plastic bags and kept in a vacuum. Adequate records of tissue specimens were kept. Use of a tissue ledger facilitated further use of the stored tissue specimens.

3.4.2.2. Thin-Sectioning of Renal Tissue (Fresh Cryosections)

The tissue was thinly sectioned using a cryostat at −20°C. The block support in the cryostat was removed to cool before usage. The aluminum foil around the OCT compound block containing the renal tissue was removed and the block was placed in

the cryostat. The adhesive tape was removed from the aluminum foil and was stuck on the cryostat. After placing a small amount of the OCT compound on the block support, the block containing the renal tissue was immediately placed on the OTC compound on the block before it had hardened and pushed slightly downward such that the tissue was at the top of the block. A short time was waited and thin sectioning was started once the OTC compound hardened. The sections should be 3–4 pm thick. After preparing the thin sections, the samples were wrapped in fresh aluminum foil, and the foil was wrapped in adhesive tape from the cryostat to preserve the samples. The thin tissue sections were placed on a glass slide. When the sections were in the center of the glass slide, a circle was drawn around the sections using a waterproof pen to avoid excessive use of antibodies.

3.4.2.3. Indirect Double-Staining Method

First, glass slides with tissue specimens were air dried for 20–30 min at room temperature. To eliminate serum protein, the glass slides were placed in the staining basket and washed three times for 5 min each time with PBS. Bovine albumin solution (4%) in PBS was applied to block non-specific endogenous antigens for 30 min. The PBS around the tissue on the glass slides was wiped off with a paper towel and the unlabeled primary antibodies (50–100 µl) were applied using a Pasteur pipette. The glass slide was placed in the staining box and reacted for 1 h at room temperature or overnight at 4°C. After washing 3 times with PBS for 5 min each time, the fluorophore-labeled secondary antibodies were applied and reacted in the same manner as primary antibodies. Aluminum foil was used as a light shield when a plastic container was utilized. The container was sealed to prevent tissue from drying out. After washing 3 times with PBS for 5 min each time, the specimen was mounted using a PD-PBS-glycerin solution, and the glass cover was attached for visualization under a fluorescent microscope (Axiovert 100, Zeiss, Germany). After mounting, the cover glass was sealed with colorless nail polish.

3.5. 2-D DIGE System and Proteomics

Proteomics is the large-scale study of proteins, particularly their structures and functions. Proteomics is typically considered the next step after genomics in studying biological systems. Proteomics is significantly more complex than genomics; although an organism's genome is generally constant, a proteome differs from cell to cell and constantly changes through biochemical interactions with the genome and environment. One organism can have radically different protein expressions in different parts of its body, different stages of its lifecycle and different environmental conditions.

3.5.1. 2-D Electrophoresis and DIGE

2-D electrophoresis is a powerful and widely utilized method for analyzing complex protein mixtures extracted from cells, tissues, or other biological samples. This technique separates proteins based on two independent characteristics in two discrete steps. The first-dimensional step, isoelectric focusing (IEF), separates proteins according to their isoelectric points (pI); the second-dimensional step, sodium dodecyl sulfate-polyacrylamide gel electrophoresis (SDS-PAGE), separates proteins based on their molecular weights (MWs, relative molecular mass). Each spot on the resulting 2-D gel potentially corresponds to a single protein species in the sample. Thousands of different proteins can thus be separated, and information such as protein pI, apparent MW, and the amount of each protein can be acquired.

The 2-D DIGE method labels protein samples prior to 2DE, facilitating accurate analysis of differences in protein abundance between samples. Up to three different samples can be separated within the same 2-D gel. This technology is based on the specific properties of spectrally resolvable dyes that have been designed as both mass- and charge-matched CyDye DIGE Fluor dyes. Consequently, identical proteins labeled with each CyDye DIGE Fluor dye migrate to the same position on a 2-D gel. This ability to separate more than one sample on a single gel permits the inclusion of up to two samples and an internal standard (internal reference) in each gel. The internal standard is prepared by mixing equal amounts of each sample in the experiment and

adding this mixture to each gel. The CyDye DIGE Fluors dyes are size- and charge-matched, pH insensitive, spectrally resolvable, highly sensitive, bright and photostable.

Figure 3.5.1 presents the main steps in the DIGE system workflow. (A) The lysates to be analyzed were labeled with the fluorescent CyDyes Cy3 and Cy5. Additionally, an internal standard was labeled with Cy2. (B) The labeled samples were mixed and then separated according to their isoelectric points (1st dimension) and molecular weight (2nd dimension) in one gel. (C) Decyder software was used to analyze differential expression level of proteins. Samples were normalized using the internal standard. (D) All differentially expressed proteins that were down- or up-regulated >1.5-fold were isolated (picked) from the gel and measured using matrix-assisted laser desorption/ionization time of flight mass spectrometer (MALDI-TOFMS). (E) Peptide mass fingerprint analysis utilized Mascot software. (F) A flowchart illustrates the experimental design for both analytical and preparative gel workflow.

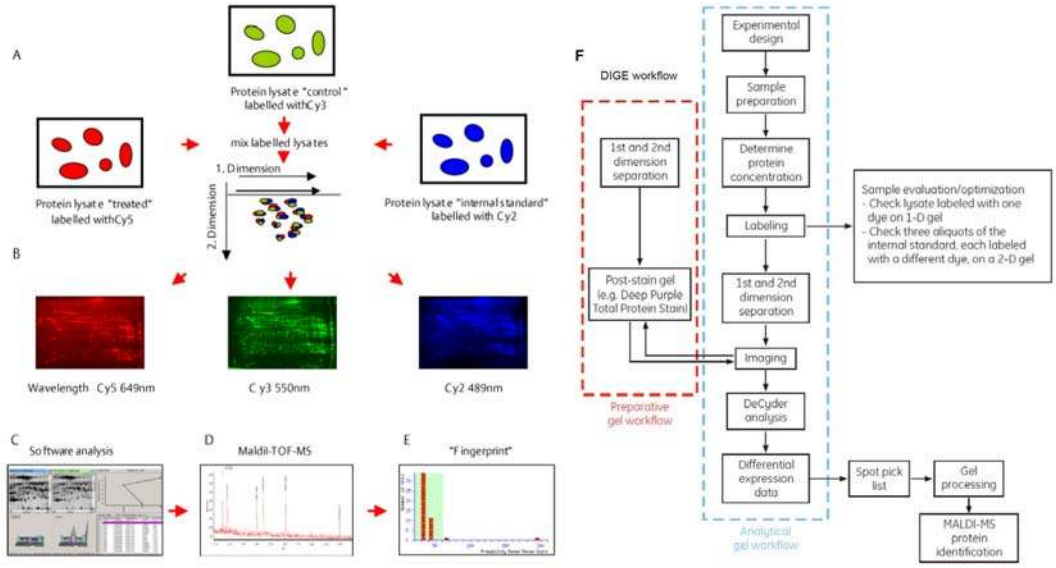

Fig. 3.5.1 Standard processes of 2-D DIGE and proteomics study

3.5.2. Methods for 2-D DIGE and Proteomic Analysis

For two-dimensional polyacrylamide gel–based analysis, podocytes were harvested and homogenized in 2DE lysis buffer (7 M Urea, 2 M Thiourea, 4% CHAPS, and 30 mM Tris) with a micro tissue grinder followed by 3 rounds of sonication (1 min) in an ice bath sonicator at 4°C. Lysates were allowed to rest on ice for 30 min and then centrifuged for 1 h at 16000g. Supernatant protein concentrations were determined as described previously. Protein pH was assessed and adjusted when the pH of the cell lysate was outside the desired range (optimal cell lysate pH is 8.5 for CyDye DIGE Fluor minimal dyes).

The protein samples from vehicle–treated and Ang II–treated podocytes were labeled with Cy3- and Cy5-CyDye DIGE Fluor minimal dyes (GE Healthcare, country), respectively, for 30 min at 4°C. A pooled sample of vehicle–treated and Ang II–treated podocyte lysates was similarly labeled with Cy2-CyDye DIGE Fluor minimal dye for use as an internal control. Excess unlabeled CyDye was inactivated by adding 1 μl 10 mM lysine to stop the reaction.

The Cy3-, Cy5-, and Cy2-labeled samples (50 μg each) were mixed with 1% Bio-Lyte 3-10 IPG buffer, 40 mM DTT, and 0.002% bromphenol blue, and isoelectrically focused on an immobilized pH-gradient strip (24 cm; pH 3–10, non-linear) with a PROTEAN IEF cell. Focusing was performed at 150 V for 3 h (rapid ramp), 300 V for 3 h (rapid ramp), 1000 V for 6 h (slow ramp), 10000 V for 3 h (slow ramp) and 10000 V for 5 h (rapid ramp) to reach approximately 80000 total voltage-hours for isoelectric focusing.

After focusing, strips were equilibrated for 15 min in a solution containing 6 M urea, 30% glycerol, 2% SDS, 50 mM Tris-HCl (pH 8.8), 0.002% bromphenol blue, and DTT (10 mg/mL) followed by a second 15-min equilibration with iodoacetamide (25 mg/mL) instead of dithiothreitol. Strips were briefly rinsed in 1× PAGE buffer and applied to a 12% polyacrylamide gel for electrophoresis at a constant current (16 mA/gel overnight or 72 mA/gel for 5 h). Samples were prepared and then

electrophoresed in triplicate.

A Typhoon scanner in fluorescence mode (GE Healthcare) was utilized to obtain Cy3, Cy5, and Cy2 images of analytical gels at a resolution of 100 µm. Images were analyzed using DeCyder software (GE Healthcare) to identify protein spots exhibiting statistical significant change between groups with the Student's t-test and ANOVA. Preparative gels (loaded to about 1 mg protein of lysate per gel) were then fixed in 30% ethanol and 7.5% acetic acid for 2 h, followed by Coomassie staining overnight for total protein visualization. Identified proteins of interest were picked from preparative gels as gel plugs. Figure 3.5.2 presents one representative preparative gel loaded with AT1R podocyte lysate and stained with Coomassie.

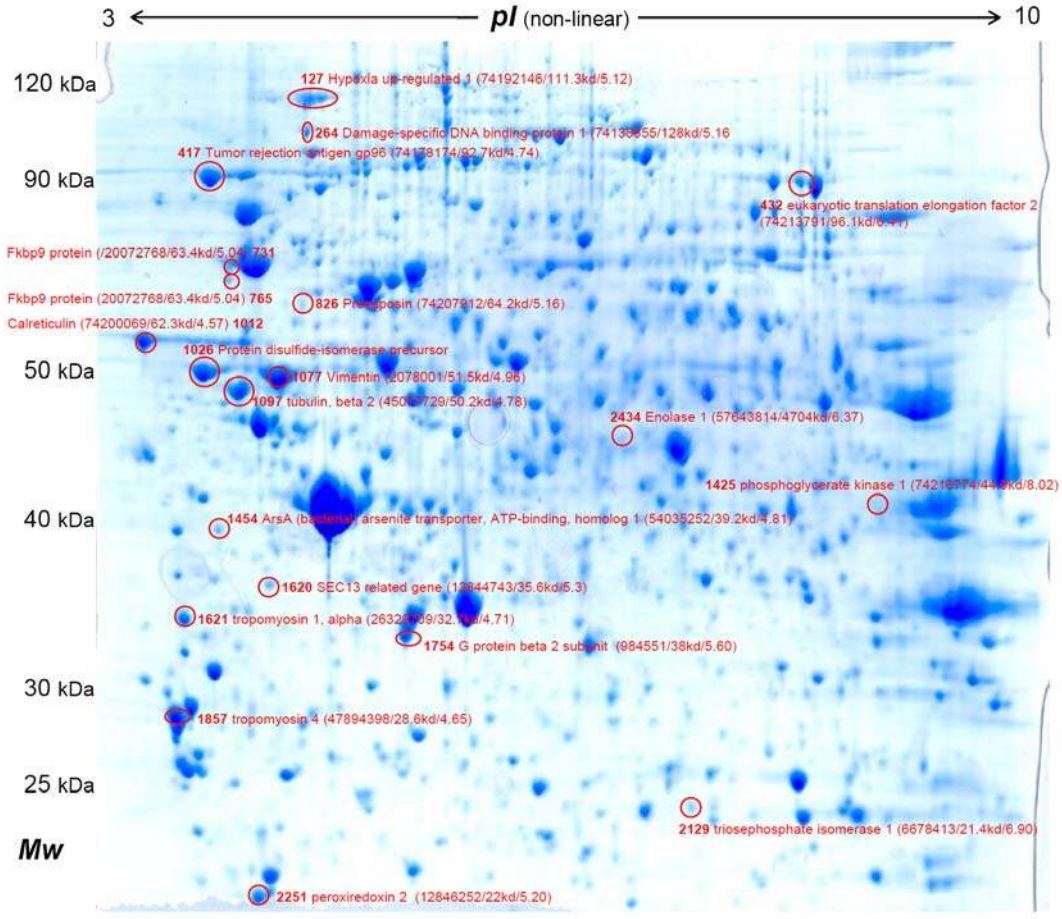

Fig 3.5.2 Coomassie was used to stain preparative gel for protein spot picking and further MS analysis Proteins with differential expression levels (proteins of interest) in the Ang II-treated podocyte proteomic study are marked in red circles.

After trypsin (GE Healthcare) digestion of gel plugs, peptides were extracted and analyzed with an UltraflexIII matrix-assisted laser desorption ionization-tandem time-of-flight mass spectrometer (MALDI-TOF/TOF MS; Bruker Daltonics, Germany), operating in reflection positive-ion mode. The Swiss-Prot database was searched with GPS Explorer software (Applied Biosystems) and the MASCOT search engine (Matrix Sciences) to identify peptide mass data acquired using MALDI-TOF/TOF MS. A peptide group was considered a positive match for a database protein when the confidence interval (CI) for the match, as determined by GPS Explorer, was at least 95% and when spot position on the two-dimensional gel reflected approximately the theoretical isoelectric point and molecular weight of the specified protein. The MASCOT scores >61 were considered significant ($p < 0.05$).

3.6. Gene Silencing

Gene silencing is a general term describing epigenetic gene regulation processes. The term gene silencing is typically utilized to describe the process of "switching off" a gene using a mechanism other than genetic modification. In other words, a gene that would be expressed (turned on) under normal circumstances is switched off by cell machinery. This process has recently been best illustrated via the application of RNA interference (RNAi) to functional genomics, which relies on the ability of double-stranded RNAs (dsRNAs), small interfering RNAs (siRNAs), or small hairpin RNAs to silence a target gene through specific destruction of that gene's mRNA.[120-122]

3.6.1. Mechanisms of RNA Interference

Gene silencing by dsRNA was first observed in plant experiments. In the late 1980s and early 1990s, genetic experiments conducted on petunias yielded unpredicted results. Introducing numerous copies of a gene coding for a deep-purple color generated plants with white or patchy blossoms, not a dark hue as was expected.[123;124] The introduction of genes had silenced both themselves and the plant's intrinsic color-coding genes.

At that time, using antisense oligonucleotides (ASOs), short single-stranded stretches of DNA or RNA with a sequence complementary to their target mRNA, was the state-of-the-art method for gene-silencing experiments. However, experimental results for petunias were not compatible with the mechanism of gene down-regulation by ASOs.

The puzzling findings for color alteration in petunias following transfection remained unexplained for nearly a decade. In 1998, Fire *et al*. determined that injecting dsRNA into Caenorhabditis elegans resulted in potent gene silencing.[120] The dsRNA, several hundred bases in length, not only caused significant gene silencing, but was clearly more active than the corresponding single-stranded antisense molecules; this study obtained a revolutionary finding in the molecular biology field. Since introduced dsRNA molecules interfered with target gene function, the process was termed 'RNA interference'.

These first mechanistic clues to RNAi machinery were obtained from experiments using Drosophila extracts. Briefly, RNAi is initiated by long stretches of dsRNA that undergo processing by an enzyme referred to as a Dicer (Fig. 3.6.1).[125] The Dicer cuts long stretches of dsRNA into duplexes with 19 paired nucleotides and 2 nucleotide overhangs at both 3′ ends.[126] These duplexes are called siRNA. The double-stranded siRNA then associates with the RNA-induced silencing complex (RISC), a fairly large (roughly 160 kDa) protein complex comprising Argonaute proteins as the catalytic core of this complex[127]. Within the RISC, the siRNA is unwound and the sense strand is removed for degradation by cellular nucleases. The antisense strand of the siRNA directs the RISC to the target an mRNA sequence, where it anneals complementarily by Watson-Crick base pairing. Finally, the target mRNA is degraded by RISC endonuclease activity.[128]

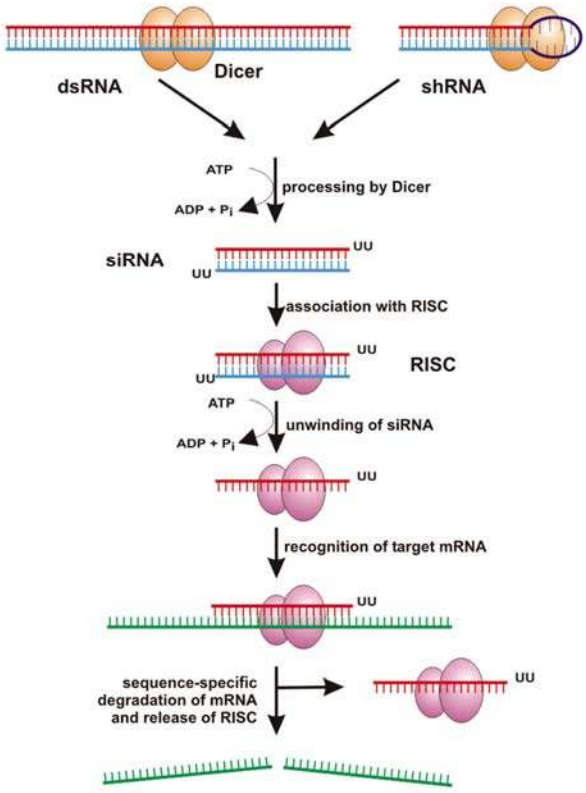

Fig. 3.6.1 The RNA interference pathway Long double-stranded RNA (dsRNA) or small hairpin RNA (shRNA) was processed by Dicer and formed a small interfering RNA (siRNA) that is associated with the RNA-induced silencing protein complex (RISC) and mediates target sequence specificity for subsequent mRNA cleavage. Rutz *et al*. Arthritis Res Ther 2004

This mechanism is fundamentally different from post-transcriptional gene silencing by ASOs. Binding of ASOs to their target mRNA hinders protein translation either by steric hindrance of the ribosomal machinery or induction of mRNA degradation by ribonuclease H (Rnase H).[129] Although gene silencing by ASOs was considered a reliable approach for targeted gene down-regulation in human cell cultures, RNAi was first studied in C. elegans and plants; whether this technique would work in mammalian cells remained unclear. In 2001, Tuschl *et al.* provided the first evidence that siRNAs mediate sequence-specific gene silencing in mammalian cells and that the dicing step can be bypassed via transfecting siRNA molecules into cells.[121] Since, RNAi could be used to study, and perhaps even influence, the molecular basis of human disease.

Notably, RNAi represents an outstanding strategy for controlling gene expression. In contrast to other mRNA-targeting strategies, RNAi utilizes physiological gene-silencing machinery, which may account for the excellent potency of RNAi.

3.6.2. Vector-Based SiRNA

Using DNA vector-based siRNA technology, a small DNA insert (approximately 70 bp) encoding a short hairpin RNA targeting gene of interest is cloned into a commercially available vector. The vector containing the insert, which expresses the short hairpin RNA can be transfected into a cell. The hairpin RNA is rapidly processed by cellular machinery into 19–22 nt double-stranded RNA (dsRNA). Key features of vector-based siRNA are as follows: vector-based siRNA is delivered as a plasmid, which is more stable and easier to handle than synthetic dsRNA and allows one to obtain a stable cell line and observe the long-term effects of RNAi.

However, one important issue must be addressed. Experimental results from synthetic dsRNA or the siRNA cassette cannot be completely transformed into a vector-based siRNA construct. The vector-based siRNA differs from synthetic siRNA oligos and siRNA cassettes. Although experimental results obtained with synthetic siRNA oligos or siRNA cassettes can suggest the most potent siRNA targets, experimental results cannot be duplicated in vector-based siRNA for unknown reasons.

3.6.3. Retroviral SiRNA Vector

The pRNA-TH1.4/Retro vectors contain elements that facilitate packaging of the siRNA construct into retroviral particles. These retroviral particles are then utilized to infect mammalian cells and cause them to express siRNA in host cells. The H1 promoter is employed to drive siRNA expression. A small DNA insert (roughly 70–80 bp) encoding a short hairpin RNA targeting the gene of interest can be cloned into this vector between the Mlu I and Xho I sites. This vector, derived from Murino sarcoma virus, is designed for mammalian transfection and carries a hygromycin resistance gene that can be used to establish a stable cell line.

3.6.4. Cloning SiRNA Insert into pRNA Vectors

Order two oligos with cohesive Xho I and Mlu I sites.

siRNA insert 1(for human peroxiredoxin 2): 71 bp.

Mlu I Xho I

ACGCGTCAAAGAGGACCACGTACTTCTTGATATCCGGAAGTACGTGGTCCTCTTTTTTTTTCCAACTCGAG

| Antisense | Loop | Sense | Termination Signal

siRNA insert 2(for mouse peroxiredoxin 2): 71 bp.

Mlu I Xho I

ACGCGTCAAAGAGGTCCACGTACTTCTTGATATCCGGAAGTACGTGGACCTCTTTTTTTTTCCAACTCGAG

| Antisense | Loop | Sense | Termination Signal

siRNA insert 3(for both human and mouse peroxiredoxin 2): 71 bp.

Mlu I Xho I

ACGCGTCATTCCTTGCTGTCATCCACTTGATATCCGGTGGATGACAGCAAGGAATTTTTTTCCAACTCGAG

| Antisense | Loop | Sense | Termination Signal

Fig. 3.6.4 Oligonucleotide sequences for vector-based short hairpin RNA (upper strand only shown).

The oligos must be PAGE-purified oligos. The oligos were dissolved in water to 1 μg/μl concentration. The two oligos were then annealed. A 20 μl annealing reaction was prepared as follows:

Top-strand oligo, 1 μl

Bottom-strand oligo, 1 μl

20 x SSC, 1 μl

Add H_2O to a final volume of 20 μl

The mixture was heated to 95°C for 10 min, then taken out and allowed to rest at room temperature for 1 h. The mixture was diluted to a final concentration of 40 ng/μl. The vector was cut with Mlu I and Xho I. A 1% agarose gel was used to purify the vector. The vector was ligated with the insert using T4 ligase (molar insert-to-vector ratio was 3:1).

The ligation mixture was transformed into competent DH5α cells and plated on Luria-Bertani Medium (LB)-ampicillin plates. At least 15 clones were chosen and grown. MiniPreps from the culture were prepared and the plasmids cut with Xho I and Mlu I. A 3% gel was run to determine whether the plasmids have the insert and select positive clones. The positive clones were sequenced to verify the insert sequence.

3.6.5. Producing Retroviral Particles and Infecting Cells

The RNA short hairpin gene-containing virus was produced by co-transfecting HEK293 cells with three plasmids (2.5 μg pMD.G, 7.5 μg pMD. gag/pol and 10 μg pRNA-TH1.4/Retro-mPrdx2/SH1) using the calcium phosphate method. The following procedures are exactly the same as described in Section 3.2.3 (Retroviral Gene Delivery).

3.7. Statistical Analysis

All data are presented as means ± SEM unless specified otherwise. Group differences were tested by Student *t*-tests. More than two groups were compared by two-way ANOVA (SPSS, Chicago, IL, USA). Statistical significance was $p < 0.05$.

4. Results

4.1. Establishment and Characterization of a Stable Ang II-Responsive Podocyte cell line

Immortalized mouse podocytes in culture were not consistently responsive to Ang II with elevated intracellular calcium concentrations ($[Ca^{2+}]_i$). To elucidate AT1R signaling mechanisms, human AT1R was stably expressed in a murine podocyte cell line known to show dominant stress fiber formation.[113] Stable human AT1R expression was verified by RT-PCR (Fig. 4.1.1), and Flag-tag immunoprecipitation (Fig. 4.1.2) and two-dimensional immunoblotting (Fig. 4.1.3).

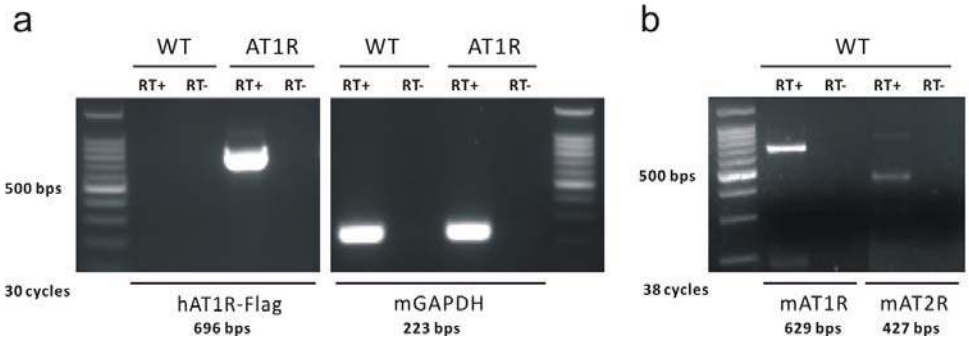

Fig. 4.1.1 RT-PCR of wild type and AT1R podocytes (a) The RT-PCR results show that Flag-tagged AT1R transgene was only expressed in transduced podocytes (AT1R cells) using Flag tag sequence containing primers. Endogenous GAPDH mRNAs were detected with the same reaction condition as that for the internal control. **(b)** Endogenous AT1R and AT2R mRNAs were detected in wild-type (WT) podocytes in the same reaction condition but with more PCR reaction cycles. RT+, reverse transcriptase added; RT-, H_2O added in stead of reverse transcriptase; hAT1R, human AT1R; mAT1R, mouse AT1R; mAT2R, mouse AT2R; mGAPDH, mouse glyceraldehyde-3-phosphate dehydrogenase; bps, base pairs.

Retroviral transduction of the human AT1R gene enables differentiated cultured podocytes to express additional AT1R (2.72 ± 0.37-fold increase) than wild-type cells (Fig. 4.1.3). Empty vector transducted cells were generated as controls.

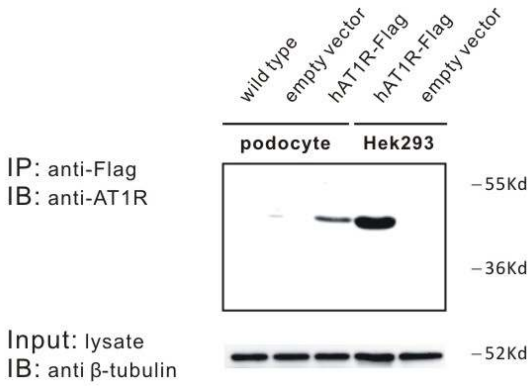

Fig. 4.1.2 Immunoprecipitation of Flag-tagged hAT1R in cultured podocytes Flag-tagged hAT1R were only precipitated in stably transducted AT1R podocytes and transiently transfected Hek cells. Immunostaining of β-tubulin demonstrates that each lane was equally loaded. IP, immunoprecipitation; IB, immunoblotting.

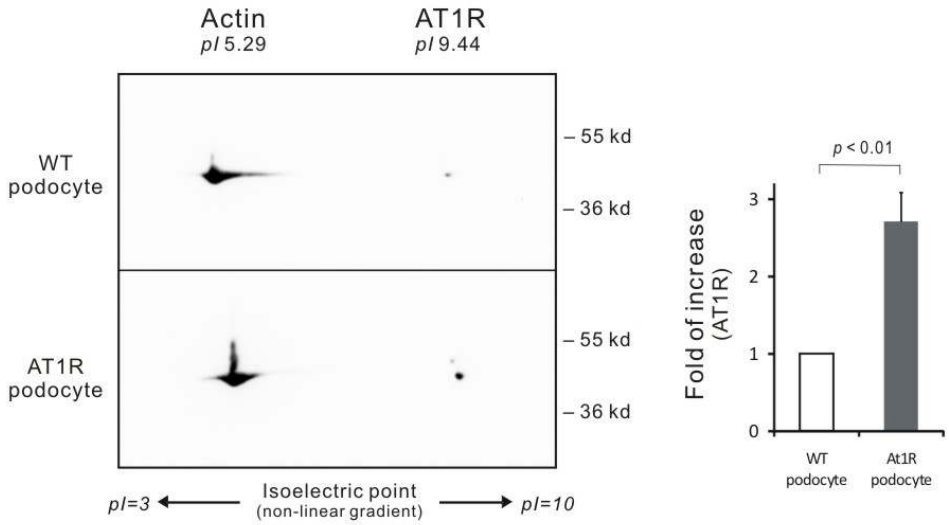

Fig. 4.1.3 Two-dimensional immunoblotting of wild type and AT1R podocytes Equal amounts of proteins (400–600 µg in each experiment) from differentiated cultured podocyte lysates were separated by two-dimensional electrophoresis followed by immunoblotting. Quantified signal intensities of AT1R representing spots (calibrated by signal intensity of actin) reveal that AT1R was increased 2.72 ± 0.37-fold in stably transducted cells (AT1R podocytes) compared with that of wild type (WT) cells (mean ± SEM, n = 4, $p < 0.01$). The second bar shows the AT1R expression level as a ratio factored for the first bar.

Intracellular Ca^{2+} measurements indicate that differentiated AT1R podocytes responded with a significant and reversible $[Ca^{2+}]_i$ increase after 100 nM Ang II stimulation (Fig. 4.1.4 a). The Ang II–triggered $[Ca^{2+}]_i$ increase was concentration-dependent (Fig. 4.1.4 b, lanes 1–5), steadily responsive (AT1R cells

versus wild-type cells) and was inhibited by pre-treatment with losartan, an AT1R-specific antagonist (Fig. 4.1.4 b, lane 6).

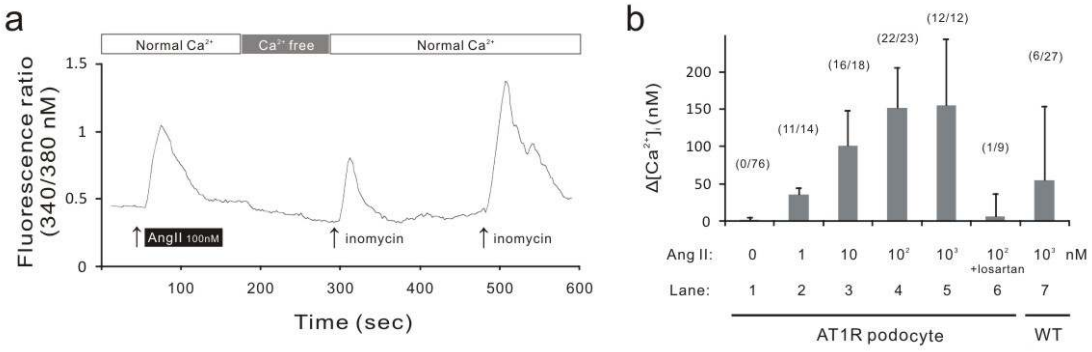

Fig. 4.1.4 Intracellular Ca^{2+} measurements of wild-type and AT1R podocytes (a) Fluorescence recordings demonstrate the effects of Ang II on $[Ca^{2+}]_i$ in AT1R podocytes (inomycin 1 μM was used to calibrate $[Ca^{2+}]_i$ after experiments). **(b)** The plot summarizes experimental results for $[Ca^{2+}]_i$ response of podocytes to different Ang II concentrations and losartan (200 nM). Wild type (WT) podocytes in culture were not consistently responsive to Ang II with elevated $[Ca^{2+}]_i$ (lane 7). Parentheses above each bar: (number of positive responses/number of stimulations).

Moreover, expression of Ang II type 2 receptors (AT2R), known to exert opposite effects on Ang II signaling,[130] was up-regulated in AT1R podocytes accompanying increased AT1R expression (Fig. 4.1.5 a). Single stimulation of AT2R achieved by combined treatment (Ang II 100 nM and losartan 200 nM) suppressed AT2R expressions in AT1R podocytes (Fig. 4.1.5 b), indicating that Ang II modulates crosstalks between AT1Rs and AT2Rs.

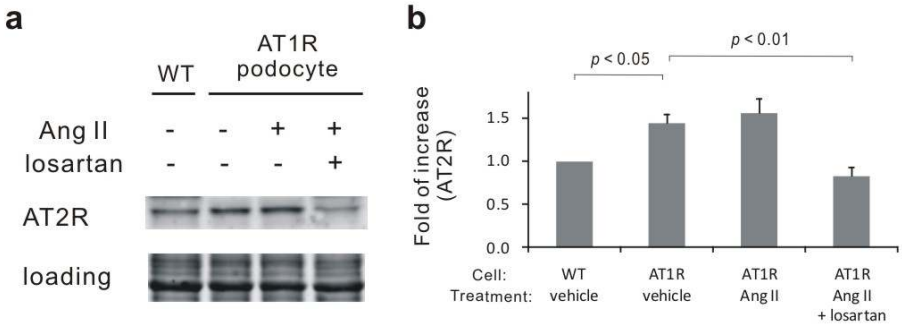

Fig. 4.1.5 AT2R in up-regulated in AT1R stably transduced podocytes in an Ang II-responsive manner Representative immunoblotting and quantitative analysis of AT2R in cultured AT1R podocytes treated with Ang II (100 nM), Ang II with losartan (200 nM) or vehicle for 24 h (n = 3). Signal intensity of each band was standardized by quantitative SYPRO Ruby gel stain to eliminate the effects of differential loading. Each bar represents protein expression levels as a ratio factored for the first bar (means ± SEM). WT, wild type cultured podocyte.

Therefore, we conclude that AT1R podocytes, which respond constantly with $[Ca^{2+}]_i$ increases, comprise a novel and reliable cultured podocyte model for investigating Ang II signal mechanisms.

4.2. Increased Rac-1 Expression in Cultured AT1R Podocytes and in Glomeruli of Neph-hAT1 TGRs

Figure 4.2 a shows that cytosolic Rac-1 expression increased after treating differentiated cultured AT1R podocytes with Ang II (100 nM, n = 3). The effects of Ang II on Rac-1 expression were limited by pre-treating cells with losartan (200 nM).

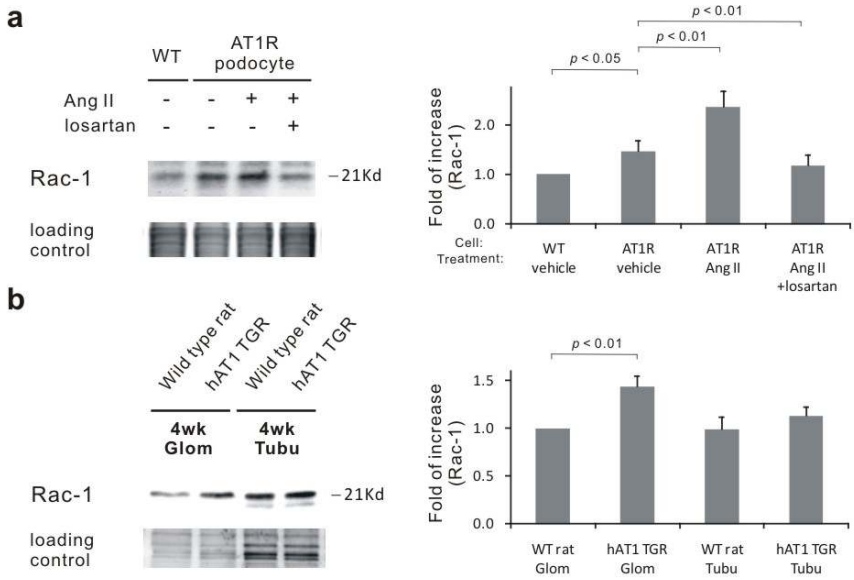

Fig. 4.2 Increased Rac-1 expression in cultured AT1R podocytes and in glomeruli of Neph-hAT1 TGRs (a) Representative immunoblotting and quantitative analysis of Rac-1 in cultured AT1R podocytes treated with Ang II (100 nM), Ang II with losartan (200 nM) or vehicle for 24 h (n = 3). Signal intensity of each band was standardized by quantitative SYPRO Ruby gel stain to eliminate the effects of differential loading. Each bar represents protein expression levels as a ratio factored for the first bar (means ± SEM). **(b)** Representative immunoblotting and quantitative analysis of Rac-1 expression in kidney tissues from 4-week-old Neph-hAT1 TGRs and age-matched littermates (WT rat). Glomerular expression of Rac-1 was significantly higher in Neph-hAT1 TGRs than in WT rats (1.44 ± 0.12-fold *versus* WT, n = 6, $p < 0.01$). Tubular Rac-1 expression levels in Neph-hAT1 TGRs and WT rats did not differ significantly. Glom, glomerulus; Tubu, tubule; WT, wild type.

To determine whether Rac-1 impacts the AT1R signaling of podocyte damage *in vivo*, the expression of Rac-1 was examined in glomeruli and tubuli from 4-week-old podocyte-specific Neph-hAT1 TGRs and WT rats.[60] At 4 weeks, Neph-hAT1 TGRs and age-matched littermates were phenotypically indistinguishable and nonproteinuric. Figure 4.2 b presents Western blotting results. Glomerular Rac-1 expression in Neph-hAT1 TGRs was 1.44-fold that of WT rats, whereas glomerular Rac-1 expression was not significantly altered in the tubuli of Neph-hAT1 TGRs (n = 6).

4.3. Effects of Ang II on ROS Generation and Migration in Podocytes

Analysis of nicotinamide adenine dinucleotide phosphate (NADPH)-dependent oxidase activity demonstrate that differentiated cultured AT1R podocytes pre-stimulated with Ang II (100 nM, 24 hrs) produced more superoxide anions ($O_2^{\cdot-}$) than those in the vehicle-treated group (Fig. 4.3.1). The ROS-activating effect of Ang II was suppressed by losartan (200 nM), implying that an AT1R-specific mechanism exists.

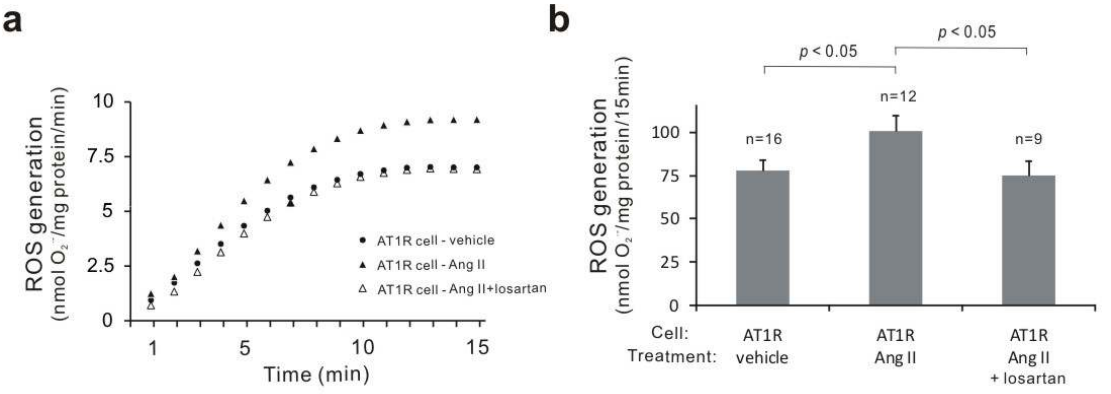

Fig. 4.3 Effects of Ang II on ROS production in podocytes (a) Illustrated time-dependent ROS ($O_2^{\cdot-}$) production in cultured AT1R podocytes with different pre-stimuli; **(b)** Summary of relative change in total ROS production in cultured AT1R podocytes pre-stimulated with Ang II (100 nM), Ang II + losartan (200 nM) or vehicle for 24 h. The NADPH-dependent ROS production increased in Ang II pre-stimulated podocytes (100.6 ± 9.2 nmol $O_2^{\cdot-}$/mg protein/15 min *versus* the vehicle-treated group: 78.0 ± 6.1 nmol $O_2^{\cdot-}$/mg protein/15min, $p < 0.05$). Losartan exhibited a significant inhibitory effect on Ang II-induced ROS production.

An *in vitro* wound healing ('scratch') assay of confluent AT1R cells reveals that Ang II (100 nM, 24 h) pre-treatment increased cell migration (Fig. 4.3.2 a). Losartan (200 nM) or SCH51344, a Rac-1 specific inhibitor (10 μM), or DMTU, a free radical scavenger (10 mM), significantly attenuated Ang II–induced cell migration. Pre-treating cells with PD123319, an AT2R specific inhibitor (200 nM), did not alter the Ang II–mediated increase in cell migration (all n = 12; Fig. 4.3.2 b).

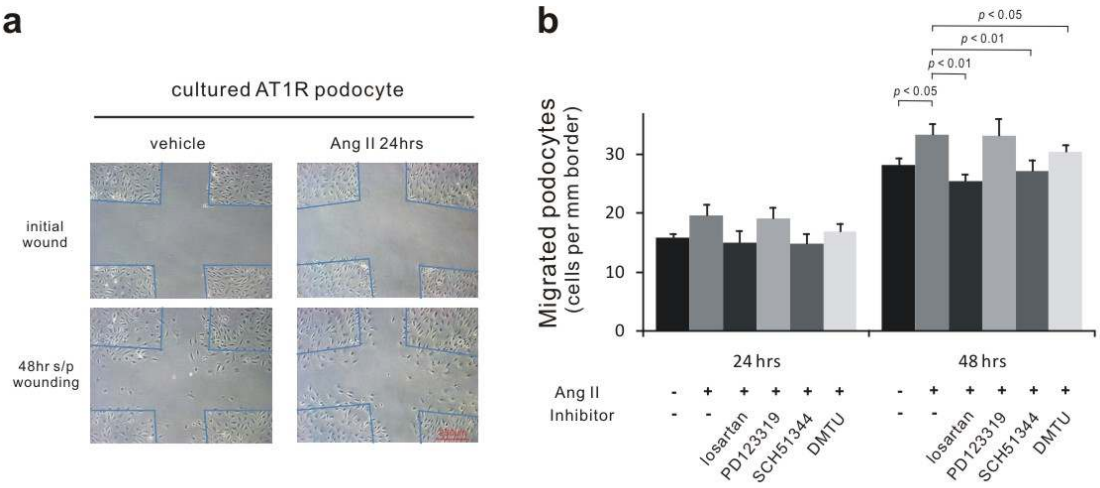

Fig. 4.3.2 Rac-1–mediated Ang II effects on cell migration in podocytes (a) The *in vitro* wound healing ('scratch') assay for assessing podocyte migration. Movement of differentiated AT1R podocytes in culture into the wound with the vehicle or Ang II (100 nM, 24 h) pre-treatments represents cell migration. **(b)** Mean values of cell migration, expressed as number of cells crossing a 1 mm wound border (cells/mm border ± SEM), were calculated at 24 h and 48 h after creating the wound (n = 12 for each group). Losartan (200 nM), PD123319 (200 nM), SCH51344 (10 μM), DMTU (10 mM), scale bar = 250 μm.

4.4. Characterization and Quantification of Rac-1-Mediated Podocyte Cytoskeletal Reorganization in AT1R Signaling

Cell imaging shows increased lamellipodium activity and membrane ruffles in Ang II–treated single podocytes (Fig. 4.4.1 a). Furthermore, fluorescence microscopy reveals features of Ang II–mediated cytoskeletal reorganization in podocytes, including cortical F-actin ring formation and stress fiber attenuation (Fig. 4.4.1 b).

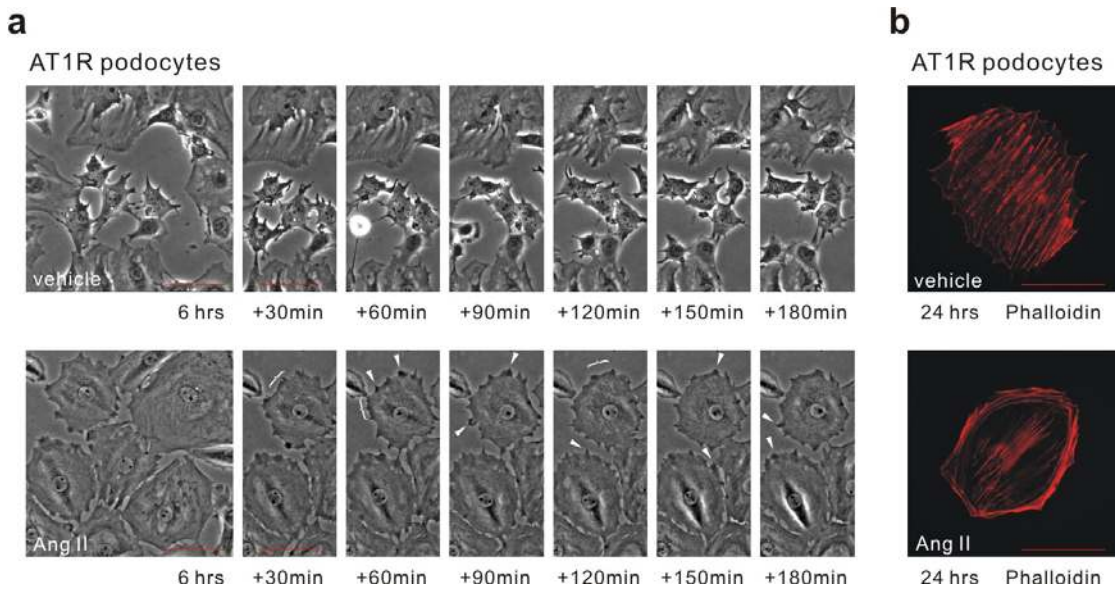

Fig. 4.4.1 Life cell imaging and staining of AT1R podocytes (a) Time-lapse phase contrast imaging of differentiated AT1R podocytes in culture Ang II–treated (100 nM) cells revealed increased lamellipodia (arrowheads) and membrane ruffles (quotation marks). **(b)** F-actin cytoskeletal reorganizations triggered by Ang II (100 nM, 24 h) in sparsely cultivated AT1R podocytes stained with fluorescein-conjugated phalloidin. All scale bar = 50 µm.

In confluent cultivated podocytes, an identical F-actin cytoskeletal rearrangement was identified following Ang II stimulation (Fig. 4.4.2).

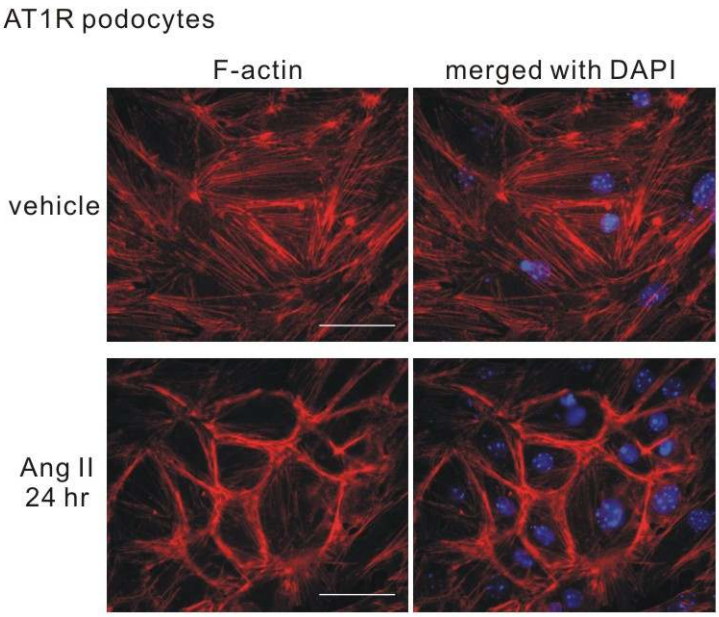

Fig. 4.4.2 Confluent cultivated AT1R podocytes revealed the same cytoskeletal change in response to Ang II stimulation Scale bar = 50 µm

A cortical F-actin score index (CFS index) (Fig. 3.4.1) was constructed to quantify the extent of cytoskeletal reorganization in cultured podocytes at varying Ang II concentrations. Figure 4.4.3a presents the concentration-response curve for the effects of Ang II on CFS index in AT1R podocytes (n = 3).

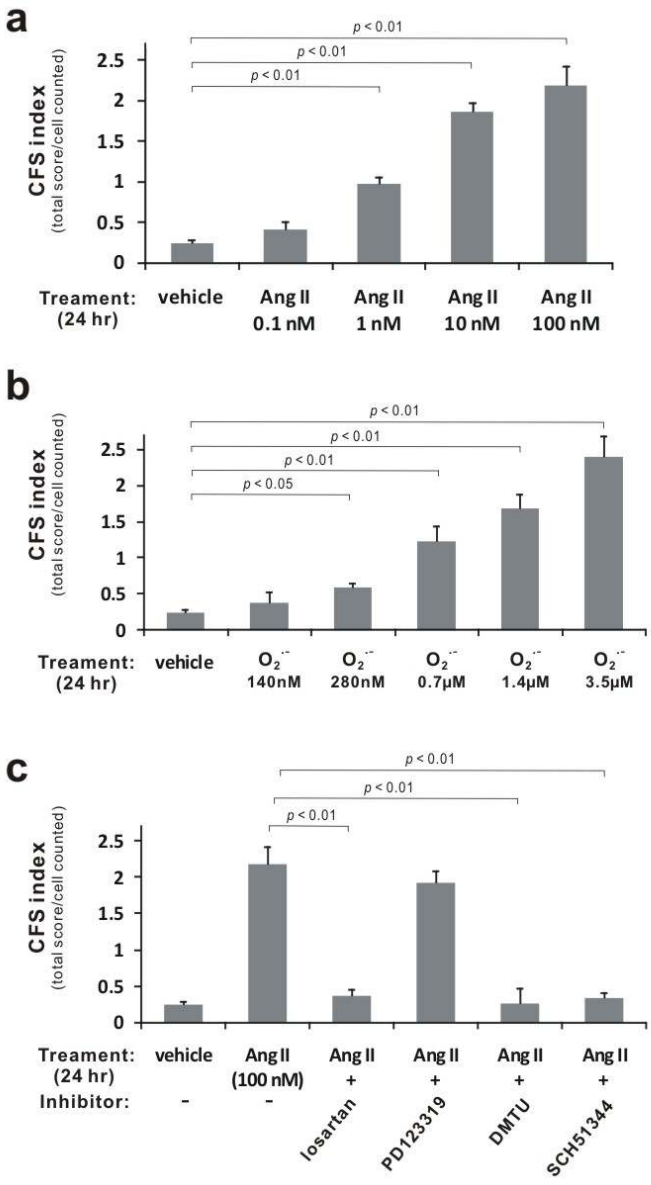

Fig. 4.4.3 Ang II and ROS induced concentration-dependent cytoskeletal changes in AT1R podocytes (a-c) Degree of F-actin cytoskeletal reorganization for each individual cell was assessed with a score of 0 to 3 based on degree of cortical F-actin formation. At minimum three independent experiments were performed, and over 600 cells were scored in each group. The CFS index for Ang II– or vehicle-treated podocytes is presented as average score for cells counted ± SEM. In **(c)**: Ang II, 100 nM; losartan, 200 nM; PD123319, 200 nM; DMTU, 10 mM; SCH51344, 10 µM.

Like Ang II, ROS induced concentration-dependent cytoskeletal changes in AT1R podocytes (Fig. 4.4.3 b, n = 3). The inhibitory effects of losartan, DMTU and SCH51344 on Ang II–induced change to the CFS index indicates that Ang II–mediated cytoskeletal reorganization in podocytes was mediated by an AT1 receptor, ROS and Rac-1 (Fig. 4.4.3 c, n = 3).

4.5. Rac-1 mediates Ang II–induced ERM protein phosphorylation

ERM proteins are crucial components linking the cortical F-actin cytoskeleton to membrane proteins at the peripheries of cells.[70] To elucidate the influences of ERM proteins on AT1R signaling pathways resulting on cytoskeletal reorganization in podocytes, Ang II–stimulated cultured AT1R podocytes were analyzed by immunofluorescent staining. Ang II induced threonine phosphorylation of ERM proteins, and localization of phosphorylated ERM (pERM) proteins existed primarily at the peripheries of AT1R podocytes (Fig. 4.5.1). The Rac-1 inhibitor SCH51344 inhibited the effects of Ang II on ERM protein phosphorylation, demonstrating that cortically distributed pERM proteins are downstream effectors of Rac-1 and mediate F-actin reorganization during AT1R signaling (Fig. 4.5.1).

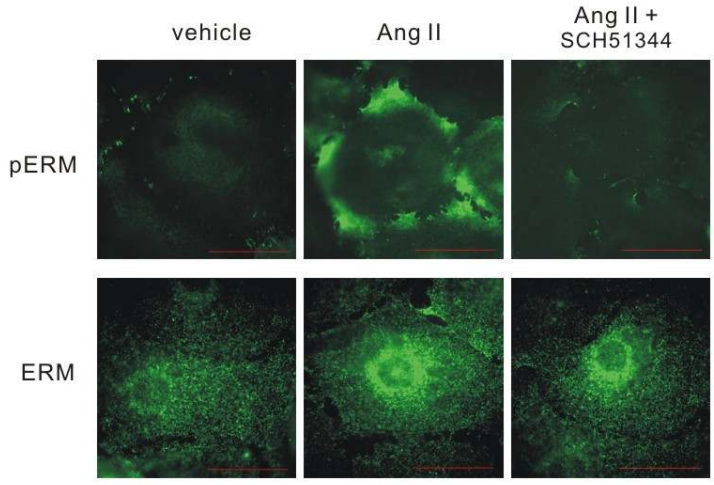

Fig. 4.5.1 The immunostainings of pERM and ERM proteins in AT1R podocytes The pERM proteins were increased and predominantly localized on the peripheries of AT1R podocytes following Ang II treatment (100 nM), and SCH51344 (10 μM) inhibited these effects. The ERM protein staining results indicate that no distributional difference exists before and after Ang II treatment (n =3, scale bar = 50 μm).

Immunoblotting results confirmed that AT1R mediates Ang II–induced ERM protein phosphorylation (Fig. 4.5.2 a). Ang II (100 nM, 24 h)–induced ERM protein phosphorylation was suppressed by losartan (200 nM), SCH51344 (10 μM) and DMTU (10 mM), indicating that AT1R, Rac-1 activation and ROS production are essential to this process. Both the absolute amount of phosphorylated pERM protein and percentage of total phosphorylated ERM protein increased in Ang II–treated AT1R podocyte (Fig. 4.5.2 b, n = 3).

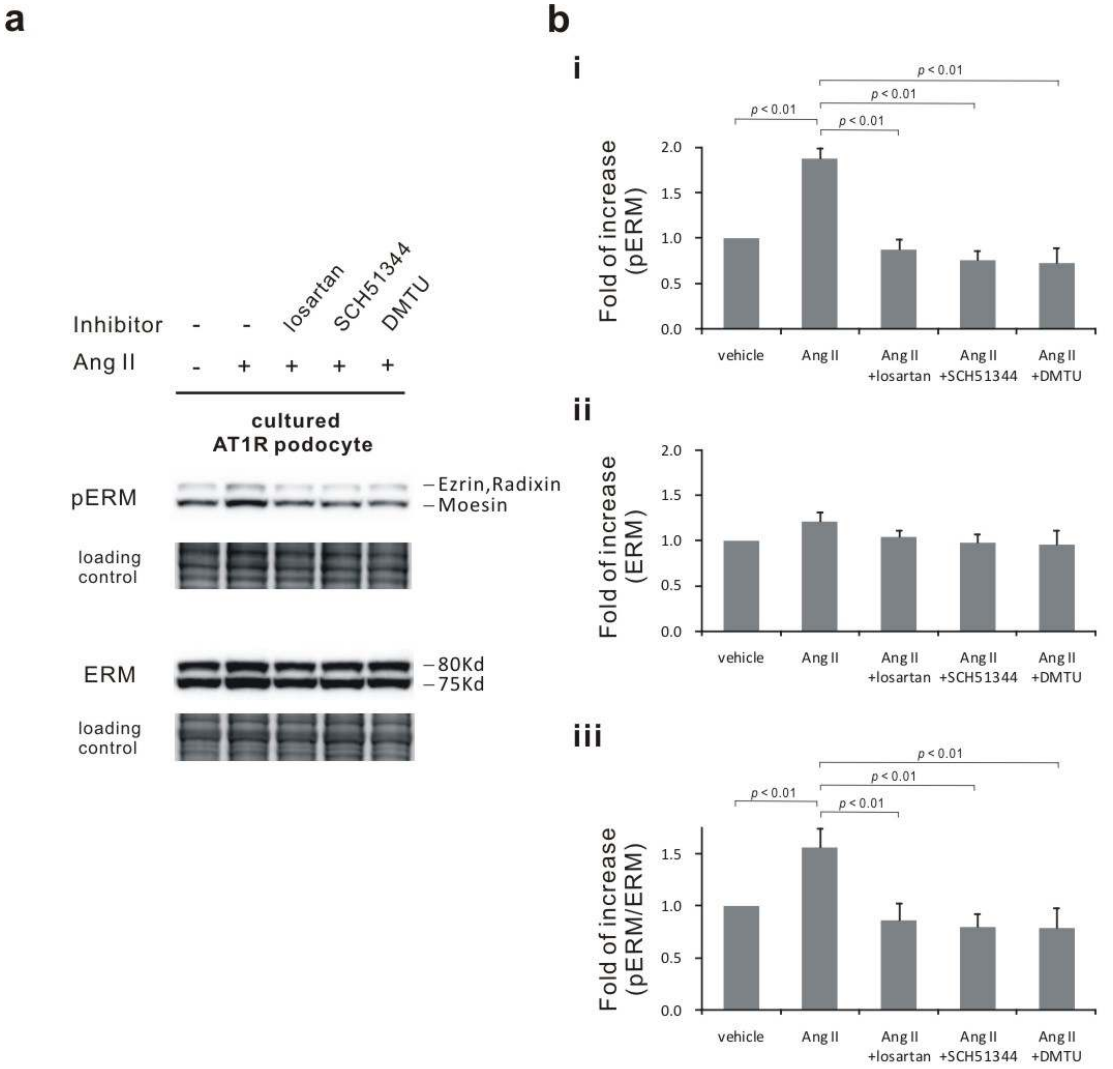

Fig. 4.5.2 Rac-1 mediates Ang II–induced ERM protein phosphorylation in immunoblotting (a) Representative immunoblotting of pERM and ERM protein expression in cultured AT1R podocytes. Ang II, 100 nM, 24h; losartan, 200 nM; SCH51344, 10 μM; DMTU, 10 mM. **(b)** Quantitative analysis plots for expression levels of (i) pERM proteins, (ii) total ERM proteins and (iii) percentage of total ERM protein phosphorylated. Signal intensity of each band was standardized as described earlier, and each bar represents protein expression levels as a ratio factored for the first bar (n = 3).

In glomeruli of Neph-hAT1 TGRs, immunoblotting results demonstrate that both total and proportional phosphorylated ERM proteins were increased compared those of age-matched littermates (Fig. 4.5.3, n = 5).

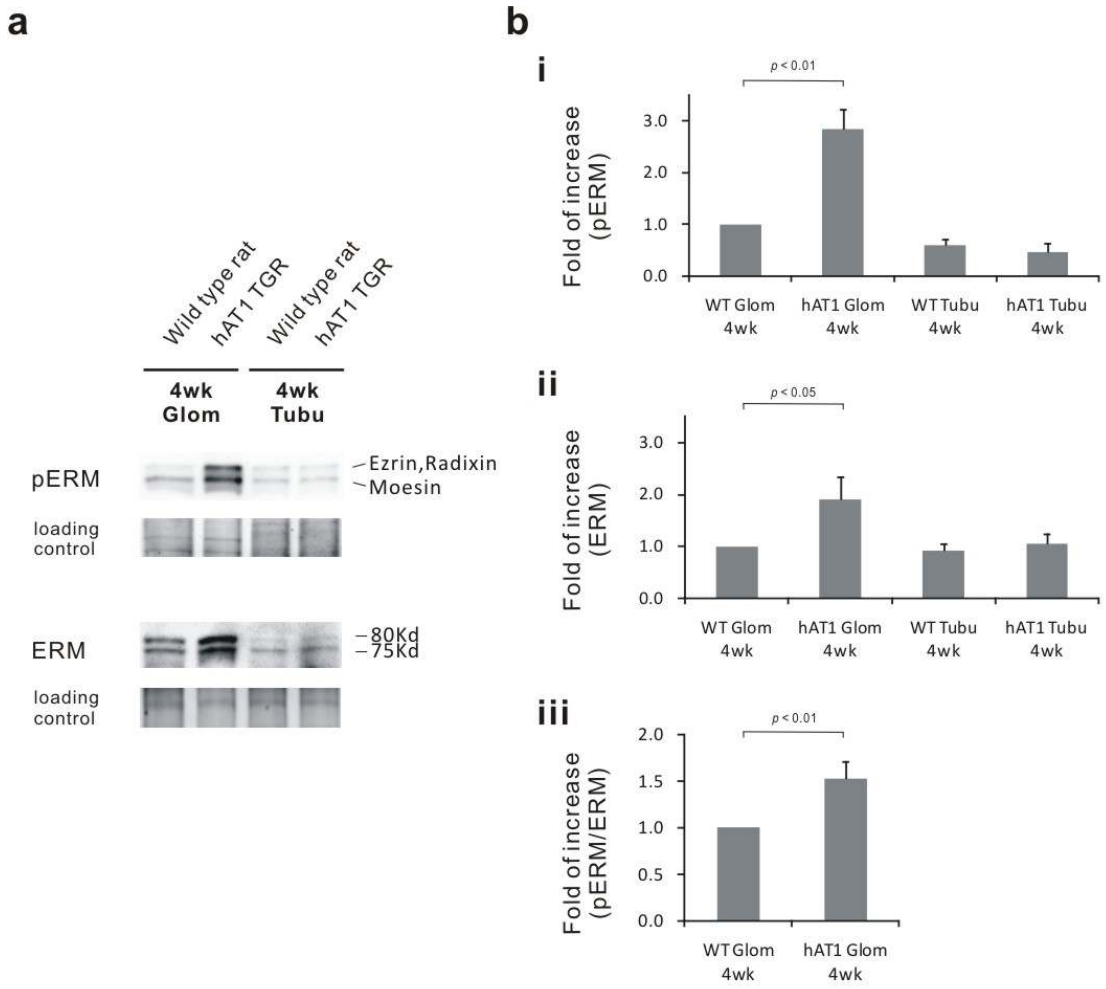

Fig. 4.5.3 pERM expression is increased in Neph-hAT1 TGR glomeruli (a) Representative immunoblotting of pERM and ERM protein expressions in kidney tissues from Neph-hAT1 TGRs and age-matched littermates (WT). **(b)** Quantitative analysis plots for expression level of (i) pERM proteins, (ii) total ERM proteins and (iii) percentage of total phosphorylated ERM protein. Signal intensity of each band was standardized as mentioned previously, and each bar represents protein expression levels as a ratio factored for the first bar (n = 5)

To elucidate signaling mechanisms resulting in ERM phosphorylation by Ang II, the effects of different serine/threonine kinase inhibitors on ERM protein phosphorylation were investigated. Heparin (a potent G protein-coupled receptor kinase 2 (GRK2) inhibitor), and not Y27632 (Rho kinase inhibitor), SB203580 (p38 MAPK inhibitor) or calphostin C (pan protein kinase C inhibitor), abated ERM protein phosphorylation in

Ang II–treated podocytes (Fig. 4.5.4, n = 3).

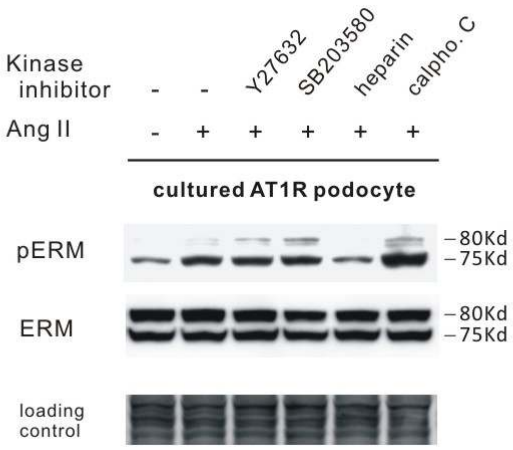

Fig. 4.5.4 Heparin inhibits ERM protein phosphorylation in AT1R signaling of podocytes Representative immunoblotting results for different signaling inhibitors after eliminating Ang II–induced ERM protein phosphorylation in cultured AT1R podocytes (n = 3). Y27632, 10 μM; SB203580, 10 μM; heparin, 10 μM; calphostin C, 0.1 μM.

Moreover, heparin inhibited the effect of Ang II on F-actin cytoskeletal reorganization of podocytes (Fig. 4.5.5).

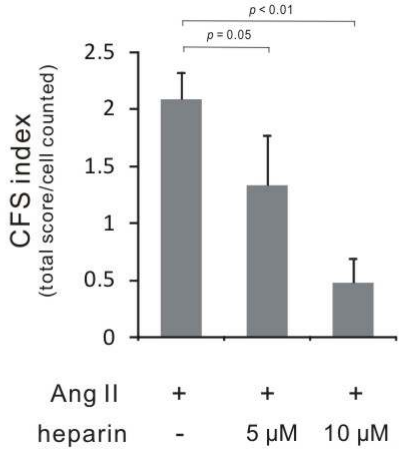

Fig. 4.5.5 Heparin inhibits the effect of Ang II on F-actin cytoskeletal reorganization of podocytes The CFS index was used to quantify the canceling effects of heparin on Ang II (100 nM, 24 h)–induced F-actin cytoskeletal reorganizations. At least three independent experiments were performed, and >600 cells were examined and scored for each group.

4.6. Alpha actinin-4 is down-regulated in Neph-hAT1 TGR glomeruli and Ang II–treated cultured podocytes

The α actinin-4, encoded by the FSGS gene ACTN4,[35] is an actin bundle cross-linker and is also required for normal podocyte adhesion.[92] To explore further the mechanisms linking chronically increased AT1R signaling in podocytes and proteinuria, expression levels of α actinin-4 in Neph-hAT1 TGRs (Fig. 4.6.1 a) were determined. Glomerular expression of α actinin-4 increased more than 2-fold in 4-week-old Neph-hAT1 TGRs (Fig. 4.6.1 b i: 2.18 ± 0.24 fold, 4-wk hAT1 TGR glom *versus* WT). Thereafter, decreased glomerular expression of α actinin-4 was detected in 15-week-old Neph-hAT1 TGRs that exhibited proteinuria (Fig. 4.6.1 b ii, 0.82 ± 0.10 fold, 15-wk hAT1 TGR glom *versus* WT).

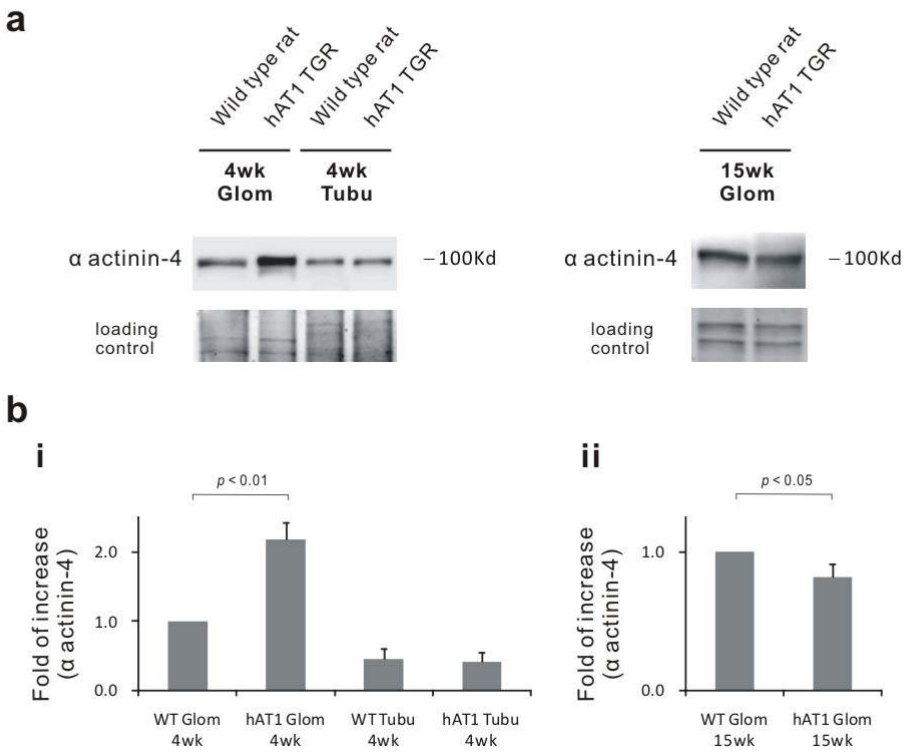

Fig. 4.6.1 Alpha actinin-4 is down-regulated in Neph-hAT1 TGR glomeruli and Ang II–treated cultured podocytes (a) Representative immunoblotting results for α actinin-4 expression in kidney tissues from 4-week-old and 15-week-old Neph-hAT1 TGRs and age-matched littermates. **(B)** Quantitative analysis plots for expression levels of α actinin-4. Signal intensity of each band was standardized as previously mentioned, and each bar shows α actinin-4 expression levels as a ratio factored for the first bar (n = 5 for 4-week-old rats, n = 3 for 15-week-old rats).

Expression of α actinin-4 was also down-regulated in cultured AT1R podocytes after 24-h treatment with Ang II (Fig. 4.6.2). Notably, SCH51344, Y27632, heparin, and not SB203580 nor calphostin C, suppressed the effects of Ang II on α actinin-4 expression in AT1R podocytes, implying that Rac-1 signaling, RhoA signaling and F-actin cytoskeletal reorganization, but neither P38MAPK nor protein kinase C, regulate α actinin-4 expression.

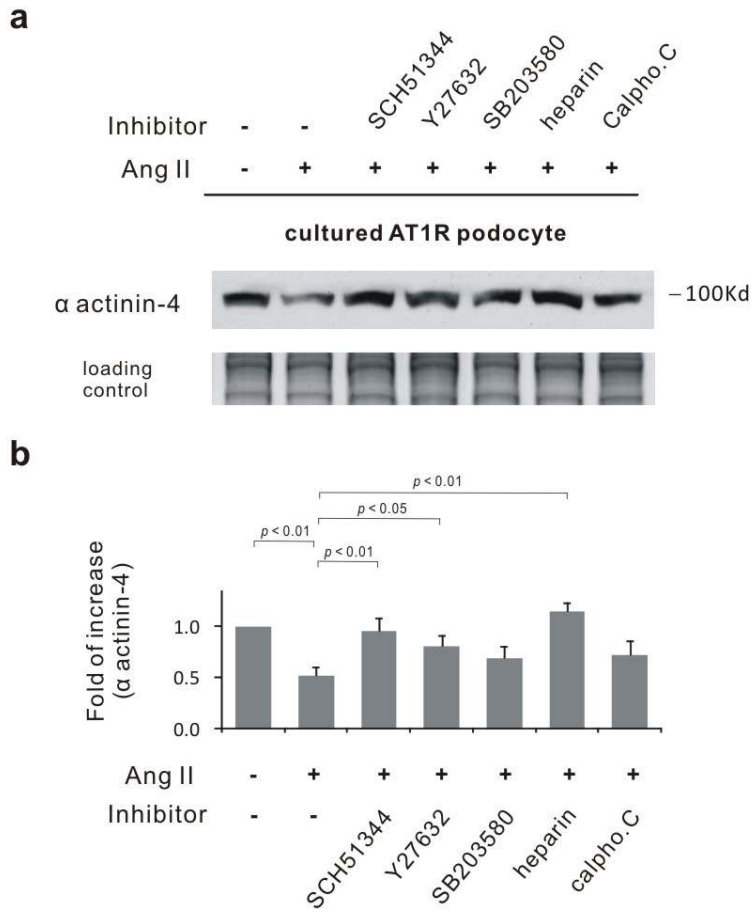

Fig.4.6.2 Rac-1 signaling, RhoA signaling and F-actin cytoskeletal reorganization regulate alpha actinin-4 expression in AT1R podocytes (a) Representative immunoblotting results for α actinin-4 expression in cultured AT1R podocytes treated with Ang II (100 nM, 24 h) combined with different inhibitors (SCH51344, 10 μM; Y27632, 10 μM; SB203580: 10 μM; heparin, 10 μM; calphostin C, 0.1 μM). **(b)** Quantitative analysis plots for expression levels of α actinin-4 in AT1R podocytes with different treatments. Signal intensity of each band was standardized as mentioned previously, and each bar represents α actinin-4 expression levels as a ratio factored for the first bar (n = 3).

Double immunostaining results demonstrate that the α actinin-4 staining of vehicle-treated podocytes was confined to F-actin stress fibers (indicated by

arrowheads) and focal adhesions at the ends of stress fibers (indicated by arrows) (Fig. 4.6.3 a). Ang II (100 nM, 24 h) treatment induced a reduction in α actinin-4 staining, down-regulation of focal adhesions and redistributed α actinin-4 to the periphery of cells as focal complexes (indicated by stars). Using the focal adhesion kinase (FAK)-specific antibody to detect cell-matrix interactions (focal adhesions and focal complexes), this study confirmed further that Ang II induced a phenotypical change, shifting from a dynamic-stable state (focal adhesions associated with F-actin stress fibers) to a migratory state (focal complexes associated with membrane ruffles). (Fig. 4.6.3 b)

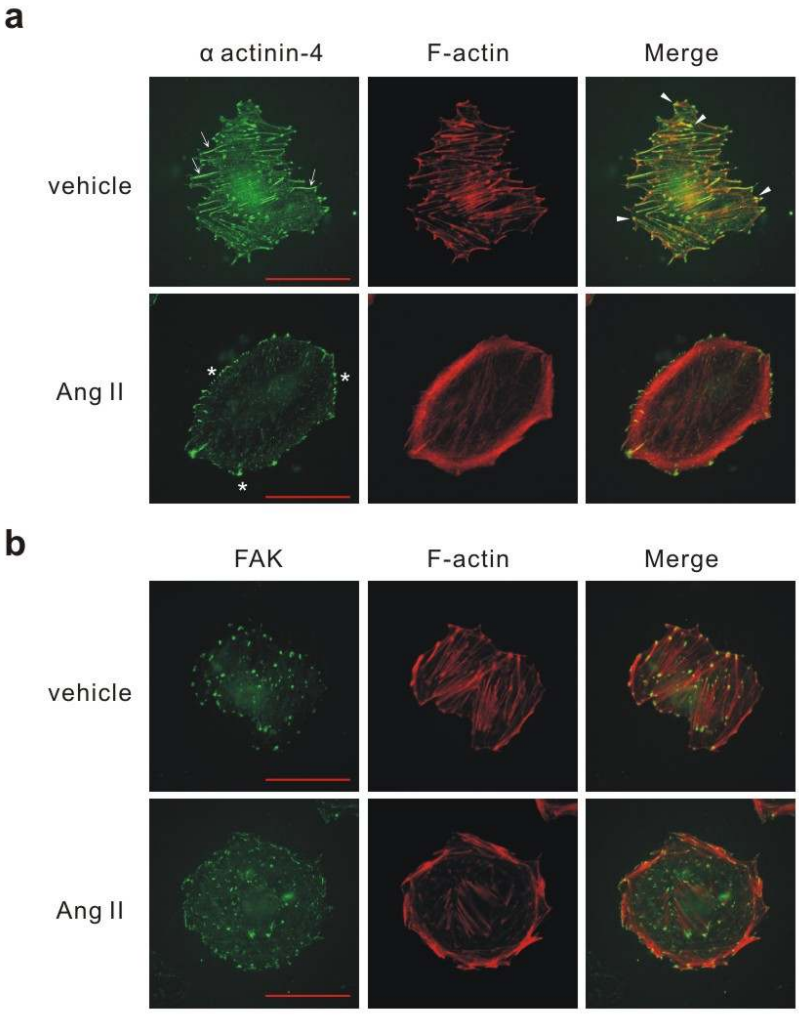

Fig. 4.6.3 Immunostaining of adhesion molecules in AT1R podocytes (a) Immunostaining results for α actinin-4 (green) and F-actin (red) in cultured AT1R podocytes. Although Ang II induced stress fiber attenuation in podocytes; the number of focal adhesions (indicated by arrowheads) was also decreased. Arrows the α actinin-4 staining, which is cross-linked with stress fibers. Stars: focal complexes. **(b)** Immunostaining of FAK (green) shows similar distribution pattern changes. Scale bar = 50 µm.

4.7. Slit Diaphragm Protein—Nephrin is Down-Regulated in AT1R signaling

The expression level of a slit diaphragm protein, nephrin, was examined to investigate molecular correlations between proteinuric phenotype and podocyte cytoskeletal reorganizations in Neph-hAT1 TGRs. Glomerular expression of nephrin decreased 40% in 4-week-old Neph-hAT1 TGRs (Figs. 4.7.1 a and b: 0.59 ± 0.01 fold, 4-wk hAT1 TGR glom *versus* WT). At 4 weeks, Neph-hAT1 TGRs and age-matched littermates are non-proteinuric and phenotypically indistinguishable.

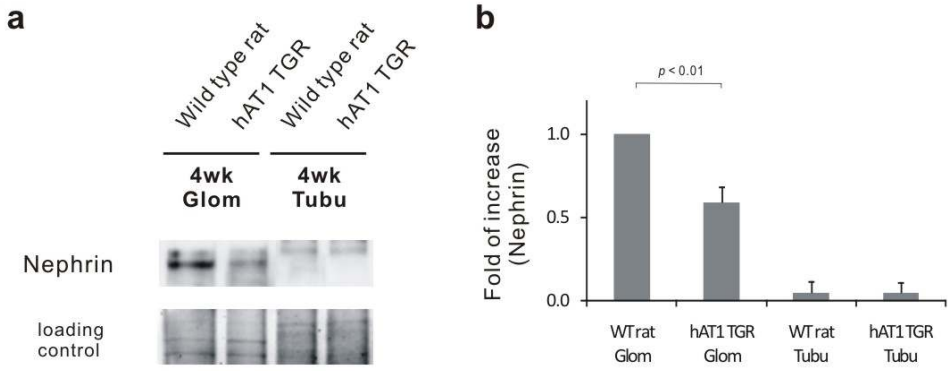

Fig. 4.7.1 Nephrin expression is down-regulated before proteinuria development in Neph-hAT1 TGRs (a) Representative immunoblotting of nephrin expression in kidney tissues from 4-week-old Neph-hAT1 TGRs and age-matched littermates. **(b)** Quantitative analysis plots for nephrin expression. Signal intensity of each band was standardized as mentioned previously, and each bar shows nephrin expression levels as a ratio factored for the first bar (n = 3).

Immunofluorescent staining results of nephrin in Ang II–treated cultured podocytes demonstrate significant distribution changes (Fig. 4.7.2). Expression of nephrin was down-regulated in cultured AT1R podocytes after 24-h Ang II treatment (Fig. 4.7.3). Notably, SCH51344, Y27632, and heparin, but not SB203580 or calphostin C, suppressed the effects of Ang II on nephrin expression in AT1R podocytes, suggesting that Rac-1 signaling, RhoA signaling and F-actin cytoskeletal reorganization, but not p38 MAPK or protein kinase C, regulate nephrin expression.

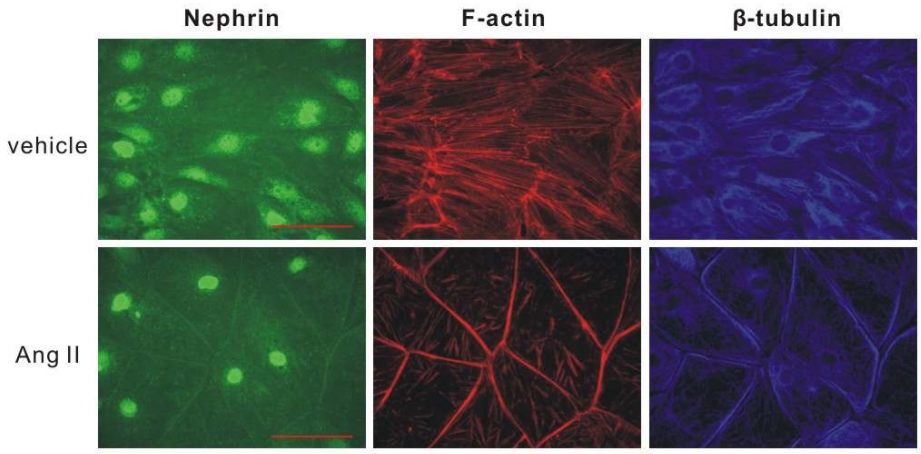

Fig. 4.7.2 Immunostaining of nephrin, F-actin and beta-tubulin in cultured AT1R podocytes While Ang II (100 nM, 24 h) induced F-actin cortical ring formation in podocytes, nephrin expression was decreased and distributed cortically. The β-tubulin cytoskeleton was also altered following Ang II stimulation. Scale bar = 50 μm.

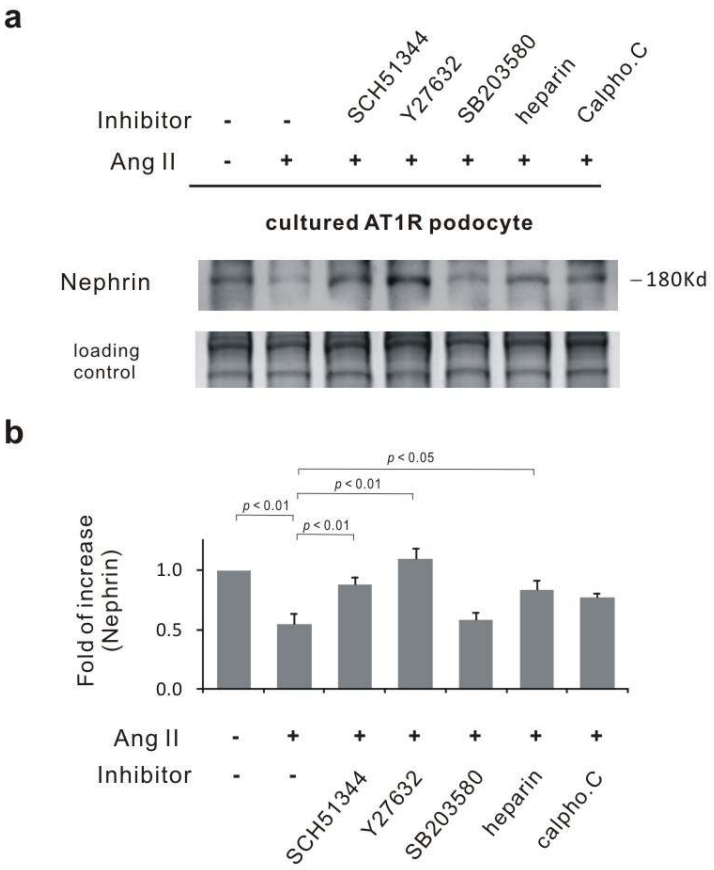

Fig. 4.7.3 Rac-1 signaling, RhoA signaling and F-actin cytoskeletal reorganization regulate nephrin expression in AT1R podocytes (a) Representative immunoblotting results for nephrin expression in cultured AT1R podocytes treated with Ang II (100 nM, 24 h) combined with different inhibitors (SCH51344, 10 μM; Y27632, 10 μM; SB203580, 10 μM; heparin, 10 μM; calphostin C, 0.1 μM). **(b)** Quantitative analysis plots for expression levels of nephrin in AT1R podocytes with different treatments. Signal intensity of each band was standardized as mentioned previously, and each bar shows nephrin expression levels as a ratio factored for the first bar (n = 4).

4.8. Proteomics of Ang II–treated podocytes

Proteomic analysis of Ang II–stimulated (100 nM, 24 h) cultured AT1R podocytes provides an overview of differential protein expression levels in AT1R signaling. With the Ettan™ DIGE system, mass spectrometry and peptide fingerprinting, this study identified 22 proteins of interest that have significant differential expression (Table 4.8.1).

Master No.	T-test	Average Ratio	Target protein	GI number	MS Status
2434	3.0e-006	2.10	Enolase 1, αnon-neuron	gi|54673814	confirmed
432	9.0e-005	1.96	Eukaryotic translation elongation factor 2	gi|74213791	confirmed
1027	0.013	1.91	Methylcrotonoyl-Coenzyme A carboxylase 2 (beta)	gi|58865926	confirmed
1425	0.0040	1.73	Phosphoglycerate kinase (PGK) 1	gi|80477474	confirmed
822	0.0071	1.64	Transketolase	gi|11066098	confirmed
826	0.0097	-1.60	Prosaposin	gi|74207912	uncertain
1454	4.5e-005	-1.61	Laminin receptor 1 (ribosomal protein SA)	gi|38014840	confirmed
127	0.00019	-1.62	Hypoxia up-regulated 1 (homology with HSP70 protein)	gi|31542333	confirmed
417	0.00023	-1.62	Tumor rejection antigen gp96 (homology with HSP90 protein)	gi|74178174	confirmed
1097	6.6e-006	-1.65	Tubulin β2-chain	gi|22165384	confirmed
264	0.00044	-1.65	Damage-specific DNA binding protein 1	gi|74138855	confirmed
765	8.1e-005	-1.66	FK506 binding protein 9	gi|20072768	confirmed
1077	6.3e-006	-1.67	Vimentin	gi|2078001	confirmed
2251	0.00017	-1.69	Peroxiredoxin 2	gi|31560539	confirmed
731	3.3e-008	-1.69	FK506 binding protein 9	gi|20072768	confirmed
1754	3.1e-008	-1.71	G protein β-2 subunit	gi|984551	confirmed
1620	5.3e-006	-1.82	SEC 13 related gene product	gi|29150272	confirmed
1012	0.0005	-1.92	Calreticulin	gi|74200069	confirmed
2129	4.1e-008	1.63	Triosephosphate isomerase 1	gi|6678413	confirmed
1026	3.3e-007	-1.68	Protein disulfide-isomerase	gi|14318713	confirmed
1857	1.3e-005	-1.62	Tropomyosin 4	gi|47894398	confirmed
1621	8.2e-006	-1.66	Tropomyosin 1, alpha-isoform	gi|78000190	confirmed

Av. Ratio : average ratio of Angiotensin II stimulated groups in comparison with vehicle treated groups

Table 4.8.1 Summary of proteomic results for Ang II–stimulated AT1R stable-responsive podocytes

Table 4.8.2 presents a summary of results of a thorough literature survey and analysis of these proteins with functional groupings. Proteomic results demonstrate that cytosolic enzymes involved in glycolysis and mitochodria enzyme MCCC2 (defects in MCCC2 are the cause of a recessive disease 3-methylcrotonylglycinuria type II [131]) are significantly up-regulated. Thus metabolic and energy consumption of podocytes may be increased following Ang II stimulation. However, proteomic analysis showed no up-regulated protein expression in protein biosynthesis, stress-responsive process or neo-synthesis of cytoskeleton-related proteins. Cytoskeleton rearrangements of differentiated podocytes after Ang II stimulation likely explain this high energy consumption identified by proteomics.

UniPort name	Protein of interest	Access#	Response	Function
Metabolic enzymes				
ENOA_MOUSE	enolase 1, αnon-neuron	P17182	up-regulated	carbohydrate degradation; glycolysis; cytoplasm
Q8K1L7_MOUSE	3-Methylcrotonyl-CoA carboxylase 2	Q8K1L7	up-regulated	leucine catabolism in mitochodria; MCGII
PGK1_MOUSE	phosphoglycerate kinase 1	P09411	up-regulated	carbohydrate degradation; glycolysis, cytoplasm
TKT_MOUSE	transketolase	P40142	up-regulated	pentose phosphate pathway;Ca^{2+} binding;WKS
TPIS_MOUSE	triosephosphate isomerase 1	P17751	up-regulated	glycolysis and gluconeogenesis; TPI deficiency
Protein biosynthesis				
Q3TJZ1_MOUSE	eukaryotic translation elongation factor 2	Q3TJZ1	up-regulated	GTP binding; translation elongation activity
PDIA1_MOUSE	protein disulfide-isomerase	P09103	down-regulated	catalyzes the formation, breakage and rearrangement of disulfide bonds
Q3TVD2_MOUSE	calreticulin	Q3TVD2	down-regulated	calcium binding chaperone promoting folding, oligomeric assembly and quality control monoglucosylated glycoproteins in ER
FKBP9_MOUSE	FK506 binding protein 9	Q9Z247	down-regulated	PPIases accelerate the folding of proteins during protein synthesis; located in ER
SEC13_MOUSE	SEC 13 related gene product	Q9D1M0	down-regulated	Intracellular protein transport;WD40 domain;ER
RSSA_MOUSE	ribosomal protein SA (laminin receptor 1)	P14206	down-regulated	structural constituent of ribosome
Stress / damage response				
Q80X75_MOUSE	hypoxia up-regulated 1 (homology with HSP70 protein)	Q80X75	down-regulated	in cytoprotective cellular mechanisms triggered by oxygen deprivation; located in ER
ENPL_MOUSE	endoplasmin (homology with HSP90 protein)	P08113	down-regulated	folding newly synthesised proteins, stabilisation & refolding denatured proteins after stress; ER
Q9WV39_MOUSE	damage-specific DNA binding protein 1	Q9WV39	down-regulated	DNA repair; located in nucleus
PRDX2_MOUSE	peroxiredoxin 2	Q61171	down-regulated	in redox regulation of the cell; located cytoplasm
Cytoskeleton / microtubule / filament				
TBB2C_MOUSE	tubulin β2-chain	P68372	down-regulated	major constituent of microtubules;Ca^{2+} binding
VIME_MOUSE	vimentin	P20152	down-regulated	class-III intermediate filaments
TPM4_MOUSE	tropomyosin 4	Q61R12	down-regulated	stabilizing cytoskeleton actin filaments
TPM1_MOUSE	tropomyosin 1, alpha-isoform	P58771	down-regulated	stabilizing cytoskeleton actin filaments
Others				
GBB2_MOUSE	G protein β-2 subunit	P62880	down-regulated	signal transduction; WD40 domain
SAP_MOUSE	prosaposin	Q61207	down-regulated	pulmonary surfactant-associated, secreted

Table 4.8.2 Functional grouping results of AT1R podocyte proteomics

4.9. Peroxiredoxin 2 is Down-Regulated in AT1R signaling

Peroxiredoxins have recently received considerable attention as a new anti-oxidant enzyme.[132] Peroxiredoxin 2 (Prx2) belongs to antioxidant families and is about 40% down-regulated based on proteomic analysis results for Ang II–treated podocytes (Fig. 4.9.1).

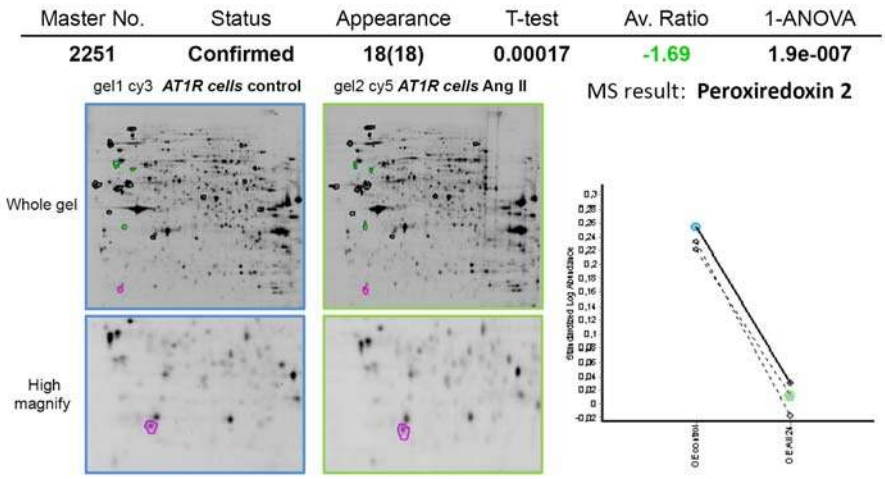

Fig. 4.9.1 2-D map of peroxiredoxin 2 analyzed using DeCyder software Proteomic map indicated the difference of Prx2 expression in AT1R podocytes treated with and without Ang II (100 nM, 24 h), and then the differential expression levels of Prx2 was confirmed statistically by a Student's *t*-test and one-way ANOVA. Spots representing Prx2 are marked with pink circles. The 2-D Cydye maps of vehicle-treated AT1R podocytes (control group) are outlined in blue, and the Ang II–treated group maps are outlined in green. Three independently treated sample pairs were examined with 2DE at the same time to eliminate interference from instruments and handling.

To validate Prx2 data, this study performed Western blot analysis of protein lysates from Ang II–treated cultured AT1R podocytes (Fig. 4.9.2), and glomeruli of Neph-hAT1 TGRs (Fig. 4.9.3). Little is known about the function of Prx2 in kidneys.[133] Additionally, this work is the first to characterize Prx2 in podocytes. This study performed a detailed immunofluorescence microscopic analysis of Prx2 protein localization in the kidney. Double immunostaining with a podocyte-specific marker WT-1 and a Prx2-specific antibody indicate that podocytes express abundant levels of Prx2 *in vivo*. (Fig. 4.9.4)

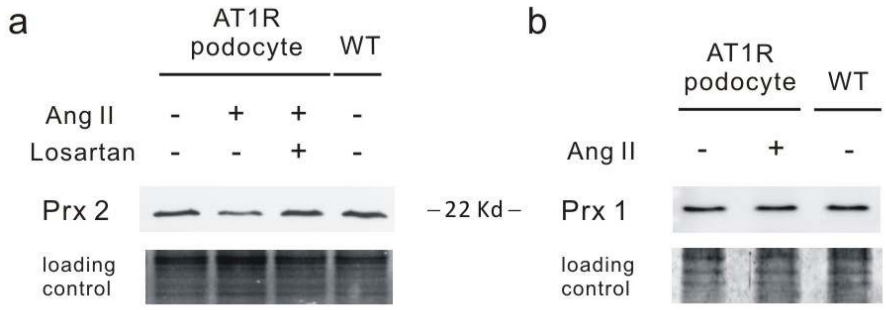

Fig. 4.9.2 Representative immunoblotting of Prx2 and Prx1 in cultured podocytes Ang II induces down-regulated expression of Prx2, but not in Prx1, another isoform of the Prx family. Wild type podocytes (WT) were used as controls. (all n = 4) **(a)** The expression level of Prx2 was down-regulated in cultured AT1R podocytes after 24-h Ang II treatment. Losartan limited the effects of Ang II on Prx2 down-regulation in AT1R podocytes, suggesting that AT1R mediates this effect. **(b)** Ang II treatment had no influence on the Prx1 expression level. Ang II, 100 nM, 24h; losartan, 200 nM.

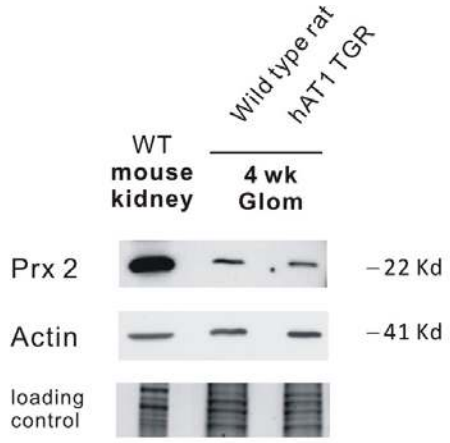

Fig. 4.9.3 Expression of Prx2 was down-regulated in Neph-hAT1 TGR glomeruli Representative immunoblotting of Prx2 and actin expression in kidney tissues from 4-week-old Neph-hAT1 TGRs and age-matched littermates (n = 3). Wild type (WT) mouse kidney lysates were used as a positive control for Prx2-specific antibody.

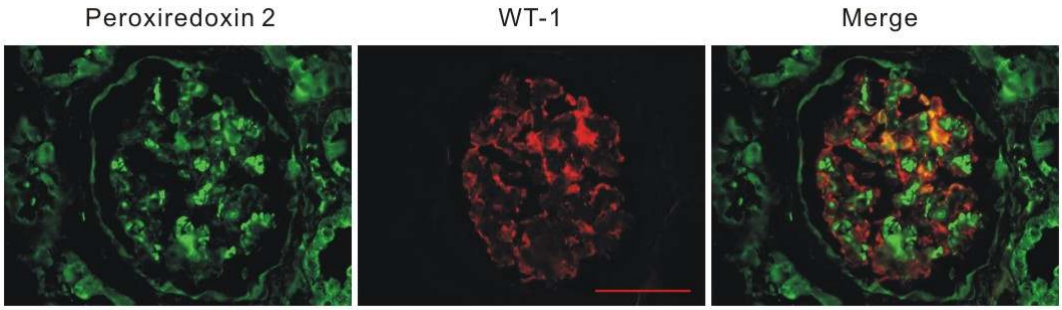

Fig. 4.9.4 Immunofluorescence staining of Prx2 and WT-1 in human glomeruli Prx2 (green, left) and podocyte-specific marker WT-1 (Wilms tumor suppressor gene; red, middle) were stained. Merging both images (right) suggests co-localization of Prx2 and WT-1 signals at podocyte cell bodies and FPs. The bright green signals within capillary loops are from red blood cells. Bar = 50 μm.

4.10. Decreased Prx2 Expression Also Causes Oxidative-Mediated ERM protein phosphorylated in Podocytes

To elucidate the effects of Prx2 down-regulation in AT1R signaling, siRNAs specifically designed for Prx2 were stably expressed in cultured murine podocytes. Sustained suppression of Prx2 expression was verified by immunoblotting (Figs. 4.10.1 a and b). Retroviral transduction of human AT1R gene facilitates differentiated cultured podocytes to express less Prx2 (48 ± 8%, n = 6) than WT cells. Empty vector and scramble sequence siRNA transducted cells were utilized as controls.

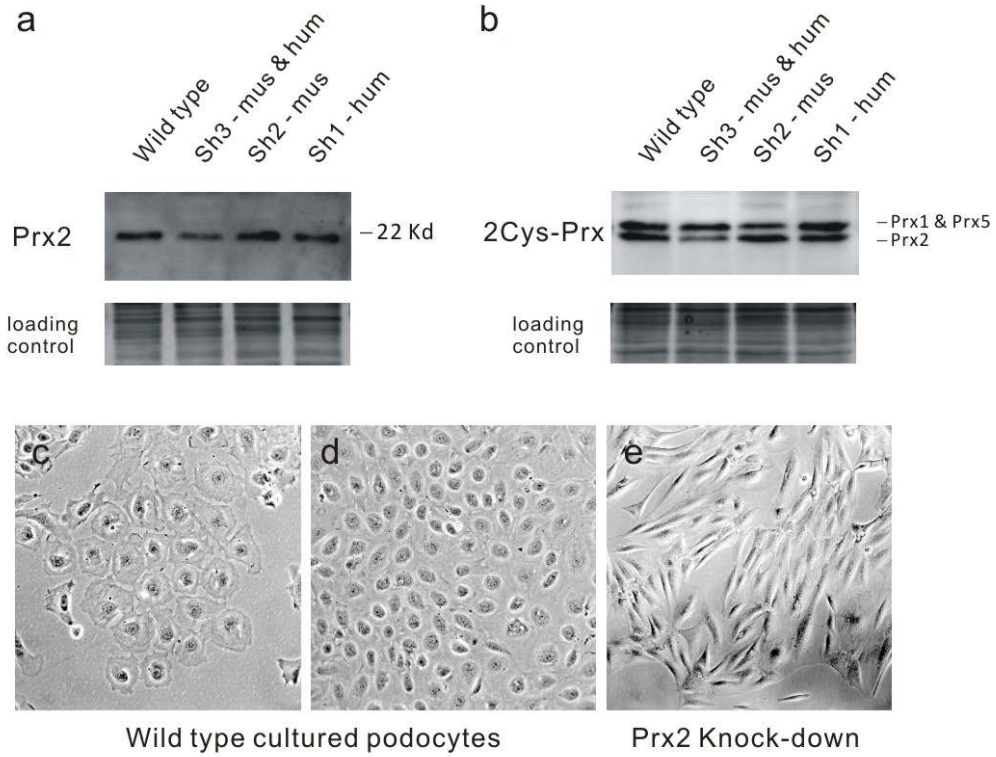

Fig 4.10.1 The Prx2 knockdown podocyte cell line created by the retroviral-vector-based siRNA method (a) With a short hairpin sequence (Sh3) targeting both human (hum) and mouse (mus) Prx2 amino acid position from 559–577, Prx2 expression level decreased 52% in a cultured mouse podocyte cell line. Short hairpin 1 and 2 had no effects on Prx2 expression by Western blotting with a mouse monoclonal antibody that specifically detects Prx2. **(b)** Using an antibody that can recognize all 2-cystine Prx isoforms (Prx1–5) further demonstrates the Prx2-specific knockdown with Sh3. Notably, Prx3 is 28Kd & distributed mainly in mitochondria, whereas Prx4 is a 31Kd secretory isoform. Neither Prx3 nor Prx4 are shown in this representative blotting. **(c, d)** Differentiated murine podocytes (wild type) in sparse (c) and confluent (d) cultured conditions, respectively. The cells exhibit an aborized phenotype and form cell-cell contacts at the monolayer confluence. **(e)** The Prx2 knockdown podocytes are morphologically generally spindle-shaped and show little cell-cell contact even at high culture density.

Differentiated Prx2 knockdown podocytes have a morphology that differs distinctly from that of control cells (Figs. 4.10.1 c–e). Prx2 knockdown podocytes are minimally aborized and have minimal cell-cell contacts. Moreover, differentiated Prx2 knockdown podocytes exhibit substantial ROS activity, which represents the anti-oxidant function of Prx2 in podocytes (Fig. 4.10.2).

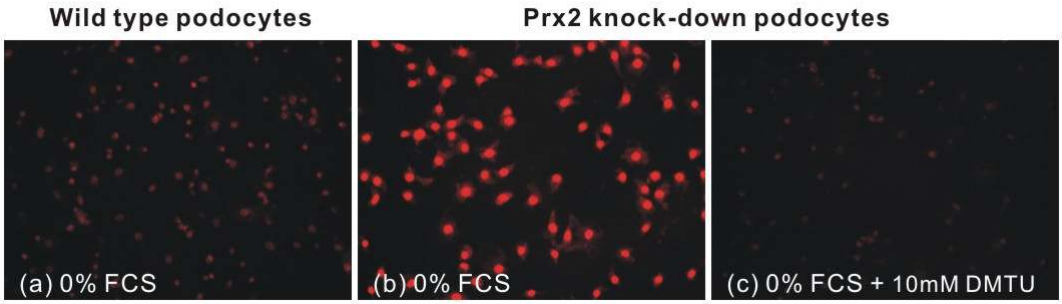

Fig. 4.10.2 Intracellular oxidants/ROS of Prx2 knockdown podocytes were analyzed using DHE fluorescence staining Compared with control cells **(a)**, Prx2 knockdown podocytes **(b)** had more reactive oxygen species activities; this effect was abolished by the free-radical scavenger DMTU **(c)**.

Compensatory up-regulated expression of catalase, another anti-oxidant protein, provides indirect evidence demonstrates oxidative stress with excess ROS in Prx2 knockdown podocytes. Similar to the Ang II effect, ERM protein phosphorylation was also observed in vehicle-treated Prx2 knockdown podocytes compared with WT cells, indicating the occurrence of F-actin cytoskeletal reorganization in podocytes. (Fig. 4.10.3).

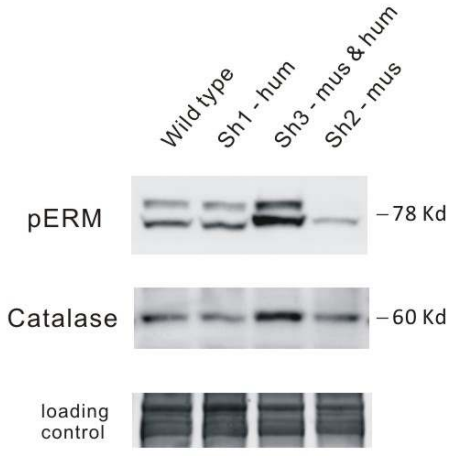

Fig. 4.10.3 Representative immunoblotting results for pERM and catalase expression in cultured podocytes The ERM proteins are more phosphorylated in Prx2 knockdown podocytes (Sh3) than in scramble siRNA (Sh1) transduced cells and WT podocytes. Additionally, catalase was up-regulated in Prx2 knockdown podocytes and compensated for increased oxidative status. (n = 2)

Combined these experimental results further confirm that ROS and the resultant oxidative stress have a central role in AT1R signaling. These effects are achieved either by activating Rac-1 to increase ROS production or by down-regulating anti-oxidant protein Prx2 to attenuate removal of ROS.

5. Discussion

5.1. Establishing an *In Vitro* Model to Explore AT1R Signaling in Podocytes

Substantial experimental and clinical evidence indicates that inhibiting Ang II and/or its receptor improves proteinuria and this benefit is independent of decreased blood pressure. Podocytes have a central role in the pathogenesis of proteinuric glomerular diseases and in progression of chronic renal failure.[1] The Ang II type 1 (AT1) and type 2 (AT2) receptors are expressed on podocytes, and their expression is elevated in the proteinuric state.[130] Furthermore, transgenic rats with overexpressed human AT1Rs in podocytes develop protein leakage and structural podocyte damage that progresses to focal segmental glomerulosclerosis (FSGS).[60] On a cellular level, Ang II increases cytosolic Ca^{2+} concentration and synthesis of VEGF and TGF-β, but decreases ZO-1 and nephrin expression, resulting in podocyte injury, hypertrophy and apoptosis.[10]

This study investigated the effects of Ang II on cytoskeletal rearrangement of podocytes using a novel cultured murine podocyte model with stable expression of functioning AT1Rs. This proposed model was developed because murine podocytes do not respond consistently to Ang II and because expression of Ang II receptors is increased in glomerular diseases. Although AT1R is not as robust as transient transfection methods, the expression level of AT1 receptors in AT1R podocytes increased only 2.7-fold compared with empty vector transducted or WT cells. However, this increase was adequate to generate a cell line that is stably responsive to Ang II. Similar to podocytes *in vivo*,[58;59] differentiated AT1R podocytes in culture responded with a significant $[Ca^{2+}]_i$ increase via nanomolar concentrations of Ang II.

The principal advantage of this AT1R podocyte cell line is that it is a convenient experimental model for investigating AT1R and AT2R signaling mechanisms. Although functional expression of the renin-angiotensin system has been characterized in human cultured podocytes, these cells do not respond constantly to Ang II with

increased $[Ca^{2+}]_i$. Culture methods for cells outgrowing from sieved glomeruli can acquire primary podocytes that respond well to Ang II; however, limited cell numbers and mesangial cell contamination still impede further signaling investigations and large-scale proteomics study. Stable transduction of human AT1R to a well-characterized immortalized murine podocyte cell line overcame these problems. Additionally, the AT1R podocyte has all features of the origin cells—dominant F-actin stress fiber formation, stable expression of nephrin and abundant formation of cell-cell contact, possessing several features of *in situ* podocyte cell-cell contact. In combination with Neph-hAT1 TGRs (developed proteinuria and glomerular damage that progressed to FSGS) and this AT1R podocyte cell line, we generated an experimental system that contains both *in vitro* and *in vivo* models.

5.2. The Vital Physiological and Pathophysiological Roles of Actin Cytoskeleton in Podocytes and Filtration Barrier

Like smooth muscles that develop isometric force over a very wide range of cell lengths—which reflects "mechanical plasticity,"—podocytes tether the underlying glomerular basement membrane via bundles of actin filaments in FPs while lining the outer aspect of the capillary loop. Podocytes, together with smooth muscle-like mesangial cells on the opposite side of capillary loop, counteract extension force due to hydraulic glomerular filtration (Fig. 5.2).

To adapt to varying filtration forces due to blood pressure change and retain glomerular capillary loops at a constant size and shape, the F-actin cytoskeleton of podocyte FPs should develop considerable plasticity. Plasticity is defined here as a persistent change in cell structure or function in response to an environmental change. Important environmental stimuli that trigger F-actin cytoskeleton plasticity encompass chemical (e.g., glucose, ROS, autacoids, and cytokines) and external mechanical signals (e.g., applied stress and strain). Both signals are likely transduced by ionic and protein kinase signaling cascades that alter gene expression patterns and induce changes in the cytoskeleton and contractile system.

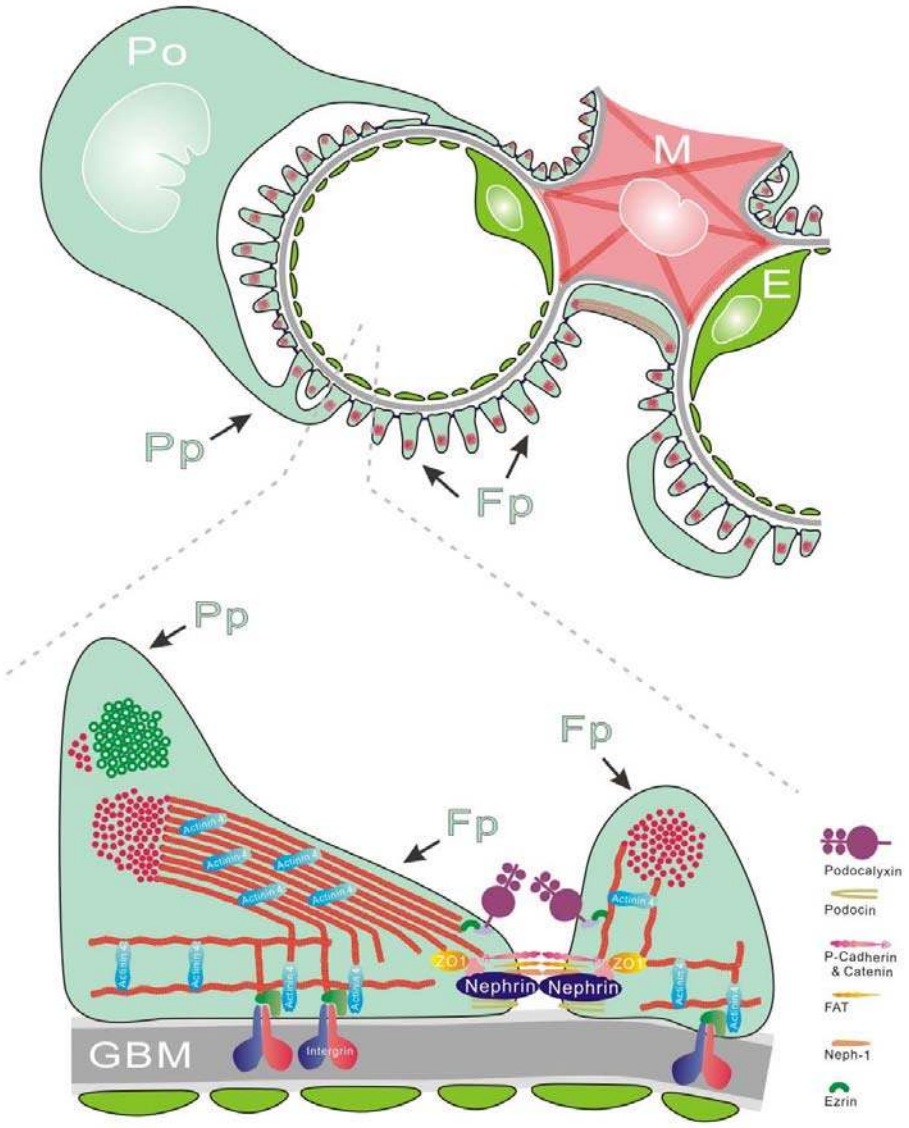

Fig. 5.2 Diagram of a single glomerular capillary The peripheral endothelial cell cytoplasm (green, E), which has pores through it, looks like a small string of sausages on a cross-sectional view. The visceral epithelial cells or podocytes (blue, Po), have foot processes (Fp) that contain F-actin cytoskeletal networks (red). The glomerular basement membrane does not completely enclose the lumen, but rather splays out over the mesangium to become the paramesangial basement membrane. This results in a functional gap in which materials from the capillary lumen or subendothelial zone (having passed through the endothelial pores) can directly enter the mesangium without traversing the basement membrane. Mesangial cells (pink, M) are concentrated between capillaries at the vascular pole of the corpuscle. Abundant contractile F-actin bundles allow mesangial cells to anchor capillary loops in the vascular stack or glomeruli. This figure is drawed by Hsu and is summarzied and modified from Kriz *et al.* Kidney Int. 1998; Pavenstädt *et al.* Physio Rev. 2003 and Meyrier A Nat Clin Pract Nephrol 2005

Defining the signaling mechanisms and effector proteins mediating phenotypic and mechanical plasticity of F-actin cytoskeletons is important in podocyte biology and pathophysiology. Some signaling cascades that are likely prominent include calcium-dependent protein kinases, small GTPases (Rho, Rac, cdc42), Rho kinase,

protein kinase C (PKC), Src family tyrosine kinases, mitogen-activated protein (MAP) kinases, and p21 activated protein kinases (PAK). Many potential targets exist for these signaling cascades, including nuclear processes, metabolic pathways, and structural components of the cytoskeleton.

A dynamic steady-state F-actin cytoskeleton organization is crucial for maintaining structural integrity of FPs and provides stability between cell-cell contacting SD and the cell-matrix contact of podocytes.[1] The ensuing actin cytoskeletal rearrangement following injury to this specialized organization causes the stereotypical response of FP effacement.[134;135]

This study demonstrates that AT1R signaling induces a ROS-mediated F-actin cytoskeletal reorganization and a migratory phenotype of podocytes. This reorganization is likely a physiological response to podocytes that counteracts the increasingly distending forces of the capillary wall and covers the enlarged capillary surfaces induced by intraglomerular renin-angiotensin system activation. However, the actin-based cytoskeleton network in podocyte FPs is linked to the GBM (the basal membrane domain (BMD), which is also known as the sole plate), the apical membrane domain (AMD), and SDs through different adaptor molecules (Fig. 1.3 a). Sustained or severe alternation of the F-actin cytoskeleton in FPs likely impairs podocyte stability and viability, and further impairs the structure of the SD causing filtration barrier failure (Fig. 1.1).

5.3. Rac-1 Orchestrates AT1R Signaling on Podocyte Cytoskeletons via ROS Formation

Using the AT1R podocyte cell model and the Neph-hAT1 TGRs, experimental data demonstrate increased Rac-1 expression after Ang II stimulation and in the early stage of podocyte injury in Neph-hAT1 TGRs. Similar to the experimental results for Neph-hAT1 TGRs, Rac-1 participates in the development of Ang II–induced cardiac hypertrophy.[136] In an animal model of cardiac hypertrophy, treatment with Ang II

activates NADPH oxidase, increases ROS production, induces cardiac fetal gene expression, and results in increased left ventricular mass. All of these effects of Ang II on the heart occurred with similar changes in blood pressure and were decreased or absent in mutant mice with decreased cardiac expression of Rac1. Notably, ROS has also been implicated in podocyte injury and diabetic nephropathy.[137;138] These experimental findings suggest that glomerular Rac-1 likely plays a pivotal role in development of proteinuria and FSGS in response to Ang II.

The Rho GTPases, members of the Ras superfamily of small GTPases, are the key regulators of actin cytoskeleton organization[62] and are composed of three subfamilies: Rho, Rac and CDC42. The Rho family also has various effectors in vascular cells and tissues. One Rho effector—Rho-kinase (ROCK)—has an important role in smooth muscle contraction. Additionally, various vasoactive factors stimulate RhoA and ROCK, resulting in enhanced vasoconstriction and migration of vascular smooth muscle cells. Therefore, small G-proteins are possible therapeutic targets in cardiovascular medicine. Three members of the Rac family (Ras-related C3 botulinum toxin substrate) show a cell type-specific expression: Rac-2 is generally restricted to hematopoietic cells; and, Rac-3 is preferentially expressed in neurons.[139] Notably, Rac-1 exhibits a ubiquitous expressional pattern and controls membrane protrusion by inducing assembly of an actin filament meshwork at the cell periphery to generate lamellipodium and membrane ruffles, thereby triggering cell migration. Additionally, Rac-1 is a crucial component of NADPH oxidase, which mediates Ang II–induced ROS production.[63-65;140;141]

Our experimental data demonstrate that Rac-1 mediates the Ang II–induced increase of ROS production, F-actin cytoskeletal rearrangements (i.e., cortical F-actin formation and stress fiber attenuation) and the switch to a migratory phenotypic in AT1R podocytes. In contrast to recent studies suggesting that RhoA maintains F-actin stress fibers of podocytes,[142-144] Rac-1 seems to orchestrate an adaptive cellular response to physiological stress or injurious stimuli in AT1R signaling, especially in the F-actin cytoskeleton modulating mechanism. As Rac-1 controls Ang II signaling in podocytes,

Rac-1 inhibitors may be thus a potential therapeutic target for protecting podocytes from excess ROS generation and cytoskeletal rearrangement.

5.4. "Rac and Rho" of AT1R Signaling in Podocytes?

The opposing effects of Rac or Cdc42 and Rho may be a general feature of these GTPases. For neurons, Rac and Cdc42 may be under the control of chemoattractants, whereas Rho can be activated by chemorepellants, leading to either localized protrusion or retraction of the growth cone.[145] In considering phagocytosis of macrophage, which is driven by reorganization of filamentous actin, this study identified two distinct mechanisms: Type I, which is used by the immunoglobulin receptor and mediated by Cdc42 and Rac; and, type II, which is utilized by the complement receptor and is mediated by Rho.[146] Moreover, significant cross-talk exists between GTPases of the Ras and Rho subfamilies: Ras can activate Rac (hence, Ras induces lamellipodia); Cdc42 can activate Rac (hence, filopodia are intimately associated with lamellipodia); and, Rac can activate Rho (although in fibroblasts, this is a weak and delayed response).[147] These observational results suggest that members of the Rho GTPase family are key regulatory molecules that link surface receptors to the organization of the actin cytoskeleton and likely act together.

Our experimental data demonstrate that in F-actin cytoskeletal reorganization of podocytes, Rac has a dominant role in the Ang II–induced ROS-pERM-cortical actin ring effector axis. With an efficient ROCK inhibitor (Y27632, 10 μM) that inhibits Rho activity in cultured podocytes, Ang II–induced ERM phosphorylation cannot be eliminated even when the cell shapes were markedly altered by F-actin stress fiber breakdown. However, in contrast to regulation of F-actin cytoskeleton, Rac and Rho are both necessary in the Ang II–associated expression regulation of α actinin-4 and nephrin. These dual activating effects of Rac-1 and RhoA signaling ("Rac and Rho" effect) are illustrated by experimental results (Figs. 4.6.2 and 4.7.3), for SCH51344, Y27632, and heparin, but not for SB203580 or calphostin C, inhibited the effects of Ang II on α actinin-4 and nephrin expression in AT1R podocytes. Distinct from Ang

II–induced cytoskeletal reorganization, during which the Rac effect prevails, down-regulated expression of α actinin-4 and nephrin is an effect of Rac and Rho interplay.

5.5. "PKC-independent Rac Activation" of AT1R Signaling in Podocytes

In vascular smooth muscle cells, vasoconstrictors, growth factors, cytokines and mechanical stretching induce intracellular signal transduction involving small GTPases and MAPKs. For instance, Ang II and endothelin (ET) stimulate transactivation of the epidermal growth factor receptor (EGFR) through its own G-protein coupled receptors. This effect occurs through a metalloprotease, such as ADAM 17, that produces mature growth factors. Activation of select small GTPases and MAPKs causes vascular diseases (Fig. 5.5 a).

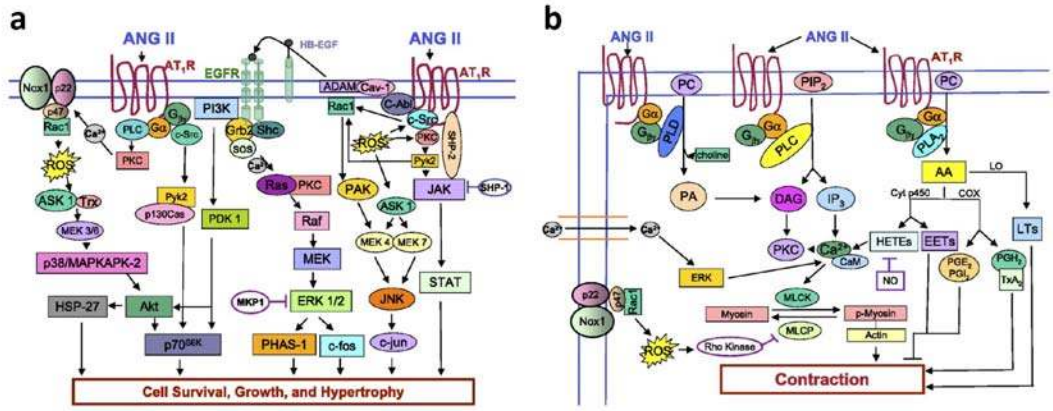

Fig. 5.5 Ang II cell signaling: physiological and pathological effects in vascular smooth muscle cells Metha *et al.* Am J Physiol Cell Physiol 2007

In this disease model, Ang II regulates vascular smooth muscle cell survival, growth, and hypertrophy. Via activation of PKC, Ang II activates NADPH oxidase, a principal source of cellular ROS with increased intracellular Ca^{2+}. In turn, NADPH-derived ROSs activate the EGFR in a c-Src–dependent manner. Once activated, AT1R transactivates numerous tyrosine and nontyrosine kinase receptors in carrying out its

pleiotrophic effects. Notably, Ang II mediates cell survival via p38 MAPK, and Akt (members of the serine/threonine-specific protein kinase family). Cell growth and hypertrophy are mediated by Ang II–mediated MAPKs, p38 MAPK, extracellular signal-regulated kinase (ERK) and C-Jun N-terminal kinases (JNK), and the Janus kinases (JAKs) and signal transducers and activators of transcription (STATs) pathway, all of which result in changes in cellular protein transcription.

Ang II induces vascular smooth muscle cell contraction in a PKC-dependent manner (Fig. 5.5 b). Experimental results show that when activated by an agonist, AT1Rs couple to $G_{\alpha q/11}$, $G_{\alpha 12/13,}$ and $G_{\beta y}$ complexes, which activate downstream effectors, including phospholipase C (PLC), phospholipase A_2 (PLA_2), and phospholipase D (PLD). Activation of PLC generates inositol-1,4,5-triphosphate (IP_3) and diacylglycerol (DAG) within seconds. The IP_3 binds to its receptor on the sarcoplasmic reticulum, opening a channel that allows calcium efflux into the cytoplasm, and Ca^{2+} binds to calmodulin and activates the myosin light chain kinase (MLCK), which phosphorylates the myosin light chain and enhances interaction between actin and myosin, causing smooth muscle cell contraction. Diacylglycerol activates PKC, which not only increases pH during cell contraction by phosphorylating Na^+/H^+ pump, but also participates as an effector in the Ras/Raf/MEK/ERK pathway (Fig. 5.5 a).

This experimental study identified a PKC-independent AT1R signaling pathway for Rac-1 activation in podocyte cytoskeletal reorganizations. By using a sufficient concentration of pan-PKC inhibitors (calphostin C or tamoxifen), PKC inhibitors did not eliminate Ang II effects on ERM protein phosphorylation, indicating that Rac-1 activation mediated cytoskeletal reorganization in cultured podocytes. Moreover, PKC inhibition augmented phosphorylation of ERM proteins in response to Ang II stimulation (Fig 4.5.4). Although ERM proteins are PKC substrates in several different cell types,[148-150] experimental findings are consistent with a recent *in vitro* study demonstrating that activation of PKC suppressed phosphorylation of ezrin and moesin in carcinosarcoma cells.[151] The mechanism of PKC's augmentative effect remains unknown, but may be explained by feedback inhibition of G protein-coupled receptor

kinase 2 (GRK2) activity by ERKs,[152] which are activated by PKC.

A very recent experimental study demonstrated that ADP-ribosylation factor 6 (ARF6) and Rac-1 are sequentially activated when HEK 293 cells expressing the AT1R are stimulated with Ang II.[153] Following receptor activation, ARF6 and Rac-1 transiently form a complex; this complex then induces AT1R expressing HEK293 cells to ruffle, form membranous protrusions, and migrate in response to agonist treatment. These experimental results also suggest that a novel PKC-independent Rac-1 activating mechanism in AT1R signaling leads to actin remodeling.

5.6. Effects of Ang II–induced ROS on the Podocyte Cytoskeleton

In vivo infusion of Ang II elevates blood pressure and generates ROSs in rat aortic rings.[154;155] Oxidative stress resulting from Ang II and NADPH oxidase machinery is believed responsible for this Ang II-induced hypertensive effect. Oxidative stress is an imbalance between ROSs generation and scavenging such as superoxide anions or hydrogen peroxide (H_2O_2). Superoxide anions are metabolized by antioxidant proteins such as superoxide dismutases, catalases, glutathione peroxidases and peroxiredoxins. These ROSs are implicated in cell signaling and bioinactivation of nitric oxide, and contribute to aging, hypertension, and cardiovascular and kidney diseases.

Reactive oxygen species are detrimental and toxic to cells and tissues as a result of injury to lipids, nucleic acids, and proteins. Lipid peroxidation of membranes causes a loss of membrane function, increases permeability and induces lipid autoperoxidation reactions. Notably, DNA damage results in mutation and cell death (apoptosis). Cross-linking or vulcanization of sulfhydryl-rich proteins causes signaling pathway dysfunction and stiff, aged proteins (specifically, collagen of the extracellular matrix).

Sustained AT1R activation in podocytes cause excess ROS production, cellular oxidative stress, actin-binding molecule exhaustion, decreased focal adhesion and podocyte depletion, all of which can cause proteinuria. Recent experimental data

suggest that ROSs damage the F-actin cytoskeleton and impair the physiological function of different cells.[156-158]

Our experimental results in this study demonstrate that ROS is a secondary messenger of AT1R signaling. Podocytes treated with Ang II (up to 10 μM) or low concentrations of superoxide anions (up to 5 μM) for 24 h did not cause cell necrosis or apoptosis. When using Ang II concentrations of 1–100 nM, which are very close to the typical physiological condition, and tiny amounts of superoxide anions (0.28–0.7 μM) to stimulate AT1R podocytes, cells present with membrane ruffles, lamellipodia and increased cell migrations. In addition to these Rac-1-specific effects, podocytes also developed F-acting cytoskeletal reorganization and ERM protein phosphorylation. The free radical scavenger DMTU eliminated Ang II–induced cell migration, ERM protein phosphorylation and cortical F-actin ring formation, demonstrating that ROS mediates the effects of Rac-1 on the migratory phenotypical switch, cytoskeletal reorganization (via ERM protein phosphorylation) and down-regulated α actinin-4 expression of podocytes.

5.7. Effects of AT1R-induced Cytoskeleton Reorganization on the Apical Membrane Domain of FPs

In the apical domain podocyte FPs, ezrin bridges the cytoplasmic domain of podocalyxin to the actin cytoskeleton through Na^+/H^+-exchanger regulatory factor 2 (NHERF2).[83] Podocalyxin, which is a heavy sialyated and sulfated membrane protein expressed on the apical surface of podocytes, functions as an antiadhesin that prevents cell-cell adhesion via charge repulsion as a result of abundant sialic acid residues, which give podocalyxin a highly negative charge. The association of the podocalyxin/NHERF2/ezrin complex with the F-actin cytoskeleton may anchor podocalyxin to specific microdomains of the apical membrane or determine its time residing on the cell surface. In damaged podocytes, the podocalyxin/NHERF2/ezrin complex is disrupted. Treatment of rats with puromycin or sialidase is associated with dephosphorylation of ezrin and uncoupling of ezrin from the cytoskeleton. These *in*

vivo findings suggest that a mechanism exists through which the loss of negative charge at the surface of podocytes alters FP morphology and stability of SD.

Conversely, little is known about the process whereby excess phosphorylation of adapter molecules—the ERM family—target the F-actin cytoskeletal during podocyte injury. Structural changes between dormant and active conformations of ERM proteins are regulated by phosphorylation.[70] Furthermore, phosphorylated ERM proteins are selectively found on cell surfaces and induce abundant formation of F-actin-membrane linkages.[159;160] In studies based on cultured cells, Rho-kinase-mediated threonine phosphorylation in ezrin weakens intramolecular head-to-tail associations and unmasks membrane protein- and actin-binding sites. Once activated, ezrin generates its associations with plasma membrane proteins and the cortical actin cytoskeleton.[13;161;162] In cultured endothelial cells, tumor necrosis factor (TNF)-alpha-induced ERM phosphorylation was accompanied by cytoskeletal changes, paracellular gap formation, and increased permeability to fluxes of dextran and albumin.[148]

Phosphorylated ERM proteins, which may indicate a high F-actin turnover rate, are increased in Ang II–stimulated cultured podocytes and in glomeruli extracts of Neph-hAT1 TGRs. Both an AT1R blocker and a Rac-1 specific inhibitor, but not a Rho kinase inhibitor (Y27632, 10 μM [142;143]), inhibit Ang II–induced F-actin cytoskeletal reorganization and ERM protein phosphorylations of cultured AT1R podocyte, indicating that, in contrast with studies of other cell types, RhoA does not predominantly mediate ERM protein phosphorylation in Ang II–stimulated podocytes.

Regulation of ERM protein localization is not completely understood; however, the involvement of Rho GTPases is likely critical. A recent study based on cultured cells demonstrated that both Rho-dependent and Rho-independent activation of ERM proteins require the presence and local accumulation of phosphatidylinositol 4,5-bisphosphate (PIP_2) at the cell membrane destination and binding of PIP_2 to the N-terminus of ERM proteins.[163] Rho-independent ERM protein activation has been

demonstrated to be dependent on Rac-1 recruited phosphatidylinositol-4-phosphate 5-kinase (PIP5K) activity, subsequently increased PIP_2 production, and actin assembly.[164]

The downstream kinase effector in podocyte AT1R signaling was elucidated by inhibiting serine/threonine kinases that have been reported using ERM proteins as substrates (i.e., Rho kinase,[13;161;162] p38MAPK,[148;165] G protein-coupled receptor kinase 2,[166] and protein kinase C [148-150]). Experimental data demonstrate that p38MAPK and protein kinase C do not phosphorylate ERM proteins in podocyte AT1R signaling. Notably, heparin, which has beneficial effects in proteinuric renal diseases,[167] effectively eliminated Ang II–induced ERM protein phosphorylation and subsequently blocked rearrangement of the podocyte F-actin cytoskeleton. Heparin is well known as a potent inhibitor (IC50: 0.15 μM) of G protein-coupled receptor kinase 2 (GRK2).[168-170] Furthermore, a recent study determined that ezrin is a novel substrate of GRK2-mediating membrane ruffles in Hep2 cells.[171] Heparin may thus exhibit glomerular protection effects on the podocyte cytoskeleton by inhibiting GRK2-mediated ERM protein phosphorylation.

5.8. Effects of AT1R Induced Cytoskeleton Reorganization on FP Basal Membrane Domain

Mutations in the α actinin-4 gene (ACTN4) cause an autosomal dominant human kidney disease.[35] Mice deficient in α actinin-4 develop a recessive phenotype characterized by kidney failure, proteinuria, retraction of glomerular podocyte FPs and FSGS.[91] Both *in vivo* models appear to be nephron degenerated pathways with slowly progressing proteinuria and late onset glomerulosclerosis. Late onset diseases likely emerge from impaired functions of the podocyte cytoskeleton, whereas early onset diseases emerge from severe structure deficiencies of various components (GBM and the slit membrane). Loss of α actinin-4 depletes podocytes.[92] Cross-linking of actin filament bundles by α actinin-4 is required for normal podocyte adhesion. Notably, α actinin-4 interacts with intergrins and strengthens podocyte-GBM interaction, thereby

stabilizing glomerular architecture and preventing podocyte detachment. Here we demonstrate that α actinin-4 expression is down-regulated in Ang II–treated podocytes. In Neph-hAT1 TGRs, decreased glomerular α actinin-4 expression was correlated with proteinuria development. Ang II–induced α actinin-4 down-regulation of podocytes was mediated by Rac-1, RhoA and pERM, demonstrating the importance of this signaling system for regulating α actinin-4 expression. Sustained Ang II signaling in podocytes, involving repeated depolymerization and polymerization of G-actins and consuming numerous actin adaptor or cross-linking proteins, may thus exhaust α actinin-4 expression and decrease the podocyte-matrix adhesion. Detachment of podocytes from the glomerular basement membrane causes gradual podocyte depletion and, finally, FSGS.

5.9. Effects of AT1R Induced Cytoskeleton Reorganization on the SD Domain of FPs

Neph-hAT1 TGRs start to develop proteinuria (selective albuminuria) at 8 weeks. Microscopic examination of the Neph-hAT1 TGR kidney revealed only mild pathological findings: 27% of glomeruli developed early podocyte lesions (pseudocysts) and the remaining glomeruli were without lesions. Under electron microscopy, morphology of the interdigitated FP is the same with Neph-hAT1 TGRs and WT rats. Moreover, pseudocyst formation is not a reasonable explanation for early onset proteinuria.

Slit diaphragm dysfunction always induces proteinuria development. This study assessed expression of nephrin, a vital SD protein, in AT1R signaling. Like other podocyte injury factors, Ang II down-regulated nephrin expression in cultured AT1R podocytes and in 4-week-old Neph-hAT1 TGR glomeruli. Signaling pathway examination demonstrated that both Rac-1 activation and RhoA signaling are essential to regulating nephrin expression by Ang II. Furthermore, immunostaining of Ang II–treated podocytes showed that nephrin is redistributed in the cell-cell contact area in parallel with F-actin cortical ring formation. Recent *in vitro* and *in vivo* studies provide

compelling evidence that nephrin tyrosine phosphorylation controls podocyte cell morphology through Nck adaptor proteins.[99;100] These experimental findings link nephrin to rearrangement of actin cytoskeleton in FPs and indicate that Nck adaptor proteins may mediate this connection. In a high actin turnover state in podocyte FPs, such as AT1R signaling activation, excess tyrosine phosphorylation may cluster nephrin with Nck adaptors and reorganized cortical F-actin filaments. This SD-associated molecule clustering may injure SD structure and result in FP effacement and proteinuria.

5.10. AT1R Signaling Down-regulates Peroxiredoxin 2 in Podocytes—"RedOx Switching"

Recent in experimental and clinical studies demonstrated that the Prx families are more than anti-oxidant proteins, but modulate many cellular processes by switching over the reductive-oxidative environment within cells. The identification of down-regulated Prx2 in Ang II–treated podocytes enables researchers to consider about ROS and oxidative stress in a manner that differs from conventional thinking.

Like hydrogen peroxide or superoxide anions, ROS has been viewed for a long time as the inevitable but unwanted by-product of aerobic existence. Now researchers know that some cellular signaling is linked to reductive-oxidative-based mechanisms. For some specific signaling pathways, ROS is produced temporally and spatially to achieve the desired cellular outcomes. Figure 5.10 presents a summary of the production, protection and signaling of ROS.

Notably, AT1R signaling in podocytes activates Rac-1 and NADPH oxidase to produce additional ROS, and down-regulates antioxidant protein Prx2 to maintain an oxidative environment that favors signal propagation. Prx2 knock-down podocytes showed an increased intracellular ROS activity and compensatory up-regulation of another antioxidant enzyme catalase. Cell morphology was also altered in Prx2 knock-down podocytes: reduced adhesion to the matrix, less aborization and loss of cell-cell contact

were observed. In addition, Prx2 knock-down causes phosphorylation of ERM proteins, which is indicative of high F-actin turnover status. Taken together, these experimental findings further indicate that Prx2 might be an important mediator of podocyte AT1R signaling.

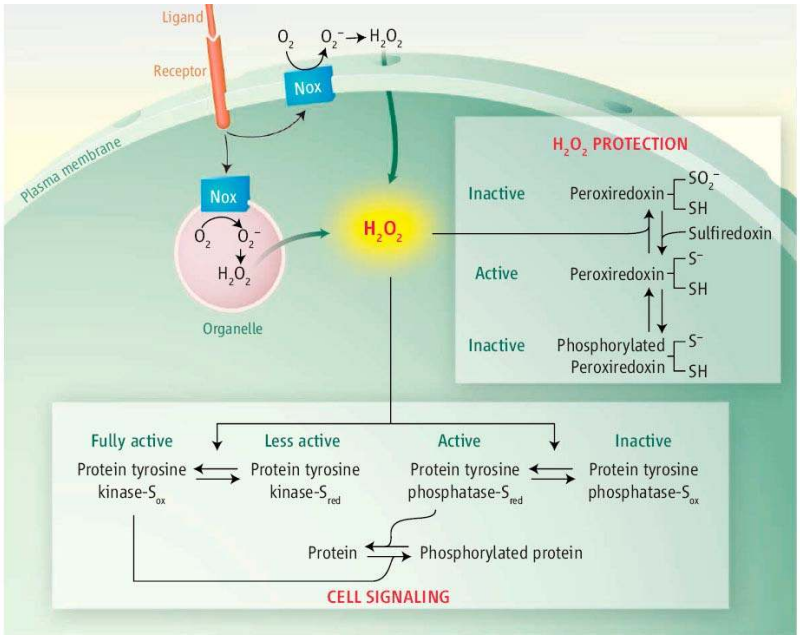

Fig. 5.10 ROS as a messenger for cell signaling Using H_2O_2 as a representation, ROS can be produced intracellularly or extracellularly by activating NADPH oxidase (Nox). Spatially produced H_2O_2 can modify the activity of key signal proteins—kinases and phosphatases. Notably, ROS catalyzing oxidation of essential cysteines eliminates phosphatase activities. Additionally, H_2O_2 promotes tyrosine phosphorylation by activating protein tyrosine kinases and creating an environment that favor proteins staying in the phosphorylated form. For H_2O_2 to serve as a signal—through modification of signaling proteins—its concentration must increase rapidly above a specific threshold. This can occur in the presence of temporarily inactivated antioxidant enzymes. During catalysis of H_2O_2 reduction, the active-site residue of Prx, Cys-SH, occasionally reacts with two molecules of H_2O_2 and, thus, becomes hyperoxidized to Cys-SOOH. Consequently, Prxs are inactivated. This inactivation, which can be reversed by sulfiredoxin, an adenosine triphosphate-dependent enzyme, likely represents a built-in mechanism that prevents suppression of the H_2O_2 signal. Ree SG Science 2006.

6. Conclusion

By using the retroviral-based gene delivery method, a murine podocyte cell line (AT1R podocyte) stably expresses human AT1R and has a constant $[Ca^{2+}]_i$ response to Ang II has been established. AT1R podocytes were a cell model for studying AT1R and AT2R signaling, and allowing performance of cellconsuming experiments. This study demonstrated that Ang II stimulation activities Rac signaling and up-regulates the expression of Rac-1 in AT1R podocytes. Ang II–stimulated podocytes revealed increased lamellipodia, membrane ruffles and cell migration — a cell phenotype typically directed by Rac-1. Elevated expression level of Rac-1 can also be confirmed in glomeruli of Neph-hAT1 TGRs that develop proteinuria, podocyte pseudocysts and finally focal segmental glomerular sclerosis.

In podocytes, Ang II induced a Rac-1–mediated and ROS–dependent rearrangement of cortical F-actin, stress fiber attenuation and a migratory phenotype switch. The Ang II–induced actin cytoskeletal remodeling was promoted further by activated Rac-1 and phosphorylated ERM proteins. Phosphorylated ERM proteins indicate that the F-actin cytoskeleton in podocytes is in a high turnover state and can affect crucial podocyte molecules in either the apical domain, basal domain or SD of FPs. Heparin, a potent G-coupled protein kinase 2 inhibitor, eliminated ERM protein phosphorylation in Ang II–treated podocytes. However, inhibition of Rho kinase, p38MAPK or protein kinase C had no effect on phosphorylation. Moreover, Ang II signaling down regulated α actinin-4 and reduced focal adhesion expression in podocytes. Nephrin, a major molecule in the SD, was also down-regulated in Ang II-treated AT1R podocytes and in glomeruli of Neph-hAT1 TGRs. Similar to α actinin-4, expression regulation of Ang II on nephrin involves both Rac-1 and RhoA signaling.

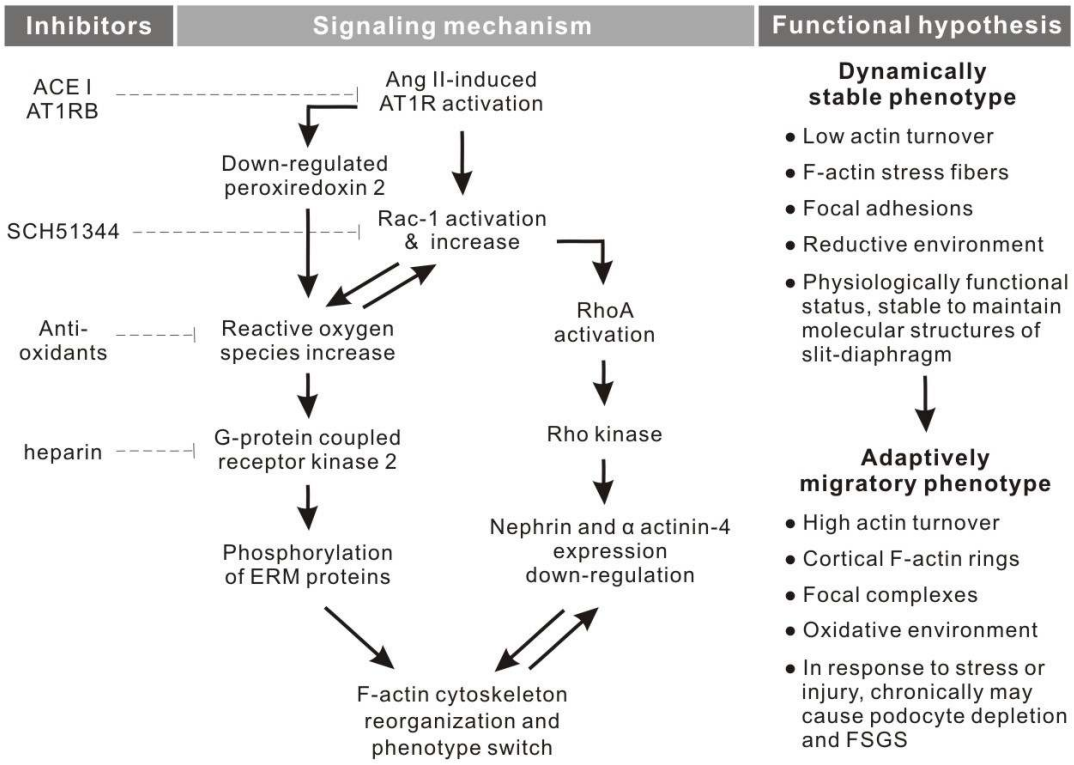

Fig. 6 Integrated model of signal transduction via AT1R and resultant effects on podocyte cytoskeletons After using Ang II to stimulate AT1R in podocytes, Rac-1 GTPases were activated in a PKC-independent manner. Additionally, Rac-1 expression was elevated. Activated Rac-1 induced NADPH-dependent oxidases to increase production of ROSs. The AT1R signaling also down-regulates expression of peroxiredoxin 2, which is a newly discovered antioxidant enzyme and cellular redox reaction modulator. Increased cytosolic ROS transformed the cellular redox environment from reductive into oxidative. Activated Rac-1 and increased ROS caused ERM protein phosphorylation and membrane redistribution by activating GRK2. Phosphorylated ERM proteins promoted de novo F-actin synthesis at the periphery of cells and triggered F-actin cytoskeletal reorganization, i.e., cortical F-actin ring formation and stress fiber attenuation. In a Rac-1-dependent manner, RhoA signaling was also activated in AT1R signaling and mediated the reduction in α actinin-4 expression. A notable finding was that increased cell migration and the cell-matrix contact pattern shifted from focal adhesions to focal complexes, thereby supporting the hypothesis of a podocyte phenotype transformation. Migratory phenotype podocytes can exert an adaptive response to physiological or injurious events. However, long-term activation of AT1R signaling may have devastating effects on podocytes. This figure also shows that inhibitors exert definitive renoprotective effects (ACEI and AT1RB) or have therapeutic potential (Rac-1 inhibitor, SCH51344; antioxidants; and, heparin).

AT1R signaling also down-regulates expression of Prx2, which is a newly discovered antioxidant enzyme and cellular redox reaction modulator. Using cultured Prx2 knock-down podocytes, we observed more intracellular ROS activity and compensatory up-regulation of catalase. Cell morphology was also altered in Prx2 knock-down podocytes: reduced adhesion to the matrix, less aborization and disruption of cell-cell contact. Increased cytosolic ROS transformed the cellular redox

environment from reductive into oxidative that favoring with phosphorylated ERM protein expression.

Chronically activated AT1R may induce a sustained phenotype shifting from a dynamically stable phenotype to an adaptively migratory phenotype. Persisting cytoskeletal reorganization in the end may exhaust podocytes via a high actin cytoskeletal turnover, deplete podocytes and subsequently cause FSGS. These experimental findings also suggest that heparin and Rac-1 inhibitors may be therapeutic tools for treating podocyte injury. (Fig. 6)

7. Prospect

The signaling mechanisms and cellular effects of Ang II–induced $[Ca^{2+}]_i$ increase still remain unknown in podocytes. By using the complete experimental system that contains *in vitro* (AT1R podocyte cell line) and *in vivo* (Neph-hAT1 TGRs) models, the angiotensin signaling network in podocytes can be uncovered. How are the PKC isoforms, and MAPKs, as well as several tyrosine kinases (JAK, Src, FAK) involved in this pleiotropic signaling cascade in podocytes? What are the cellular responses to Ang II stimulation in cultured or *in vivo* podocytes (contraction, migration, cell survival, growth, hypertrophy, adhesion and extracellular matrix formation)? Some consequences of AT1R activation are counteracted by the structurally dissimilar AT2R, which antagonizes the effects of AT1R–mediated growth responses on several cell types. The results of AT2R actions in podocytes remain unclear.

Proteins regulating the plasticity of the podocyte actin cytoskeleton are extremely important for maintenance of glomerular filter function. Podocyte cell shape changes, such as retraction of FPs, occur in minimal-change nephropathy, membranous nephropathy, focal segmental glomerulosclerosis, chronic glomerulonephritis, and diabetic nephropathy. What are the molecular mechanism orchestrate F-actin cytoskeleton reorganization in these clinical pathological entities? Heparin, a potent GRK2 inhibitor and exerting clinical therapeutic effects, may indicate the *in vivo* involvement of ERM protein phosphorylation in these proteinuric diseases.

Small GTPases including Ras, Rho, Rac and their downstream MAPKs, including extracellular signal-regulated kinase (ERK), c-Jun NH2-terminal kinase (JNK) and p38MAPK, play central roles in cellular responses such as cell proliferation, apoptosis, migration and gene expression. Small GTPases act as molecular switches controlled by a GDP/GTP-binding cycle, thereby regulating gene expression, cytoskeletal reorganization, intracellular vesicle trafficking and microtubule organization during the cell cycle, and other signaling events. The mechanisms of how Ang II signaling,

oxidative stress, mechanical stress, vasoconstrictors and growth factors activate small GTPases in podocytes remain unclear. It is noteworthy that if these signal molecules are also significantly activated in glomerulus of Neph-hAT1 TGRs. Using specific small GTPase catalytic pathway inhibitors, the cellular effects of small GTPase in podocyte AT1R signaling can be investigated in both *in vitro* and *in vivo* experimental models.

Recent clinical and experimental data demonstrate podocyte is the key player in diabetic nephropathy, the most frequent cause of end-stage renal disease. Podocytopenia is likely to be at the origin of proteinuria and segmental sclerosis in diabetic nephropathy. Podocyte loss has been reported in diabetic patients and many rodent experimental models. Notably, loss of podocytes is an early event in type 2 diabetic patients and the number of podocytes is the only morphologic parameter which predicts disease progression. ACEIs and AT1RBs reduce proteinuria and moderate the decline in glomerular filtration rate in patients with diabetic renal disease. These clinical data imply that angiotensin signaling mediates injuries in diabetic podocytes. Preliminary data affiliated with this work showed ERM protein of cultured podocytes is extensively phosphorylated in a hyperglycemic environment. This pathophysiological implication of a high actin turnover rate in diabetic podocyte may correlate with sustained RAS activation The podocyte injury hypothesis and experimental findings of this work can be extended by investigating the role of RAS in the pathogenesis of diabetic nephropathy.

8. Appendix

List of Figures and Tables

9. Reference

Reference List

1. Pavenstadt H, Kriz W, Kretzler M: Cell biology of the glomerular podocyte. *Physiol Rev* 83:253-307, 2003
2. Kriz W, Hackenthal E, Nobiling R, Sakai T, Elger M, Hahnel B: A role for podocytes to counteract capillary wall distension. *Kidney Int* 45:369-376, 1994
3. Drumond MC, Kristal B, Myers BD, Deen WM: Structural basis for reduced glomerular filtration capacity in nephrotic humans. *J Clin Invest* 94:1187-1195, 1994
4. Drenckhahn D, Franke RP: Ultrastructural organization of contractile and cytoskeletal proteins in glomerular podocytes of chicken, rat, and man. *Lab Invest* 59:673-682, 1988
5. Laurens W, Battaglia C, Foglieni C, De VR, Malanchini B, Van DB, Vanrenterghem Y, Remuzzi G, Remuzzi A: Direct podocyte damage in the single nephron leads to albuminuria in vivo. *Kidney Int* 47:1078-1086, 1995
6. Pavenstadt H: The charge for going by foot: modifying the surface of podocytes. *Exp Nephrol* 6:98-103, 1998
7. LeHir M, Kriz W: New insights into structural patterns encountered in glomerulosclerosis. *Curr Opin Nephrol Hypertens* 16:184-191, 2007
8. Kriz W, Gretz N, Lemley KV: Progression of glomerular diseases: is the podocyte the culprit? *Kidney Int* 54:687-697, 1998
9. Kerjaschki D: Dysfunctions of cell biological mechanisms of visceral epithelial cell (podocytes) in glomerular diseases. *Kidney Int* 45:300-313, 1994
10. Shankland SJ: The podocyte's response to injury: role in proteinuria and glomerulosclerosis. *Kidney Int* 69:2131-2147, 2006
11. Wolf G, Ziyadeh FN: Cellular and molecular mechanisms of proteinuria in diabetic nephropathy. *Nephron Physiol* 106:26-31, 2007
12. Kerjaschki D: Caught flat-footed: podocyte damage and the molecular bases of focal glomerulosclerosis. *J Clin Invest* 108:1583-1587, 2001
13. Schmieder S, Nagai M, Orlando RA, Takeda T, Farquhar MG: Podocalyxin activates RhoA and induces actin reorganization through NHERF1 and Ezrin in MDCK cells. *J Am Soc Nephrol* 15:2289-2298, 2004
14. Orlando RA, Takeda T, Zak B, Schmieder S, Benoit VM, McQuistan T, Furthmayr H, Farquhar MG: The glomerular epithelial cell anti-adhesin podocalyxin associates with the actin cytoskeleton through interactions with ezrin. *J Am Soc Nephrol* 12:1589-1598, 2001
15. Takeda T, McQuistan T, Orlando RA, Farquhar MG: Loss of glomerular foot

processes is associated with uncoupling of podocalyxin from the actin cytoskeleton. *J Clin Invest* 108:289-301, 2001

16. Braden GL, Mulhern JG, O'Shea MH, Nash SV, Ucci AA, Jr., Germain MJ: Changing incidence of glomerular diseases in adults. *Am J Kidney Dis* 35:878-883, 2000
17. Simon P, Ramee MP, Autuly V, Laruelle E, Charasse C, Cam G, Ang KS: Epidemiology of primary glomerular diseases in a French region. Variations according to period and age. *Kidney Int* 46:1192-1198, 1994
18. Cattran DC, Rao P: Long-term outcome in children and adults with classic focal segmental glomerulosclerosis. *Am J Kidney Dis* 32:72-79, 1998
19. Wehrmann M, Bohle A, Held H, Schumm G, Kendziorra H, Pressler H: Long-term prognosis of focal sclerosing glomerulonephritis. An analysis of 250 cases with particular regard to tubulointerstitial changes. *Clin Nephrol* 33:115-122, 1990
20. Cameron JS, Turner DR, Ogg CS, Chantler C, Williams DG: The long-term prognosis of patients with focal segmental glomerulosclerosis. *Clin Nephrol* 10:213-218, 1978
21. Beaufils H, Alphonse JC, Guedon J, Legrain M: Focal glomerulosclerosis: natural history and treatment. A report of 70 cases. *Nephron* 21:75-85, 1978
22. Van DB, Tardanico R, Vanrenterghem Y, Desmet V: Adhesions, focal sclerosis, protein crescents, and capsular lesions in membranous nephropathy. *J Pathol* 161:47-56, 1990
23. Kriz W, Hartmann I, Hosser H, Hahnel B, Kranzlin B, Provoost A, Gretz N: Tracer studies in the rat demonstrate misdirected filtration and peritubular filtrate spreading in nephrons with segmental glomerulosclerosis. *J Am Soc Nephrol* 12:496-506, 2001
24. Stout LC, Kumar S, Whorton EB: Insudative lesions--their pathogenesis and association with glomerular obsolescence in diabetes: a dynamic hypothesis based on single views of advancing human diabetic nephropathy. *Hum Pathol* 25:1213-1227, 1994
25. Le HM, Keller C, Eschmann V, Hahnel B, Hosser H, Kriz W: Podocyte bridges between the tuft and Bowman's capsule: an early event in experimental crescentic glomerulonephritis. *J Am Soc Nephrol* 12:2060-2071, 2001
26. Kriz W, LeHir M: Pathways to nephron loss starting from glomerular diseases-insights from animal models. *Kidney Int* 67:404-419, 2005
27. Kriz W, Hahnel B, Hosser H, Ostendorf T, Gaertner S, Kranzlin B, Gretz N, Shimizu F, Floege J: Pathways to recovery and loss of nephrons in anti-Thy-1 nephritis. *J Am Soc Nephrol* 14:1904-1926, 2003
28. Nagata M, Kriz W: Glomerular damage after uninephrectomy in young rats. II. Mechanical stress on podocytes as a pathway to sclerosis. *Kidney Int* 42:148-160, 1992
29. Fries JW, Sandstrom DJ, Meyer TW, Rennke HG: Glomerular hypertrophy and epithelial cell injury modulate progressive glomerulosclerosis in the rat. *Lab Invest*

60:205-218, 1989

30. Wharram BL, Goyal M, Wiggins JE, Sanden SK, Hussain S, Filipiak WE, Saunders TL, Dysko RC, Kohno K, Holzman LB, Wiggins RC: Podocyte depletion causes glomerulosclerosis: diphtheria toxin-induced podocyte depletion in rats expressing human diphtheria toxin receptor transgene. *J Am Soc Nephrol* 16:2941-2952, 2005
31. Asano T, Niimura F, Pastan I, Fogo AB, Ichikawa I, Matsusaka T: Permanent genetic tagging of podocytes: fate of injured podocytes in a mouse model of glomerular sclerosis. *J Am Soc Nephrol* 16:2257-2262, 2005
32. Ichikawa I, Ma J, Motojima M, Matsusaka T: Podocyte damage damages podocytes: autonomous vicious cycle that drives local spread of glomerular sclerosis. *Curr Opin Nephrol Hypertens* 14:205-210, 2005
33. Matsusaka T, Xin J, Niwa S, Kobayashi K, Akatsuka A, Hashizume H, Wang QC, Pastan I, Fogo AB, Ichikawa I: Genetic engineering of glomerular sclerosis in the mouse via control of onset and severity of podocyte-specific injury. *J Am Soc Nephrol* 16:1013-1023, 2005
34. Kriz W: TRPC6 - a new podocyte gene involved in focal segmental glomerulosclerosis. *Trends Mol Med* 11:527-530, 2005
35. Kaplan JM, Kim SH, North KN, Rennke H, Correia LA, Tong HQ, Mathis BJ, Rodriguez-Perez JC, Allen PG, Beggs AH, Pollak MR: Mutations in ACTN4, encoding alpha-actinin-4, cause familial focal segmental glomerulosclerosis. *Nat Genet* 24:251-256, 2000
36. Weins A, Kenlan P, Herbert S, Le TC, Villegas I, Kaplan BS, Appel GB, Pollak MR: Mutational and Biological Analysis of alpha-actinin-4 in focal segmental glomerulosclerosis. *J Am Soc Nephrol* 16:3694-3701, 2005
37. Timmermans PB, Wong PC, Chiu AT, Herblin WF, Benfield P, Carini DJ, Lee RJ, Wexler RR, Saye JA, Smith RD: Angiotensin II receptors and angiotensin II receptor antagonists. *Pharmacol Rev* 45:205-251, 1993
38. de GM, Catt KJ, Inagami T, Wright JW, Unger T: International union of pharmacology. XXIII. The angiotensin II receptors. *Pharmacol Rev* 52:415-472, 2000
39. Weber KT, Sun Y, Campbell SE: Structural remodelling of the heart by fibrous tissue: role of circulating hormones and locally produced peptides. *Eur Heart J* 16 Suppl N:12-18, 1995
40. Griffin SA, Brown WC, MacPherson F, McGrath JC, Wilson VG, Korsgaard N, Mulvany MJ, Lever AF: Angiotensin II causes vascular hypertrophy in part by a non-pressor mechanism. *Hypertension* 17:626-635, 1991
41. Dzau VJ, Gibbons GH: Autocrine-paracrine mechanisms of vascular myocytes in systemic hypertension. *Am J Cardiol* 60:99I-103I, 1987
42. Ferrario CM, Iyer SN: Angiotensin-(1-7): a bioactive fragment of the

renin-angiotensin system. *Regul Pept* 78:13-18, 1998

43. Wright JW, Krebs LT, Stobb JW, Harding JW: The angiotensin IV system: functional implications. *Front Neuroendocrinol* 16:23-52, 1995
44. Ferrario CM, Brosnihan KB, Diz DI, Jaiswal N, Khosla MC, Milsted A, Tallant EA: Angiotensin-(1-7): a new hormone of the angiotensin system. *Hypertension* 18:III126-III133, 1991
45. Schiavone MT, Khosla MC, Ferrario CM: Angiotensin-[1-7]: evidence for novel actions in the brain. *J Cardiovasc Pharmacol* 16 Suppl 4:S19-S24, 1990
46. Peach MJ: Renin-angiotensin system: biochemistry and mechanisms of action. *Physiol Rev* 57:313-370, 1977
47. Parving HH, Lehnert H, Brochner-Mortensen J, Gomis R, Andersen S, Arner P: The effect of irbesartan on the development of diabetic nephropathy in patients with type 2 diabetes. *N Engl J Med* 345:870-878, 2001
48. Maschio G, Alberti D, Janin G, Locatelli F, Mann JF, Motolese M, Ponticelli C, Ritz E, Zucchelli P: Effect of the angiotensin-converting-enzyme inhibitor benazepril on the progression of chronic renal insufficiency. The Angiotensin-Converting-Enzyme Inhibition in Progressive Renal Insufficiency Study Group. *N Engl J Med* 334:939-945, 1996
49. Remuzzi G, Benigni A, Remuzzi A: Mechanisms of progression and regression of renal lesions of chronic nephropathies and diabetes. *J Clin Invest* 116:288-296, 2006
50. Zoja C, Donadelli R, Corna D, Testa D, Facchinetti D, Maffi R, Luzzana E, Colosio V, Bertani T, Remuzzi G: The renoprotective properties of angiotensin-converting enzyme inhibitors in a chronic model of membranous nephropathy are solely due to the inhibition of angiotensin II: evidence based on comparative studies with a receptor antagonist. *Am J Kidney Dis* 29:254-264, 1997
51. Haddad G, Amiri F, Garcia R: Modulation of renal glomerular angiotensin II receptors by ace inhibition and AT1 receptor antagonism. *Regul Pept* 68:111-117, 1997
52. Perico N, Amuchastegui CS, Malanchini B, Bertani T, Remuzzi G: Angiotensin-converting enzyme inhibition and calcium channel blockade both normalize early hyperfiltration in experimental diabetes, but only the former prevents late renal structural damage. *Exp Nephrol* 2:220-228, 1994
53. Remuzzi A, Perico N, Amuchastegui CS, Malanchini B, Mazerska M, Battaglia C, Bertani T, Remuzzi G: Short- and long-term effect of angiotensin II receptor blockade in rats with experimental diabetes. *J Am Soc Nephrol* 4:40-49, 1993
54. Lafayette RA, Mayer G, Park SK, Meyer TW: Angiotensin II receptor blockade limits glomerular injury in rats with reduced renal mass. *J Clin Invest* 90:766-771, 1992
55. Lafayette RA, Mayer G, Park SK, Meyer TW: Angiotensin II receptor blockade limits glomerular injury in rats with reduced renal mass. *J Clin Invest* 90:766-771, 1992

56. Henger A, Huber T, Fischer KG, Nitschke R, Mundel P, Schollmeyer P, Greger R, Pavenstadt H: Angiotensin II increases the cytosolic calcium activity in rat podocytes in culture. *Kidney Int* 52:687-693, 1997
57. Gloy J, Henger A, Fischer KG, Nitschke R, Bleich M, Mundel P, Schollmeyer P, Greger R, Pavenstadt H: Angiotensin II modulates cellular functions of podocytes. *Kidney Int Suppl* 67:S168-S170, 1998
58. Gloy J, Henger A, Fischer KG, Nitschke R, Mundel P, Bleich M, Schollmeyer P, Greger R, Pavenstadt H: Angiotensin II depolarizes podocytes in the intact glomerulus of the Rat. *J Clin Invest* 99:2772-2781, 1997
59. Nitschke R, Henger A, Ricken S, Gloy J, Muller V, Greger R, Pavenstadt H: Angiotensin II increases the intracellular calcium activity in podocytes of the intact glomerulus. *Kidney Int* 57:41-49, 2000
60. Hoffmann S, Podlich D, Hahnel B, Kriz W, Gretz N: Angiotensin II type 1 receptor overexpression in podocytes induces glomerulosclerosis in transgenic rats. *J Am Soc Nephrol* 15:1475-1487, 2004
61. Kretzler M, Koeppen-Hagemann I, Kriz W: Podocyte damage is a critical step in the development of glomerulosclerosis in the uninephrectomised-desoxycorticosterone hypertensive rat. *Virchows Arch* 425:181-193, 1994
62. Hall A: Rho GTPases and the actin cytoskeleton. *Science* 279:509-514, 1998
63. Zuo L, Ushio-Fukai M, Ikeda S, Hilenski L, Patrushev N, Alexander RW: Caveolin-1 is essential for activation of Rac1 and NAD(P)H oxidase after angiotensin II type 1 receptor stimulation in vascular smooth muscle cells: role in redox signaling and vascular hypertrophy. *Arterioscler Thromb Vasc Biol* 25:1824-1830, 2005
64. Zimmerman MC, Dunlay RP, Lazartigues E, Zhang Y, Sharma RV, Engelhardt JF, Davisson RL: Requirement for Rac1-dependent NADPH oxidase in the cardiovascular and dipsogenic actions of angiotensin II in the brain. *Circ Res* 95:532-539, 2004
65. Hordijk PL: Regulation of NADPH oxidases: the role of Rac proteins. *Circ Res* 98:453-462, 2006
66. Otis M, Gallo-Payet N: Differential involvement of cytoskeleton and rho-guanosine 5'-triphosphatases in growth-promoting effects of angiotensin II in rat adrenal glomerulosa cells. *Endocrinology* 147:5460-5469, 2006
67. Bretscher A: Purification of an 80,000-dalton protein that is a component of the isolated microvillus cytoskeleton, and its localization in nonmuscle cells. *J Cell Biol* 97:425-432, 1983
68. Lankes WT, Furthmayr H: Moesin: a member of the protein 4.1-talin-ezrin family of proteins. *Proc Natl Acad Sci U S A* 88:8297-8301, 1991
69. Tsukita S, Hieda Y, Tsukita S: A new 82-kD barbed end-capping protein (radixin) localized in the cell-to-cell adherens junction: purification and characterization. *J Cell*

Biol 108:2369-2382, 1989

70. Bretscher A, Edwards K, Fehon RG: ERM proteins and merlin: integrators at the cell cortex. *Nat Rev Mol Cell Biol* 3:586-599, 2002
71. Khanna C, Wan X, Bose S, Cassaday R, Olomu O, Mendoza A, Yeung C, Gorlick R, Hewitt SM, Helman LJ: The membrane-cytoskeleton linker ezrin is necessary for osteosarcoma metastasis. *Nat Med* 10:182-186, 2004
72. Yu Y, Khan J, Khanna C, Helman L, Meltzer PS, Merlino G: Expression profiling identifies the cytoskeletal organizer ezrin and the developmental homeoprotein Six-1 as key metastatic regulators. *Nat Med* 10:175-181, 2004
73. Lamb RF, Ozanne BW, Roy C, McGarry L, Stipp C, Mangeat P, Jay DG: Essential functions of ezrin in maintenance of cell shape and lamellipodial extension in normal and transformed fibroblasts. *Curr Biol* 7:682-688, 1997
74. Takeuchi K, Sato N, Kasahara H, Funayama N, Nagafuchi A, Yonemura S, Tsukita S, Tsukita S: Perturbation of cell adhesion and microvilli formation by antisense oligonucleotides to ERM family members. *J Cell Biol* 125:1371-1384, 1994
75. Reczek D, Berryman M, Bretscher A: Identification of EBP50: A PDZ-containing phosphoprotein that associates with members of the ezrin-radixin-moesin family. *J Cell Biol* 139:169-179, 1997
76. Bretscher A, Reczek D, Berryman M: Ezrin: a protein requiring conformational activation to link microfilaments to the plasma membrane in the assembly of cell surface structures. *J Cell Sci* 110 (Pt 24):3011-3018, 1997
77. Gary R, Bretscher A: Ezrin self-association involves binding of an N-terminal domain to a normally masked C-terminal domain that includes the F-actin binding site. *Mol Biol Cell* 6:1061-1075, 1995
78. Tebbi K, Rubin S, Cowan DH, McCulloch EA: A comparison of granulopoiesis in culture from blood and marrow cells of nonleukemic individuals and patients with acute leukemia. *Blood* 48:235-243, 1976
79. Ishikawa H, Tamura A, Matsui T, Sasaki H, Hakoshima T, Tsukita S, Tsukita S: Structural conversion between open and closed forms of radixin: low-angle shadowing electron microscopy. *J Mol Biol* 310:973-978, 2001
80. Barret C, Roy C, Montcourrier P, Mangeat P, Niggli V: Mutagenesis of the phosphatidylinositol 4,5-bisphosphate (PIP(2)) binding site in the NH(2)-terminal domain of ezrin correlates with its altered cellular distribution. *J Cell Biol* 151:1067-1080, 2000
81. Niggli V, Andreoli C, Roy C, Mangeat P: Identification of a phosphatidylinositol-4,5-bisphosphate-binding domain in the N-terminal region of ezrin. *FEBS Lett* 376:172-176, 1995
82. Nakamura F, Amieva MR, Furthmayr H: Phosphorylation of threonine 558 in the

carboxyl-terminal actin-binding domain of moesin by thrombin activation of human platelets. *J Biol Chem* 270:31377-31385, 1995

83. Takeda T: Podocyte cytoskeleton is connected to the integral membrane protein podocalyxin through Na+/H+-exchanger regulatory factor 2 and ezrin. *Clin Exp Nephrol* 7:260-269, 2003
84. Orlando RA, Takeda T, Zak B, Schmieder S, Benoit VM, McQuistan T, Furthmayr H, Farquhar MG: The glomerular epithelial cell anti-adhesin podocalyxin associates with the actin cytoskeleton through interactions with ezrin. *J Am Soc Nephrol* 12:1589-1598, 2001
85. Hugo C, Nangaku M, Shankland SJ, Pichler R, Gordon K, Amieva MR, Couser WG, Furthmayr H, Johnson RJ: The plasma membrane-actin linking protein, ezrin, is a glomerular epithelial cell marker in glomerulogenesis, in the adult kidney and in glomerular injury. *Kidney Int* 54:1934-1944, 1998
86. Broderick MJ, Winder SJ: Spectrin, alpha-actinin, and dystrophin. *Adv Protein Chem* 70:203-246, 2005
87. Djinovic-Carugo K, Gautel M, Ylanne J, Young P: The spectrin repeat: a structural platform for cytoskeletal protein assemblies. *FEBS Lett* 513:119-123, 2002
88. Ylanne J, Scheffzek K, Young P, Saraste M: Crystal structure of the alpha-actinin rod reveals an extensive torsional twist. *Structure* 9:597-604, 2001
89. Young P, Ferguson C, Banuelos S, Gautel M: Molecular structure of the sarcomeric Z-disk: two types of titin interactions lead to an asymmetrical sorting of alpha-actinin. *EMBO J* 17:1614-1624, 1998
90. Ohtsuka H, Yajima H, Maruyama K, Kimura S: The N-terminal Z repeat 5 of connectin/titin binds to the C-terminal region of alpha-actinin. *Biochem Biophys Res Commun* 235:1-3, 1997
91. Kos CH, Le TC, Sinha S, Henderson JM, Kim SH, Sugimoto H, Kalluri R, Gerszten RE, Pollak MR: Mice deficient in alpha-actinin-4 have severe glomerular disease. *J Clin Invest* 111:1683-1690, 2003
92. Dandapani SV, Sugimoto H, Matthews BD, Kolb RJ, Sinha S, Gerszten RE, Zhou J, Ingber DE, Kalluri R, Pollak MR: Alpha-actinin-4 is required for normal podocyte adhesion. *J Biol Chem* 282:467-477, 2007
93. Hallman N, Norio R, Rapola J: Congenital nephrotic syndrome. *Nephron* 11:101-110, 1973
94. Huttunen NP: Congenital nephrotic syndrome of Finnish type. Study of 75 patients. *Arch Dis Child* 51:344-348, 1976
95. Kestila M, Lenkkeri U, Mannikko M, Lamerdin J, McCready P, Putaala H, Ruotsalainen V, Morita T, Nissinen M, Herva R, Kashtan CE, Peltonen L, Holmberg C, Olsen A, Tryggvason K: Positionally cloned gene for a novel glomerular

protein--nephrin--is mutated in congenital nephrotic syndrome. *Mol Cell* 1:575-582, 1998

96. Ruotsalainen V, Ljungberg P, Wartiovaara J, Lenkkeri U, Kestila M, Jalanko H, Holmberg C, Tryggvason K: Nephrin is specifically located at the slit diaphragm of glomerular podocytes. *Proc Natl Acad Sci U S A* 96:7962-7967, 1999
97. Putaala H, Soininen R, Kilpelainen P, Wartiovaara J, Tryggvason K: The murine nephrin gene is specifically expressed in kidney, brain and pancreas: inactivation of the gene leads to massive proteinuria and neonatal death. *Hum Mol Genet* 10:1-8, 2001
98. Rodewald R, Karnovsky MJ: Porous substructure of the glomerular slit diaphragm in the rat and mouse. *J Cell Biol* 60:423-433, 1974
99. Jones N, Blasutig IM, Eremina V, Ruston JM, Bladt F, Li H, Huang H, Larose L, Li SS, Takano T, Quaggin SE, Pawson T: Nck adaptor proteins link nephrin to the actin cytoskeleton of kidney podocytes. *Nature* 440:818-823, 2006
100. Verma R, Wharram B, Kovari I, Kunkel R, Nihalani D, Wary KK, Wiggins RC, Killen P, Holzman LB: Fyn binds to and phosphorylates the kidney slit diaphragm component Nephrin. *J Biol Chem* 278:20716-20723, 2003
101. Tryggvason K, Patrakka J, Wartiovaara J: Hereditary proteinuria syndromes and mechanisms of proteinuria. *N Engl J Med* 354:1387-1401, 2006
102. Winyard PG, Moody CJ, Jacob C: Oxidative activation of antioxidant defence. *Trends Biochem Sci* 30:453-461, 2005
103. Butterfield LH, Merino A, Golub SH, Shau H: From cytoprotection to tumor suppression: the multifactorial role of peroxiredoxins. *Antioxid Redox Signal* 1:385-402, 1999
104. Fujii J, Ikeda Y: Advances in our understanding of peroxiredoxin, a multifunctional, mammalian redox protein. *Redox Rep* 7:123-130, 2002
105. Chae HZ, Robison K, Poole LB, Church G, Storz G, Rhee SG: Cloning and sequencing of thiol-specific antioxidant from mammalian brain: alkyl hydroperoxide reductase and thiol-specific antioxidant define a large family of antioxidant enzymes. *Proc Natl Acad Sci U S A* 91:7017-7021, 1994
106. Wonsey DR, Zeller KI, Dang CV: The c-Myc target gene PRDX3 is required for mitochondrial homeostasis and neoplastic transformation. *Proc Natl Acad Sci U S A* 99:6649-6654, 2002
107. Kang SW, Chae HZ, Seo MS, Kim K, Baines IC, Rhee SG: Mammalian peroxiredoxin isoforms can reduce hydrogen peroxide generated in response to growth factors and tumor necrosis factor-alpha. *J Biol Chem* 273:6297-6302, 1998
108. Jin DY, Chae HZ, Rhee SG, Jeang KT: Regulatory role for a novel human thioredoxin peroxidase in NF-kappaB activation. *J Biol Chem* 272:30952-30961, 1997
109. Kim H, Lee TH, Park ES, Suh JM, Park SJ, Chung HK, Kwon OY, Kim YK, Ro HK,

Shong M: Role of peroxiredoxins in regulating intracellular hydrogen peroxide and hydrogen peroxide-induced apoptosis in thyroid cells. *J Biol Chem* 275:18266-18270, 2000

110. Wong CM, Chun AC, Kok KH, Zhou Y, Fung PC, Kung HF, Jeang KT, Jin DY: Characterization of human and mouse peroxiredoxin IV: evidence for inhibition by Prx-IV of epidermal growth factor- and p53-induced reactive oxygen species. *Antioxid Redox Signal* 2:507-518, 2000
111. Park SH, Chung YM, Lee YS, Kim HJ, Kim JS, Chae HZ, Yoo YD: Antisense of human peroxiredoxin II enhances radiation-induced cell death. *Clin Cancer Res* 6:4915-4920, 2000
112. Chung YM, Yoo YD, Park JK, Kim YT, Kim HJ: Increased expression of peroxiredoxin II confers resistance to cisplatin. *Anticancer Res* 21:1129-1133, 2001
113. Schiwek D, Endlich N, Holzman L, Holthofer H, Kriz W, Endlich K: Stable expression of nephrin and localization to cell-cell contacts in novel murine podocyte cell lines. *Kidney Int* 66:91-101, 2004
114. Nickel C, Benzing T, Sellin L, Gerke P, Karihaloo A, Liu ZX, Cantley LG, Walz G: The polycystin-1 C-terminal fragment triggers branching morphogenesis and migration of tubular kidney epithelial cells. *J Clin Invest* 109:481-489, 2002
115. Stachon A, Stegemann H, Hohage H, Rahn KH, Schlatter E: Effects of diadenosine polyphosphates on the intracellular Ca2+ concentration in endothelial cells. *Cell Physiol Biochem* 8:175-184, 1998
116. Grynkiewicz G, Poenie M, Tsien RY: A new generation of Ca2+ indicators with greatly improved fluorescence properties. *J Biol Chem* 260:3440-3450, 1985
117. Ohara Y, Peterson TE, Harrison DG: Hypercholesterolemia increases endothelial superoxide anion production. *J Clin Invest* 91:2546-2551, 1993
118. Bek MF, Bayer M, Muller B, Greiber S, Lang D, Schwab A, August C, Springer E, Rohrbach R, Huber TB, Benzing T, Pavenstadt H: Expression and function of C/EBP homology protein (GADD153) in podocytes. *Am J Pathol* 168:20-32, 2006
119. Carter WO, Narayanan PK, Robinson JP: Intracellular hydrogen peroxide and superoxide anion detection in endothelial cells. *J Leukoc Biol* 55:253-258, 1994
120. Fire A, Xu S, Montgomery MK, Kostas SA, Driver SE, Mello CC: Potent and specific genetic interference by double-stranded RNA in Caenorhabditis elegans. *Nature* 391:806-811, 1998
121. Elbashir SM, Harborth J, Lendeckel W, Yalcin A, Weber K, Tuschl T: Duplexes of 21-nucleotide RNAs mediate RNA interference in cultured mammalian cells. *Nature* 411:494-498, 2001
122. Echeverri CJ, Perrimon N: High-throughput RNAi screening in cultured cells: a user's guide. *Nat Rev Genet* 7:373-384, 2006

123. Napoli C, Lemieux C, Jorgensen R: Introduction of a Chimeric Chalcone Synthase Gene into Petunia Results in Reversible Co-Suppression of Homologous Genes in trans. *Plant Cell* 2:279-289, 1990
124. van der Krol AR, Mur LA, Beld M, Mol JN, Stuitje AR: Flavonoid genes in petunia: addition of a limited number of gene copies may lead to a suppression of gene expression. *Plant Cell* 2:291-299, 1990
125. Bernstein E, Caudy AA, Hammond SM, Hannon GJ: Role for a bidentate ribonuclease in the initiation step of RNA interference. *Nature* 409:363-366, 2001
126. Elbashir SM, Lendeckel W, Tuschl T: RNA interference is mediated by 21- and 22-nucleotide RNAs. *Genes Dev* 15:188-200, 2001
127. Hammond SM, Bernstein E, Beach D, Hannon GJ: An RNA-directed nuclease mediates post-transcriptional gene silencing in Drosophila cells. *Nature* 404:293-296, 2000
128. Martinez J, Tuschl T: RISC is a 5' phosphomonoester-producing RNA endonuclease. *Genes Dev* 18:975-980, 2004
129. Opalinska JB, Gewirtz AM: Nucleic acid therapeutics: a work in progress. *Curr Opin Investig Drugs* 3:928-933, 2002
130. Suzuki K, Han GD, Miyauchi N, Hashimoto T, Nakatsue T, Fujioka Y, Koike H, Shimizu F, Kawachi H: Angiotensin II type 1 and type 2 receptors play opposite roles in regulating the barrier function of kidney glomerular capillary wall. *Am J Pathol* 170:1841-1853, 2007
131. Baumgartner MR, Almashanu S, Suormala T, Obie C, Cole RN, Packman S, Baumgartner ER, Valle D: The molecular basis of human 3-methylcrotonyl-CoA carboxylase deficiency. *J Clin Invest* 107:495-504, 2001
132. Woo HA, Chae HZ, Hwang SC, Yang KS, Kang SW, Kim K, Rhee SG: Reversing the inactivation of peroxiredoxins caused by cysteine sulfinic acid formation. *Science* 300:653-656, 2003
133. Soini Y, Kallio JP, Hirvikoski P, Helin H, Kellokumpu-Lehtinen P, Kang SW, Tammela TL, Peltoniemi M, Martikainen PM, Kinnula VL: Oxidative/nitrosative stress and peroxiredoxin 2 are associated with grade and prognosis of human renal carcinoma. *APMIS* 114:329-337, 2006
134. Whiteside CI, Cameron R, Munk S, Levy J: Podocytic cytoskeletal disaggregation and basement-membrane detachment in puromycin aminonucleoside nephrosis. *Am J Pathol* 142:1641-1653, 1993
135. Durvasula RV, Shankland SJ: Podocyte injury and targeting therapy: an update. *Curr Opin Nephrol Hypertens* 15:1-7, 2006
136. Satoh M, Ogita H, Takeshita K, Mukai Y, Kwiatkowski DJ, Liao JK: Requirement of Rac1 in the development of cardiac hypertrophy. *Proc Natl Acad Sci U S A*

103:7432-7437, 2006

137. Wolf G: New insights into the pathophysiology of diabetic nephropathy: from haemodynamics to molecular pathology. *Eur J Clin Invest* 34:785-796, 2004
138. Gill PS, Wilcox CS: NADPH oxidases in the kidney. *Antioxid Redox Signal* 8:1597-1607, 2006
139. Bustelo XR, Sauzeau V, Berenjeno IM: GTP-binding proteins of the Rho/Rac family: regulation, effectors and functions in vivo. *Bioessays* 29:356-370, 2007
140. Seshiah PN, Weber DS, Rocic P, Valppu L, Taniyama Y, Griendling KK: Angiotensin II stimulation of NAD(P)H oxidase activity: upstream mediators. *Circ Res* 91:406-413, 2002
141. Schmitz U, Thommes K, Beier I, Wagner W, Sachinidis A, Dusing R, Vetter H: Angiotensin II-induced stimulation of p21-activated kinase and c-Jun NH2-terminal kinase is mediated by Rac1 and Nck. *J Biol Chem* 276:22003-22010, 2001
142. Asanuma K, Yanagida-Asanuma E, Faul C, Tomino Y, Kim K, Mundel P: Synaptopodin orchestrates actin organization and cell motility via regulation of RhoA signalling. *Nat Cell Biol* 8:485-491, 2006
143. Endlich N, Kress KR, Reiser J, Uttenweiler D, Kriz W, Mundel P, Endlich K: Podocytes respond to mechanical stress in vitro. *J Am Soc Nephrol* 12:413-422, 2001
144. Morigi M, Buelli S, Angioletti S, Zanchi C, Longaretti L, Zoja C, Galbusera M, Gastoldi S, Mundel P, Remuzzi G, Benigni A: In response to protein load podocytes reorganize cytoskeleton and modulate endothelin-1 gene: implication for permselective dysfunction of chronic nephropathies. *Am J Pathol* 166:1309-1320, 2005
145. Kozma R, Sarner S, Ahmed S, Lim L: Rho family GTPases and neuronal growth cone remodelling: relationship between increased complexity induced by Cdc42Hs, Rac1, and acetylcholine and collapse induced by RhoA and lysophosphatidic acid. *Mol Cell Biol* 17:1201-1211, 1997
146. Caron E, Hall A: Identification of two distinct mechanisms of phagocytosis controlled by different Rho GTPases. *Science* 282:1717-1721, 1998
147. Nobes CD, Hall A: Rho, rac, and cdc42 GTPases regulate the assembly of multimolecular focal complexes associated with actin stress fibers, lamellipodia, and filopodia. *Cell* 81:53-62, 1995
148. Koss M, Pfeiffer GR, Wang Y, Thomas ST, Yerukhimovich M, Gaarde WA, Doerschuk CM, Wang Q: Ezrin/radixin/moesin proteins are phosphorylated by TNF-alpha and modulate permeability increases in human pulmonary microvascular endothelial cells. *J Immunol* 176:1218-1227, 2006
149. Ng T, Parsons M, Hughes WE, Monypenny J, Zicha D, Gautreau A, Arpin M, Gschmeissner S, Verveer PJ, Bastiaens PI, Parker PJ: Ezrin is downstream effector of

trafficking PKC-integrin complexes involved in the control of cell motility. *EMBO J* 20:2723-2741, 2001

150. Pietromonaco SF, Simons PC, Altman A, Elias L: Protein kinase C-theta phosphorylation of moesin in the actin-binding sequence. *J Biol Chem* 273:7594-7603, 1998
151. Rossy J, Gutjahr MC, Blaser N, Schlicht D, Niggli V: Ezrin/moesin in motile Walker 256 carcinosarcoma cells: signal-dependent relocalization and role in migration. *Exp Cell Res* 313:1106-1120, 2007
152. Pitcher JA, Tesmer JJ, Freeman JL, Capel WD, Stone WC, Lefkowitz RJ: Feedback inhibition of G protein-coupled receptor kinase 2 (GRK2) activity by extracellular signal-regulated kinases. *J Biol Chem* 274:34531-34534, 1999
153. Cotton M, Boulay PL, Houndolo T, Vitale N, Pitcher JA, Claing A: Endogenous ARF6 interacts with Rac1 upon angiotensin II stimulation to regulate membrane ruffling and cell migration. *Mol Biol Cell* 18:501-511, 2007
154. Laursen JB, Rajagopalan S, Galis Z, Tarpey M, Freeman BA, Harrison DG: Role of superoxide in angiotensin II-induced but not catecholamine-induced hypertension. *Circulation* 95:588-593, 1997
155. Rajagopalan S, Kurz S, Munzel T, Tarpey M, Freeman BA, Griendling KK, Harrison DG: Angiotensin II-mediated hypertension in the rat increases vascular superoxide production via membrane NADH/NADPH oxidase activation. Contribution to alterations of vasomotor tone. *J Clin Invest* 97:1916-1923, 1996
156. Usatyuk PV, Romer LH, He D, Parinandi NL, Kleinberg ME, Zhan S, Jacobson JR, Dudek SM, Pendyala S, Garcia JG, Natarajan V: Regulation of Hyperoxia-induced NADPH Oxidase Activation in Human Lung Endothelial Cells by the Actin Cytoskeleton and Cortactin. *J Biol Chem* 282:23284-23295, 2007
157. Saenz-Morales D, Escribese MM, Stamatakis K, Garcia-Martos M, Alegre L, Conde E, Perez-Sala D, Mampaso F, Garcia-Bermejo ML: Requirements for proximal tubule epithelial cell detachment in response to ischemia: role of oxidative stress. *Exp Cell Res* 312:3711-3727, 2006
158. Schreibelt G, Kooij G, Reijerkerk A, van DR, Gringhuis SI, van der PS, Weksler BB, Romero IA, Couraud PO, Piontek J, Blasig IE, Dijkstra CD, Ronken E, de Vries HE: Reactive oxygen species alter brain endothelial tight junction dynamics via RhoA, PI3 kinase, and PKB signaling. *FASEB J* 2007
159. Gautreau A, Louvard D, Arpin M: Morphogenic effects of ezrin require a phosphorylation-induced transition from oligomers to monomers at the plasma membrane. *J Cell Biol* 150:193-203, 2000
160. Hayashi K, Yonemura S, Matsui T, Tsukita S: Immunofluorescence detection of ezrin/radixin/moesin (ERM) proteins with their carboxyl-terminal threonine

phosphorylated in cultured cells and tissues. *J Cell Sci* 112 (Pt 8):1149-1158, 1999

161. Matsui T, Maeda M, Doi Y, Yonemura S, Amano M, Kaibuchi K, Tsukita S, Tsukita S: Rho-kinase phosphorylates COOH-terminal threonines of ezrin/radixin/moesin (ERM) proteins and regulates their head-to-tail association. *J Cell Biol* 140:647-657, 1998
162. Sagara Y, Hirooka Y, Nozoe M, Ito K, Kimura Y, Sunagawa K: Pressor response induced by central angiotensin II is mediated by activation of Rho/Rho-kinase pathway via AT1 receptors. *J Hypertens* 25:399-406, 2007
163. Yonemura S, Matsui T, Tsukita S, Tsukita S: Rho-dependent and -independent activation mechanisms of ezrin/radixin/moesin proteins: an essential role for polyphosphoinositides in vivo. *J Cell Sci* 115:2569-2580, 2002
164. Auvinen E, Kivi N, Vaheri A: Regulation of ezrin localization by Rac1 and PIPK in human epithelial cells. *Exp Cell Res* 313:824-833, 2007
165. Lan M, Kojima T, Murata M, Osanai M, Takano K, Chiba H, Sawada N: Phosphorylation of ezrin enhances microvillus length via a p38 MAP-kinase pathway in an immortalized mouse hepatic cell line. *Exp Cell Res* 312:111-120, 2006
166. Cant SH, Pitcher JA: G protein-coupled receptor kinase 2-mediated phosphorylation of ezrin is required for G protein-coupled receptor-dependent reorganization of the actin cytoskeleton. *Mol Biol Cell* 16:3088-3099, 2005
167. Schwarz A: New aspects of the treatment of nephrotic syndrome. *J Am Soc Nephrol* 12 Suppl 17:S44-S47, 2001
168. Benovic JL, Stone WC, Caron MG, Lefkowitz RJ: Inhibition of the beta-adrenergic receptor kinase by polyanions. *J Biol Chem* 264:6707-6710, 1989
169. Benovic JL: Purification and characterization of beta-adrenergic receptor kinase. *Methods Enzymol* 200:351-362, 1991
170. Kassack MU, Hogger P, Gschwend DA, Kameyama K, Haga T, Graul RC, Sadee W: Molecular modeling of G-protein coupled receptor kinase 2: docking and biochemical evaluation of inhibitors. *AAPS PharmSci* 2:E2, 2000
171. Cant SH, Pitcher JA: G protein-coupled receptor kinase 2-mediated phosphorylation of ezrin is required for G protein-coupled receptor-dependent reorganization of the actin cytoskeleton. *Mol Biol Cell* 16:3088-3099, 2005

10. Acknowledgements

I would like to thank my supervisors, Professor Dr. Hermann Pavenstädt, for his friendly advices and encouragements throughout the three and a quarter years leading to submission of this thesis, and for providing me with the first class resources. I also would like to thank the iGEL (Interdepartmental Graduate-Program for Experimental Life Sciences) of Universität Münster for providing me supports.

It has been a great pleasure working with the faculty, staff, and students at the Universitätsklinikum Münster, Medizinische Klinik und Poliklinik D, Molekulae Nephrologie during my tenure as a doctoral student. I would like to thank my current and former colleagues (in a chronological order): PD Dr. Martin Bek, Dr. Michael Bayer, Dr. Christian Reinhardt, Dr. Eric Springer, Dr. Christina Schäfer, Katja Brinkmann, Truc van Le, Dr. Stefanie Kreußer, Dr. Beate Vollenbröker, PD Dr. Detlef Lang, Miriam Stölting, Dr. Kerstin Duning, Dr. Giovana Seno di Marco, Dr. Marc Schlüter, Dr. Thomas Weide, Nina Meyer, Roman Preston and Anja Hillmann for providing me a sweet and unforgettable memory.

I would like to thank all the people at Experimentelle Nephrologie who have made it such a great place to work with. Particular thanks go to Prof. Dr. Eberhard Schlatter, PD Dr. Giuliano Ciarimboli, Dr. Bayram Edemir and Dr. Ana Velic for creative discussions and technical assistances.

Especially, thanks and good luck go out to Dr. Eva-Maria Schurek. She and her dog helped me to survive from several low-tides. We spent a lot of time in the zoo discussing how to beat those difficulties.

Finally, I would like to thank my wife and my parents for their love and support. Thank you for everything.

11. Curriculum Vitae